A Model-based Fault Recovery for the Attitude Control Subsystem of a Satellite using Magnetic Torquers

Jessica Nathalia Parra Bernal

A Thesis

in

The Department

of

Electrical and Computer Engineering

Presented in Partial Fulfillment of the Requirements

for the Degree of Master of Applied Science (Electrical & Computer Engineering) at

Concordia University

Montréal, Québec, Canada

August 2008

Your file Votre référence
ISBN: 978-0-494-45319-3
Our file Notre référence
ISBN: 978-0-494-45319-3

ABSTRACT

A Model-based Fault Recovery for the Attitude Control

Subsystem of a Satellite using Magnetic Torquers

Jessica Nathalia Parra Bernal

Concordia University, 2008

The interest in small satellites for scientific missions and Earth observations has been increasing steadily in recent years and magnetic torquers have been found attractive as suitable choice of actuators for the purpose of attitude control. Magnetic torquers are commonly used for momentum desaturation of reaction wheels, damping augmentation in gravity gradient stabilized spacecraft, and reorientation of the spin axis in spin-stabilized spacecraft. Furthermore, their use as sole actuators for 3-axis stabilization of satellites in Low-Earth Orbit (LEO) has also been proven effective and advantageous when compared to other types of actuators.

The autonomy of complex dynamical systems that are vulnerable to failures has been an important topic of research during the past few years. Particularly, in aerospace applications, where several constraints such as telemetry and hardware redundancy limitations make the management of on-board problems, a difficult task for ground control.

With this in mind, an autonomous recovery from faults in magnetic torquers in LEO

satellites constitutes the main focus of the work investigated in this dissertation. A self-recovery mechanism, which extends the capabilities of the attitude control subsystem to operate under the presence of actuator faults is developed. The solution generated takes into account the management of the control authority in the system by taking advantage of the non-faulty actuators. In other words, the recovery mechanism that is proposed in this thesis does not utilize hardware redundancy as the existing actuators are used to perform the required control action.

The effects of the delay in initiating the recovery solution, the presence of noise in the magnetic field measurement, and the responses of the system that is recovered from concurrent faults are also investigated through numerical simulations. These simulations are carried out by using a model that includes relevant environmental disturbances and a realistic model of the geomagnetic field. A reduction in the average steady state error is obtained in response to and due to the application of the proposed recovery mechanism, which is applicable to the system even in the presence of fault detection delays, presence of noise in the magnetic field measurement and concurrent faults.

A mi papá Diego, mi mamá Alba y a mis hermanos Erika y Andres...

Gracias siempre por su amor, su apoyo

y paciencia incondicionales.

ACKNOWLEDGEMENTS

I would like to express my most sincere gratitude to my supervisor, Dr. Kashayar Khorasani for his continuous patience and support. For his trust and guidance in the development of this thesis. It was an honor for me to be part of his group of students.

Thanks to Ehsan Sobhani for having contributed in great manner to the start of this thesis and to Shauheen Zahirazami for having given me a first push into the realization of this goal.

To Mani, for his valuable time and affection during these two years. For having lent me his shoulder and his heart when I needed the most.

To Ganesh Koraginjala and Mohsen Azizi for sharing with me priceless advice and encouragement. For allowing us cheerful moments during working hours.

To Mr. Antun Katalenic, thank you very much for your confidence, your friendship and wise counsel.

And finally, I thank my family and friends, whom have always been present throughout my life in spite of the distance.

TABLE OF CONTENTS

LIST OF FIGURES xi

LIST OF TABLES xix

LIST OF SYMBOLS xx

1 Introduction **1**

1.1 Problem Statement 2

1.2 Thesis Objectives 2

1.3 Literature Review 3

1.3.1 Attitude Control of Satellites using Magnetic Torquers 3

1.3.2 Fault Detection, Isolation and Recovery 4

1.3.2.1 Process-Model Based Techniques 6

1.3.2.2 Process History-Based Methods 7

1.3.3 Fault Recovery 8

1.4 Methodology 10

1.5 Contributions of This Thesis 11

1.6 Thesis Outline 12

2 Theory and Fundamentals of Attitude Control Subystem **15**

2.1 Coordinate Systems 16

2.2 Satellite Attitude Modeling 18

2.3 Disturbance Modeling 20

2.3.1 Model of the Geomagnetic Field in LEO 21

2.3.2 Other Environmental Disturbances 27
2.4 Magnetic Torquers 29
2.4.1 Model of Magnetic Torquers 30
2.4.2 Size of the Magnetic Torquers 32
2.4.3 Magnetic Torquers and the Attitude Control Law 33
2.4.4 The Cross Product Between the Desired Torque and the Magnetic Field 35
2.4.5 Closest Vector in Perpendicular Plane to the Geomagnetic Field . . 37
2.5 Nonlinear Attitude Controller 40
2.6 Stability Analysis 43
2.7 Chapter Summary 46

3 Satellite Fault Recovery using Magnetic Torquers 48

3.1 Types of Faults 48
3.2 Definitions and Models of Faults in Magnetic Torquers 51
3.3 Recovery From Actuator Faults 53
3.4 Implementation of a Fault Recovery System 54
3.5 Control Reallocation Problem 57
3.6 Analytical Solutions to the Unconstrained Control Reallocation Problem . . 59
3.6.1 System Subject to Float Fault 60
3.6.2 System Subject to LOE Fault 61
3.6.3 System Subject to LIP or HO Fault 62
3.7 Analytical Solutions to the Constrained Control Reallocation Problem . . . 63

3.7.1 System Subject to a Float Fault 67
3.7.2 System Subject to an LIP Fault 71
3.7.3 System Subject to an HO Fault 74
3.7.4 System Subject to an LOE Fault 75
3.8 System Subject to Concurrent Faults 76
3.8.1 Constrained Optimization Algorithm 77
3.9 Stability Analysis of System Recovered From Fault 78
3.9.1 Float and HO Faults 79
3.9.2 LOE Fault 81
3.9.3 LIP Fault 82
3.10 Chapter Summary 84

4 Simulation Results **85**

4.1 System Parameters, Specifications and Constraints 85
4.1.1 Satellite Model Parameters 86
4.1.2 Orbital Trajectory and Geomagnetic Field 87
4.1.3 Size and Limitations of the Magnetic Torquers 88
4.2 Response of Satellite Without Fault 92
4.3 Satellite Response Under Actuator Faults 99
4.4 Response of the Recovered Satellite From Faults 121
4.4.1 Constrained Recovery 122
4.4.2 Recovery From HO Fault 139
4.5 Effects of Delay of Fault Diagnosis in the Recovery System 140

4.6 Recovery of the System that is Subject to Faults and Measurement Noise . . 151

4.7 Recovery From Concurrent Faults 156

4.8 Chapter Summary 165

5 Conclusions and Future Work **167**

5.1 Conclusions 167

5.2 Future Work 170

Bibliography **172**

LIST OF FIGURES

2.1 Orbital elements and inertial reference frame (Adapted from [1]). 17

2.2 Geomagnetic field elements and coordinates (Adapted from [2]). 23

2.3 Orbital elements. (Adapted from [3]). 24

2.4 Illustration of the attitude control system using magnetic torquers 34

2.5 Illustration of the operation to calculate the required magnetic moment. . . 37

2.6 Torque and magnetic moment vectors in orthogonal planes. 38

3.1 Illustration of faults in a typical control signal. 50

3.2 Attitude control subsystem augmented with a fault recovery for faults in the magnetic torquers. 55

4.1 Circular LEO to be used in the simulation results. 88

4.2 Geomagnetic field during two orbits as calculated in the geocentric coordinates. 90

4.3 Time varying trajectory. Reference with respect to the inertial frame. 93

4.4 Slow time varying trajectory. Reference with respect to the inertial frame. . 93

4.5 Response of the satellite without fault following a zero reference with respect to the inertial frame. 95

4.6 Response of the satellite without fault following the time varying reference in Figure 4.3. 96

4.7 Response of the satellite without fault following the time varying reference in Figure 4.4. 97

4.8 Quaternion errors. Responses from the system without a fault. 98

4.9 Quaternion errors. Response from the system without a fault following the trajectory of Figure 4.4. 99

4.10 Response of the satellite following a zero reference trajectory. System is subject to a float fault that is applied at time $T_f = 13$ oribts. 101

4.11 Response of the satellite following the time varying reference in Figure 4.3. System is subject to a float fault that is applied at time $T_f = 13$ orbits. . . . 102

4.12 Response of the satellite following the time varying reference in Figure 4.4. System is subject to a float fault that is applied at time $T_f = 21$ orbits. . . . 103

4.13 Quaternion errors. System is subject to a float fault that is applied at time $T_f = 13$ orbits. 104

4.14 Quaternion errors. Response from the system following the trajectory in Figure 4.4. The system is subject to a float fault that is applied at time $T_f = 21$ orbits. 105

4.15 Response of the satellite following a zero reference with respect to the inertial frame. System is subject to a LIP fault that is applied at time $T_f = 21$ orbits. 106

4.16 Response of the satellite following the time varying reference in Figure 4.4. System is subject to a LIP fault that is applied at time $T_f = 21$ orbits. 107

4.17 Quaternion errors. System is subject to a LIP fault that is applied at time $T_f = 21$ orbits. 108

4.18 Response of the satellite following a zero reference. System is subject to a 90% LOE fault that is applied at time $T_f = 21$ orbits. 109

4.19 Response of the satellite following the time varying reference in Figure 4.4. System is subject to a 90% LOE fault that is applied at time $T_f = 21$ orbits. 110

4.20 Response of the satellite following a zero reference. System is subject to a 90% LOE fault that is applied at time $T_f = 21$ orbits. 111

4.21 Response of the satellite following the time varying reference in Figure 4.4. System is subject to a 75% LOE fault that is applied at time $T_f = 21$ orbits. 112

4.22 Quaternion errors. System is subject to a 90% LOE fault that is applied at time $T_f = 21$ orbits. 113

4.23 Quaternion errors. System is subject to a 75% LOE fault that is applied at time $T_f = 21$ orbits. 114

4.24 Response of the satellite following a zero reference with respect to the inertial frame. System is subject to an HO fault that is applied at time $T_f = 21$ orbits. 115

4.25 Response of the satellite following the time varying reference in Figure 4.4. System is subject to an HO fault that is applied at time $T_f = 22$ orbits. . . . 116

4.26 Quaternion errors. System is subject to an HO fault that is applied at time $T_f = 21$ and $T_f = 22$ orbits. 117

4.27 A typical calculation of the settling time and the steady state values. 118

4.28 Mean and standard deviation of the quaternion errors according to Table 4.5. Satellite is following a zero reference and subject to faults without recovery. 119

4.29 Mean and standard deviation of the quaternion errors according to Table 4.6. Satellite is following a time varying trajectory subject to faults without recovery. 120

4.30 Response of the satellite following a zero reference with respect to the inertial frame. System is recovered from a float fault that is applied at time $T_f = 13$ orbits. 123

4.31 Response of the satellite following the time varying reference in figure 4.3. System is recovered from a float fault that is applied at time $T_f = 21$ orbits. 124

4.32 Response of the satellite following the time varying reference in Figure 4.4. System is recovered from a float fault that is applied at time $T_f = 21$ orbits. 125

4.33 Quaternion errors. System is recovered from a float fault that is applied at time $T_f = 13$ and $T_f = 21$ orbits, respectively. 126

4.34 Quaternion errors of system following the trajectory from Figure 4.4. System is recovered from a float fault that is applied at time $T_f = 21$ orbits. . . 127

4.35 Response of the satellite following a zero reference. System is recovered from a LIP fault that is applied at time $T_f = 21$ orbits. 128

4.36 Response of the satellite following the time varying reference in Figure 4.3. System is recovered from a LIP fault that is applied at time $T_f = 21$ orbits. . 129

4.37 Response of the satellite following the time varying reference in Figure 4.4. System is recovered from a LIP fault that is applied at time $T_f = 21$ orbits. . 130

4.38 Quaternion errors. System is recovered from a LIP fault that is applied at time $T_f = 21$ orbits. 131

4.39 Quaternion errors of system following the trajectory from Figure 4.4. System is recovered from a LIP fault that is applied at time $T_f = 21$ orbits. . . . 132

4.40 Response of the satellite following a zero reference. System is recovered from a 90% LOE fault that is applied at time $T_f = 21$ orbits. 133

4.41 Response of the satellite following a zero reference. System is recovered from a 75% LOE fault that is applied at time $T_f = 21$ orbits. 134

4.42 Quaternion errors of system following a zero reference trajectory. System is recovered from LOE faults that are applied at time $t_f = 21$ orbits. 135

4.43 Comparison of response of the system with fault and recovered from fault. System is following a time varying reference. 136

4.44 Mean and the standard deviation of the quaternion errors according to Table 4.7. Satellite is recovered from faults while following a zero reference trajectory. 137

4.45 Mean and the standard deviation of quaternion errors according to Table 4.8. Satellite is recovered from faults while following a time varying trajectory. 138

4.46 Response of the satellite that is recovered from a float fault after a 2000s delay (T_r) from the time $T_f = 21$ orbits when the fault is applied. Satellite is following the time varying reference of Figure 4.4. 141

4.47 Quaternion errors. Response of the satellite that is recovered from a float fault after a 2000s (T_r) delay from the time $T_f = 21$ orbits when the fault is applied. Satellite is following the time varying reference of Figure 4.4. . . . 142

4.48 Response of the satellite that is recovered from a float fault after a 5000s delay (T_r) from the time T_f when the fault is applied. System is following the time varying trajectory of Figure 4.4. 143

4.49 Quaternion errors. Response of the satellite that is recovered from a float fault after a 5000s delay (T_r) from the time $T_f = 21$ orbits when the fault is applied. Satellite is following the time varying reference of Figure 4.4. . . . 144

4.50 Response of the satellite that is recovered from an LIP fault after a 5000s delay (T_r) from the time $T_f = 21$ orbits when the fault is applied. Satellite is following a zero reference. 145

4.51 Quaternion errors. Response of the satellite that is recovered from an LIP fault after a 5000s delay (T_r) from the time $T_f = 21$ orbits when the fault is applied. Satellite is following a zero reference. 146

4.52 Response of the satellite that is recovered from an HO fault (with a $0.001 Am^2/s$ rate of change) after a 5000s delay (T_r) from the time $T_f = 21$ orbits when the fault is applied. Satellite is following a zero reference. 147

4.53 Quaternion errors. Response of the satellite that is recovered from an HO fault (with a $0.001 Am^2/s$ rate of change) after a 5000s delay (T_r) from the time $T_f = 21$ orbits when the fault is applied. Satellite is following a zero reference. 148

4.54 Response of the satellite that is recovered from an HO fault (with a $0.005 Am^2/s$ rate of change) after a 4500s (T_r) delay from the time $T_f = 21$ orbits when the fault is applied. Satellite is following a zero reference. 149

4.55 Quaternion errors. Response of the satellite that is recovered from an HO fault (with a $0.005 Am^2/s$ rate of change) after a 4500s (T_r) delay from the time $T_f = 21$ orbits when the fault is applied. Satellite is following a zero reference. 150

4.56 Comparison of steady state errors of system without and with measurement noise. System is following a zero trajectory. 152

4.57 Response of the satellite under normal conditions that is subject to measurement noise from the magnetometers. Satellite is following a zero reference. 153

4.58 Response of the satellite under normal conditions that is subject to measurement noise from the magnetometers. Satellite is following a zero reference. 154

4.59 Quaternion errors. Response of the satellite under normal conditions and satellite that is recovered from a float fault that is applied at time $T_f =$ orbits. Satellite is following a zero reference. 155

4.60 Response of the satellite that is subject to 90% LOE faults that are applied at times $T_{f1} = 21$ orbits and $T_{f2} = 43$ orbits in the torquers alligned to the X and Y axis, respectively. Satellite is following a zero reference. 158

4.61 Quaternion errors. Response of the satellite that is subject to 90% LOE faults that are applied at times $T_{f1} = 21$ orbits and $T_{f2} = 43$ orbits in the torquers alligned to the X and Y axis, respectively. Satellite is following a zero reference. 159

4.62 Response of the satellite that is recovered from 90% LOE faults that are applied at times $T_{f1} = 21$ orbits and $T_{f2} = 43$ orbits in the torquers alligned to the X and Y axis, respectively. Satellite is following a zero reference. . . 160

4.63 Quaternion errors. Response of the satellite that is recovered from a 90% LOE fault at time $T_{f1} = 21$ orbits and a second LOE of 90% at time $T_{f2} =$ 43 orbits in the torquers alligned to the X and Y axis, respectively. Satellite is following a zero reference. 161

4.64 Response of the satellite that is subject to 75% LOE and LIP faults that are applied at times $T_{f1} = 21$ orbits and $T_{f2} = 43$ orbits in the torquers alligned to the Y and Z axis, respectively. Satellite is following a zero reference. . . 162

4.65 Quaternion errors. Response of the satellite that is subject to 75% LOE and LIP faults that are applied at times $T_{f1} = 21$ orbits and $T_{f2} = 43$ orbits in the torquers alligned to the Y and Z axis, respectively. Satellite is following a zero reference. 163

4.66 Response of the satellite that is recovered from 75% LOE and LIP faults that are applied at times $T_{f1} = 21$ orbits and $T_{f2} = 43$ orbits in the torquers alligned to the Y and Z, respectively. Satellite is following a zero reference. 164

4.67 Quaternion errors. Response of the satellite that is recovered from a 75% LOE and LIP faults that are applied at times $T_{f1} = 21$ orbits and $T_{f2} = 43$ orbits in the torquers alligned to the Y and Z axis, respectively. Satellite is following a zero reference. 165

LIST OF TABLES

2.1 Disturbance torques (Adapted from [4]). 28

4.1 Physical characteristics of a typical satellite [5]. 86

4.2 Orbital elements for a typical simulation ([6] and [7]). 87

4.3 Simplified disturbance torques ([4]). 89

4.4 The environmental parameters that are defined for a typical satellite. 90

4.5 Mean and standard deviation of quaternion errors in steady state. Healthy and faulty system following a zero reference trajectory. 119

4.6 Mean and standard deviation of the quaternion errors in steady state. Healthy and faulty satellite following a time varying trajectory. 120

4.7 Mean and standard deviation of the quaternion errors in steady state. Satellite is recovered from faults while following a zero reference trajectory. . . 138

4.8 Mean and the standard deviation of quaternion errors in steady state. Satellite is recovered from faults while following a time varying trajectory. . . . 139

LIST OF SYMBOLS AND CONSTANTS

$G = 6.6695 \times 10^{-11}\,[Nm^2/kg^2]$	Gravitational constant
$R_E = 6,378\,[Km]$	Mean equatorial radius of the Earth
r_s	Attitude of satellite with respect to mean radius of the Earth
$\mu = G(m_1 + m_2)$	Gravitational parameter of two-body system
$M_E = 5.9742 \times 10^{24}\,[kg]$	Mass of the Earth
$M_e = 7.96 \times 10^{15}\,[Tm^3]$	Magnetic moment of the Earth
$\overrightarrow{B}_b\,[nT]$	Geomagnetic field in body frame
$\hat{b_x}, \hat{b_y}, \hat{b_z}$	Unit vectors describing body fixed frame
$\hat{i_x}, \hat{i_y}, \hat{i_z}$	Unit vectors describing Earth centered inertial frame
$\hat{o_x}, \hat{o_y}, \hat{o_z}$	Unit vectors describing orbital reference frame
$\hat{r_x}, \hat{r_y}, \hat{r_z}$	Unit vectors describing control reference frame
$Q = [q_1, q_2, q_3, q_4] = [\mathbf{q}, q_4]$	Quaternion vector
ϕ, θ, ψ	Roll, Pitch and Yaw angles
C_a^b	Cosine rotation matrix of frame a with respect to frame b
$C_a^b(i)$	i^{th} Column of cosine rotation matrix C_a^b
$J = diag[J_x, J_y, J_y]$	Moment of inertia matrix $[Kgm^2]$
ω_a^b	Angular velocity of frame a with respect to b
ω_o	Orbital rate or orbital angular velocity
$\|\cdot\|$	Vector euclidean norm
T_a	Magnetic torque produced by magnetic torquers $[Nm]$
T_c	Control torque

T_d	Disturbance torque
T_{des}	Desired control torque
T_g	Gravity gradient torque $[Nm]$
M	Magnetic moment
$\overline{M}_i$	Lock-in-place value for magnetic moment in axis $i = x, y, z$ of body frame
M_{sat}	Saturation moment
A_i	Cross sectional area of the i^{th} actuator's solenoid
i_i	Applied current to the coil of the i^{th} magnetic torquer
k_i	Magnetic permeability of the core in the i^{th} actuator (air, ferrite, etc.)
N_i	Number of coils in the i^{th} actuator's solenoid
ASL	Above Sea Level (Altitude)
HO	Hard over failure
IGRF	International Geomagnetic Reference Field
LOE	Loss of effectiveness failure
LEO	Low Earth Orbit
LIP	Lock in place failure
t_{fi}	Instant of failure at i_{th} effector
WMM	World Magnetic Model

Chapter 1

Introduction

The use of small satellites for scientific missions and Earth observations is more attractive due to lower complexity, shorter construction time, and reduced power consumption, when compared to a large size spacecraft. Recently, researchers have focused their attention on the attitude stabilization of small satellites using magnetic torquers (also known as magnetic rods). This type of actuator generates a torque when the magnetic moment (produced by the current passing through an electric coil) interacts with the geomagnetic field. The utilization of magnetic torquers is applicable in the attitude stabilization of small satellites in Low-Earth Orbit (LEO), where the strength of the geomagnetic field is sufficient to generate the required control torques.

Considerable efforts have been invested in the development of tools to make dynamical systems capable of operating satisfactorily, regardless of the presence of faults. Reliability, safety and extended degree of autonomy are shown to be achieved by incorporating Fault Diagnosis, Isolation and Recovery (FDIR) mechanisms in the design of the control

system.

In view of the above reasons, the present work is focused on proposing a model-based actuator-fault recovery strategy as applied to magnetic torquers in the attitude control subsystem of a LEO satellite.

The following subsections introduce the statement of the problem considered, objectives of the dissertation, a summary regarding relevant literature, contributions of the thesis, and an outline of the remaining chapters.

1.1 Problem Statement

To propose a self-recovery mechanism for the attitude control subsystem of a satellite that is actuated by magnetic torquers.

1.2 Thesis Objectives

The purpose of this work is to propose a self-recovery mechanism for the attitude control subsystem of a satellite that is actuated by magnetic torquers. Our goal is to demonstrate that it is possible to reallocate the required control effort obtained by means of a reconfigured control law so that under faulty conditions the performance of the attitude control subsystem remains still satisfactory.

1.3 Literature Review

1.3.1 Attitude Control of Satellites using Magnetic Torquers

The attitude control of a satellite using magnetic torquers is to be differentiated from the control using reaction wheels, thrusters, or other types of actuators. The fact that the torque produced is a function of the variation of the magnetic field at the orbital position of the satellite makes the attitude control problem distinct from other control mechanisms. The following descriptions correspond to the work that are found in the literature regarding the development of attitude control laws for satellites using magnetic torquers.

References [8], [9], [10], and [11], deal with the design of state feedback stabilizing controllers and reference [12] addressed the solution through an LQR controller. In reference [13] the authors considered the case of isoinertial satellites and developed outer and inner-loop controllers with state feedback and sliding mode control. In reference [14] the authors presented an explicit model-predictive control law, and in reference [15] the authors introduced the solution to the attitude control problem of magnetic actuated satellites using neural networks in the implementation of the controller.

In [16] a pulse width modulation control for low power consumption torquers is developed. The work described in [17] combines the design of adaptive control for the attitude control, using two magnetic torquers and one reaction wheel, with a fuzzy logic supervisor in charge of managing a multilevel controller for different operating modes.

Model predictive control is used in the regulation of magnetically actuated satellites in [18].

References [5], [19] and [20] introduced the use of continuous-sliding mode control, while [21] and [22] utilized optimum control techniques with LQR in the linearized equations of the satellite. An energy based control was also presented in [5], in which a type of error cross product control was implemented and the stability of the system was justified using an energy function that characterizes the motion of the satellite.

Among the work in the literature as reviewed above, a model-based nonlinear control strategy is considered to be quite adequate for the application of our proposed fault recovery solution. This type of control scheme that is derived from a "better" approximation of the real system (not obtained by means of linearization of the equations of motion) as shown is believed to provide a more appropriate control torque that is required for stabilizing the attitude of the satellite for a larger range of operations.

1.3.2 Fault Detection, Isolation and Recovery

A Fault Diagnosis, Isolation and Recovery (FDIR) module is in charge of detecting, identifying and generating a mechanism to allow acceptable performance of the system that is subject to a fault. The following are some of the main concepts that are used in the field of FDIR:

- A **fault** is considered as a departure from an acceptable range of an observed variable or a calculated parameter associated with a process [23],
- The event or root cause of a fault, is also referred as a **malfunction** or a **failure**. It is defined, as well, as a permanent interruption or stoppage of a systems ability to perform a required function under specified operation conditions [24],
- a system which includes the capacity of detecting, isolating, identifying or classifying faults is called a **fault diagnosis system** [25],
- **Failure mode** is a particular way/approach in which a failure/malfunction could occur,
- **Fault detection** is the determination of the presence of fault(s) in a system,
- **Fault isolation** corresponds to the recognition of the kind, location, and time of the detected fault. It follows the fault detection/recognition step,
- **Fault identification** is the determination of the size and time-variant behavior of a fault: It follows the fault segregation/isolation step,
- **Fault diagnosis** includes the fault isolation and identification, and
- **Fault modeling** is the definition of a linguistic and mathematical model to describe a specific fault effect.

In order to determine the nature of faults, a general classification of the types of faults can be found in [23]. This classification separates the faults according to their cause, which could be:

- Gross parameter changes in a model due to unmodeled processes or interaction of disturbances entering the system through model variables, or
- Structural changes or hard failures in the equipment such that the model equations should be restructured or rederived in order to describe the current process situation, or
- Malfunctioning sensors and actuators which cause deviation of plant state variables beyond acceptable values.

Models for failures in actuators, sensors and structural damage can be found in [26], [27], and [28].

The existing methods for implementing fault detection are classified into qualitative, quantitative and process-history based methods in [23], [29] and [30]. These references explain that qualitative and quantitative methods belong to the type of detection that is based on process model information. The characteristics of these approaches are briefly explained below.

1.3.2.1 Process-Model Based Techniques

To apply these techniques as addressed in [31], among others, it is of great importance to have a fundamental understanding of the process. The interaction between process variables should be defined through qualitative causal models or quantitative models as described below.

- **Qualitative Causal Methods**:

  A cause-effect reasoning about the system's behavior is employed, instead of mathematical relations between variables of the system [32]. These methods mimic human reasoning by generating hypotheses on the status of the process; however, they might be found to be computationally costly and less certain than other methods.

- **Quantitative Methods**:

  The objective of using these approaches [25] is to generate information about the location and timing of a fault, using the measurements available in the system as well as precise mathematical relationships among them. It is assumed that a precise model of the plant is available. State estimation, parameter estimation and parity equation approaches are the major sub-classes of model-based fault detection and isolation (FDI).

1.3.2.2 Process History-Based Methods

In process history based methods, the availability of large amount of historical process data is required [30]. The data is transformed and presented as *a priori* knowledge to a diagnostic system (expert systems and trend modeling methods are widely used in this stage of the fault detection). They can also be classified into *quantitative* and *qualitative* techniques. However, there is not a single method to handle all the requirements of a good detection system. Hybrid mechanisms such as those presented in [31] and [33] have been used to

overcome these limitations.

1.3.3 Fault Recovery

Upon detection of a fault, an "optimal" selection of the possible configurations of non-faulty components is one of the goals of the fault recovery mechanism. It is also required that the quality of the performance under faulty conditions be maintained despite the presence of faults.

In [34], it is stated that generating a plan to correct an on-board anomaly, fault, or failure remained almost exclusively a ground responsibility. However, considering the cost of telemetry and data analysis, as well as the risks of communication delays or failure, on-board recovery is, nowadays, a desirable feature in aerospace applications.

Several methods have been studied in the literature such as [35],[36],[37],[38], [39], and [27], among others, for applications to control reconfiguration of systems subject to failure. A brief review of these work that are employed in fault recovery is described below.

Reference [40] is an extensive survey on the state of the art on reconfigurable fault-tolerant control systems. The authors detail that the existing model-based reconfigurable control design methods are classified into the following approaches: (a) linear quadratic

regulator; (b) eigenstructure assignment; (c) pseudo-inverse; (d) model-following; (e) adaptive control; (f) gain scheduling or linear parameter varying; (g) variable structure and sliding mode control; (h) model predictive control; (i) feedback linearization and dynamic inversion, among others. Other classifications are based on the criteria of the mathematical tools used, design approaches, and the way of achieving reconfiguration.

Multiple-model based reconfiguration methods can be found in [28], [41], and [42]. These references have in common the definition of a bank of multiple models and corresponding controllers, according to the type of faults that could affect the system. A switching mechanism among the models and the corresponding controllers is also a component of this solution.

The use of model-predictive methods is addressed in [43]. A state-space approach and a nonlinear-in-parameters neural network is used in [38] to estimate the fault and to reconfigure the controller.

An example of fault recovery using magnetic torquers is found in [35]. The recovery action was determined from ground control (not on-board) and it was commanded via telemetry to the failing satellite. Other example of fault recovery in a satellite that uses magnetic torquers for momentum damping due to the effect of the attitude control with reaction wheels is found in [?], where an optimization mechanism is used to calculate the required outputs from the magnetic actuators.

The control allocation in over-actuated systems is presented in [45], [46], [47] and [48]. The authors introduce algorithms by means of which the control effort is allocated among the available actuation resources.

1.4 Methodology

The methodology pursued in this thesis can be partitioned in the following steps: First, mathematical equations that are needed to represent the system under healthy operating conditions will be employed in the implementation of a model. This model will include relevant environmental disturbances, and the design and implementation of an adequate controller that guarantees the desirable performance of the attitude control system. It will also include the model characterizing the dynamics of the actuators.

Then, the effects of different types of failures in the magnetic torquers will be analyzed and formulated. Based on the model of the system that is operating under faulty conditions, the problem of reallocating the required control effort, among the non-faulty actuators will be studied.

Assuming the availability of a fault diagnosis system, the solution to the reallocation problem will then be implemented according to the analysis that is made regarding the effects of each type of fault and the reallocation problem. The solution will be tested through

simulations by assuming that the fault detection system has a delay in determining the presence of a fault. The response of the recovery mechanism will also be evaluated under the effect of noise in the magnetic field measurement.

The implementation of the recovery solution will as well be extended to the reallocation of the control effort and the recovery of the system that is subject to the presence of concurrent faults.

1.5 Contributions of This Thesis

To the best of the author's knowledge, the problem of autonomous fault recovery in magnetic torquers is still an open area of research and the present work constitutes a contribution to the study of additional capabilities and properties of these type of actuators for the attitude control of satellites. A comprehensive analysis of the operation of the magnetic torquers is made. The nonlinear control scheme chosen from [19], [5], and [20] is analyzed by using the results obtained and the stability of the equilibrium point in the system without faults is presented.

The solution developed takes into account the management of the control authority in the system by taking advantage of the non-faulty actuators. In other words, the recovery mechanism that is proposed in this thesis does not utilize hardware redundancy as the existing actuators are used to perform the required control action. A comprehensive stability analysis of the faulty system under the recovery mechanism proposed is also included.

The effects of the delay in initiating the recovery solution, the presence of noise in the magnetic field measurement, and the responses of the system that is recovered from concurrent faults are also investigated through numerical simulations. These simulations are carried out by using a model that includes relevant environmental disturbances and a realistic model of the geomagnetic field.

A reduction in the average steady state error has been found in response to the recovery mechanism. Positive results include, also, the successful recovery regardless of finite delay in the detection of the failure and concurrent failure of two magnetic torquers for certain applicable cases.

1.6 Thesis Outline

This dissertation is divided into five chapters that are described as follows. Chapter one introduces the objectives of this thesis. An overview of the motivations, the statement of the problem and a brief discussion regarding FDIR approaches are made. Furthermore, the contributions of this thesis are also detailed.

The second chapter presents the theory and fundamentals of the attitude control subsystem of a satellite. In the first place, it will describe the different coordinate systems that serve as reference to the relative and absolute positions of a satellite. It describes the

dynamics and kinematics equations that model the angular rates and positions of a satellite. The discussion on the various environmental disturbances to which a spacecraft is subject to is also presented. A section of the chapter is dedicated to describing the model that is used to represent the geomagnetic field, as well as the generation of its values at satellite's position in the orbit. This chapter also introduces the concepts related to the operation of the magnetic torquers, the control law used in the development of the present work and stability considerations.

Chapter three contains the details regarding the fault recovery mechanism that is proposed. It shows the model representing each type of failure to which the actuators will be subject to, such as Float, Hard Over (HO), Lock-In-Place (LIP) and Loss of Effectiveness (LOE). The formulation to the recovery reallocation solution is described and the analytical results are described. The stability analysis of the closed-loop system recovered from failures are also discussed.

The fourth chapter presents the results that are obtained from the simulations of the proposed recovery mechanism. The responses of the system under each type of failure are shown followed by the corresponding recovery results using constrained solutions to the control effort reallocation problem. The simulations results including finite delays in the initiation of the recovery after a failure occurs are presented. Furthermore, the responses of the system recovered from failures considering the presence of noise in the magnetic field measurement are shown. Finally, the responses of the recovery system from the application of concurrent faults are also included.

The last chapter lists the conclusions and the work accomplished in this thesis as well as the open problems that the author considers to be addressed and investigated in future.

Chapter 2

Theory and Fundamentals of Attitude Control Subystem

In this chapter, the concepts that are used in the modeling of the satellite attitude control subsystem will be described. First, different coordinate systems that serve as reference to the relative and absolute positions of a satellite will be presented. The calculations of the position and rate of the satellite are described by means of dynamics and kinematics equations.

In addition, the models for the geomagnetic field are formulated, along with the generation of the values at the satellite's position in the orbit. This model is required for the simulation of the operation of the magnetic torquers. In the following sections, the various environmental disturbances to which a spacecraft is subject to, such as aerodynamic drag, solar radiation and magnetic disturbance torques are also explained. Finally, the operation of the magnetic torquers, the control law used in the present work and the corresponding

stability considerations are presented.

2.1 Coordinate Systems

Different coordinate systems are used in order to identify the diverse forces and torques that are acting on the spacecraft as well as to determine its orientation and motion rate. The attitude control problem is defined as the generation of a control input so that the desired orientation of the spacecraft with respect to a reference frame is achieved.

Earth Centered Inertial Frame

This is the inertial frame located at the geographical center of the Earth, as illustrated in Figure 2.1. The axes that represent the relative position of any point around the Earth are defined as:

- $\hat{i}_x$: Pointing toward the vernal equinox
- $\hat{i}_y$: Completing the orthogonal axes frame
- $\hat{i}_z$: Along Earth's polar axis of rotation

Orbital Frame

The Orbital frame represents the position of the satellite as a point rotating around the Earth. Each axis is defined as follows:

- $\hat{o}_x$: Along the orbit direction
- $\hat{o}_y$: Perpendicular to the orbit plane

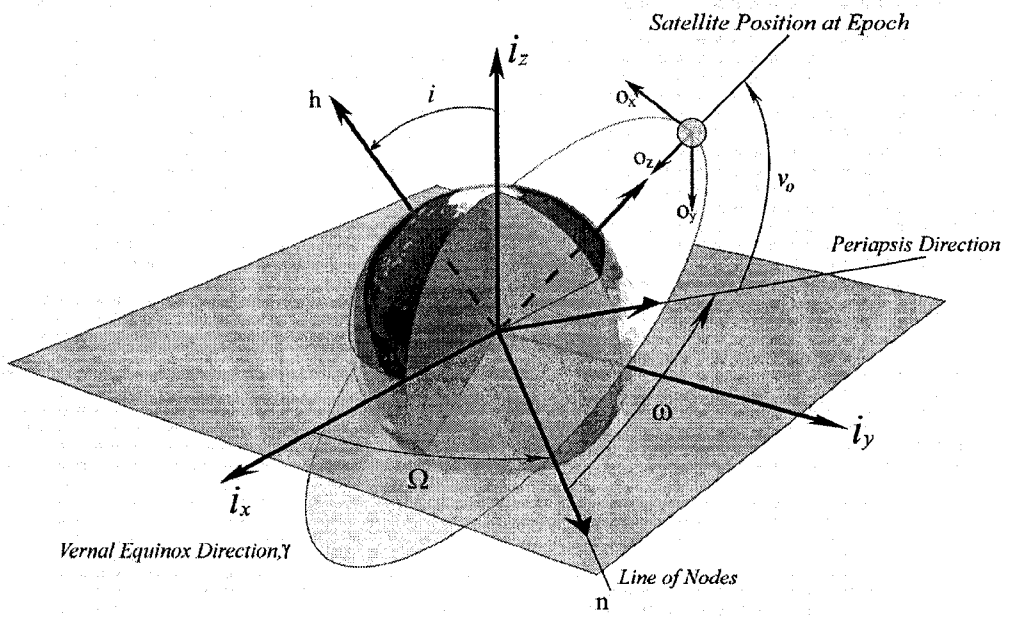

Figure 2.1: Orbital elements and inertial reference frame (Adapted from [1]).

- $\hat{o}_z$: Toward the center of the Earth

Body Fixed Frame

This frame is centered in the geometrical center of the body of the satellite. It has been defined to be alligned with the axis of the principal moments of inertia J_x, J_y, J_z, namely

- $\hat{b}_x$: Aligned with the principal moment of inertia J_x
- $\hat{b}_y$: Aligned with the principal moment of inertia J_y
- $\hat{b}_z$: Aligned with the principal moment of inertia J_z

Control Reference Frame

This reference frame is centered in the body of the satellite. The objective of the attitude control is to make the body axis align with the control reference frame. The axis of this system of coordinates are defined as:

- $\hat{r}_x$: To be aligned with $\hat{b}_x$
- $\hat{r}_y$: To be aligned with $\hat{b}_y$
- $\hat{r}_z$: To be aligned with $\hat{b}_z$

2.2 Satellite Attitude Modeling

The kinematics and dynamics equations characterize the angular position and angular rate of the system relative to a reference frame, respectively. This section will introduce the modeling equations that are employed to calculate the variables ω and $\mathbf{q}$, representing the attitude of the satellite in the orbit.

The differential equation of the angular rate of the satellite's body frame with respect to the Earth centered inertial frame, is described by [3]

$$J\dot{\omega}_b^i = -\omega_b^i \times J\omega_b^i + T_c + T_d \tag{2.1}$$

where $J = diag\{J_x, J_y, J_z\}$ is the moments of inertia matrix, ω_b^i is the vector in $\Re^3$ describing the angular velocity of the body axis with respect to the inertial frame, and T_c and T_d are the control and disturbance torques, respectively.

As it can be seen, equation (2.1) is written in terms of the angular rate ω_b^i, defined at the body's axis with respect to the inertial frame. The angular rate of interest for the purpose of attitude control for tracking a reference trajectory corresponds to the rate of the body with respect to the reference frame ω_b^r. Thus, it is necessary to obtain a representation of the vector ω_b^r, in terms of the calculated ω_b^i and the reference rate ω_r^i. The relation between the angular velocity of the body, with respect to the inertial and the reference frames, is defined as follows:

$$\omega_b^i = \omega_b^r + C_b^r \omega_r^i \tag{2.2}$$

where C_b^r is the cosine rotation matrix [3] defined in terms of the quaternion parameters q_1, q_2, q_3, q_4 as:

$$C_b^r = \begin{bmatrix} 1-2(q_2^2+q_3^2) & 2(q_1q_2+q_3q_4) & 2(q_1q_3-q_2q_4) \\ 2(q_1q_2-q_3q_4) & 1-2(q_1^2+q_3^2) & 2(q_2q_3+q_1q_4) \\ 2(q_1q_3+q_2q_4) & 2(q_2q_3-q_1q_4) & 1-2(q_1^2+q_2^2) \end{bmatrix} \tag{2.3}$$

The matrix in equation (2.3) relates the body and the reference frames. The matrix (2.3) can also be represented as:

$$C_b^r = (q_4^2 - \mathbf{q}^T\mathbf{q})I + 2\mathbf{q}^T\mathbf{q} - 2q_4\mathbf{Q},$$

where $\mathbf{Q}$ is defined as the matrix:

$$\mathbf{Q} = \begin{bmatrix} 0 & -q_3 & q_2 \\ q_3 & 0 & -q_1 \\ -q_2 & q_1 & 0 \end{bmatrix}$$

and the quaternions $\mathbf{q} = [q_1, q_2, q_3]$ and q_4 express, in this case, the angular position of the body axes with respect to the reference frame. The equations that formulate the attitude kinematics are function of the quaternions and are defined as:

$$\dot{\mathbf{q}} = \frac{1}{2}(q_4 \omega_b^o - \omega_b^o \times \mathbf{q})$$
$$\dot{q}_4 = -\frac{1}{2}(\omega_b^o)^T q \tag{2.4}$$

Equations (2.1), (2.2) and (2.4) are used in the derivation of the attitude control law and the fault recovery solution.

2.3 Disturbance Modeling

The environmental disturbances affect the attitude and orbital control of the satellite; however, for simplicity it is assumed that the disturbances to the orbital control system are compensated for. This section will present the types of disturbances that are taken into account in the model of the attitude control subsystem.

The model of the geomagnetic field in Low-Earth Orbit (LEO) is described first. Since the geomagnetic field varies with the position of the satellite with respect to the inertial frame, the model of the orbital trajectory followed by the satellite will also be described. The section concludes with an introduction to the other types of environmental disturbances and explains which of these disturbances will be included in the attitude control model.

2.3.1 Model of the Geomagnetic Field in LEO

The model of the geomagnetic field is a function of the magnetic potential expressed in spherical harmonics [2], as indicated in the following equation

$$\vec{B}(\phi,\lambda,r) = -\nabla V(\phi,\lambda,r)$$

where $\vec{B}$ is the geomagnetic field and V is the magnetic potential. The parameters ϕ, λ, r are the latitude, longitude, and altitude of a point respectively, in the *Earth-centered equatorial coordinates*. The magnetic vector potential is formulated with the following function:

$$V = a\{\sum_{n=1}^{N}[g_n^m(t)\cos(m\lambda) + h_n^m(t)\sin(m\lambda)](\frac{a}{r})^{(n+1)}\breve{P}_n^m \sin(\phi)\},$$

where $\breve{P}_n^m sin(\phi)$ are the Schmidt semi-normalized associated Legendre functions and the parameters $g_n^m(t)$and $h_n^m(t)$ are calculated as follows:

$$g_n^m(t) = g_n^m + \dot{g}_n^m(t - t_0)$$

$$h_n^m(t) = h_n^m + \dot{h}_n^m(t - t_0)$$

Parameters g_n^m, $\dot{g}_n^m$, h_n^m and $\dot{h}_n^m$ are provided in the geomagnetic field measurement results such as those referred in [2] and [49], and $t_0 = 2005$ is chosen for simplicity as the reference date of the model and t is the time given in decimal years. The estimation of values of the geomagnetic field, using the model parameters in [2] or [49] could be made up to the year 2010.

The geomagnetic field vector $\vec{B}$ is described by 7 elements [2]. These are: the orthogonal components X (northerly intensity), Y (easterly intensity), and Z (vertical intensity,

positive downwards), total intensity F, horizontal intensity H, inclination (or dip) I (the angle between the horizontal plane and the field vector, measured positive downwards), and declination (or magnetic variation) D (the horizontal angle between true north and the field vector, measured positive eastwards). These elements are calculated with the following equations [2]:

$$X(\phi,\lambda,r) = -\sum_{n=1}^{12}(\frac{a}{r})^{(n+2)}\sum_{m=0}^{n}(g_n^m(t)\cos(m\lambda)+h_n^m(t)\sin(m\lambda))\frac{d\breve{P}_n^m(\sin(\phi))}{d\phi} \tag{2.5}$$

$$Y(\phi,\lambda,r) = \frac{1}{\cos(\phi)}\sum_{n=1}^{12}(\frac{a}{r})^{(n+2)}\sum_{m=0}^{n}m(g_n^m(t)\sin(m\lambda)-h_n^m(t)\cos(m\lambda))\breve{P}_n^m(sin(\phi)) \tag{2.6}$$

$$Z(\phi,\lambda,r) = -\sum_{n=1}^{12}(n+1)(\frac{a}{r})^{(n+2)}\sum_{m=0}^{n}(g_n^m(t)\cos(m\lambda)+h_n^m(t)\sin(m\lambda))\breve{P}_n^m(\sin(\phi)) \tag{2.7}$$

$$F = \sqrt{H^2+Z^2} \tag{2.8}$$

$$H = \sqrt{X^2+Y^2} \tag{2.9}$$

$$I = \arctan(\frac{Z}{H}) \tag{2.10}$$

$$D = \arctan(\frac{Y}{X}) \tag{2.11}$$

The elements of interest for the application of this thesis are the North, East and Vertical intensities as indicated in Figure 2.2. These values conform the vector $B = [B_x, B_y; B_z]^T$ which, when transformed to the coordinates of the satellite body will represent the effects of the magnetic field in each one of the directions where the attitude control is applied.

Low Earth Orbit Trajectory

The types of orbits that a geocentric satellite can be designed to follow, according to its altitude, could be placed at Low-Earth (LEO), Middle-Earth (MEO) or High-Earth (HEO)

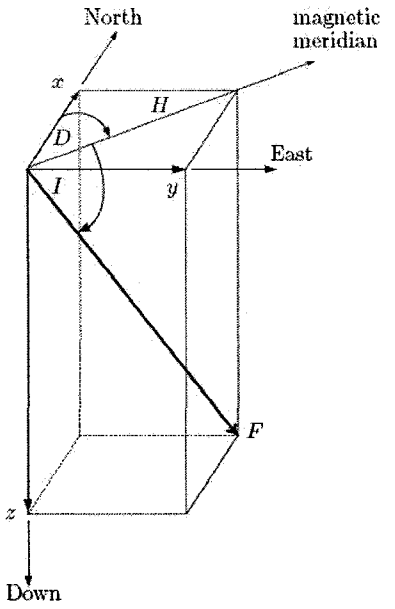

Figure 2.2: Geomagnetic field elements and coordinates (Adapted from [2]).

altitudes with respect to the Earth-centered inertial frame. A satellite would be considered to be placed in a LEO if its altitude is less than 2000 *Km*. On the other hand, if the altitude of the satellite surpasses 2000 *Km* but less than 35,786 *Km*, it is said to be on a MEO. Satellites orbiting at higher altitudes will be at HE orbits.

The application of magnetic torques for attitude control of satellites is possible at LEO because at such altitudes the intensity of the geomagnetic field is enough to allow the generation of required magnetic torques for the control action. For this reason, and because the geomagnetic field is a function of the position of the satellite with respect to the inertial frame, the equations to model the orbital trajectory [3] (specifically LEO) will be described in this part of the chapter.

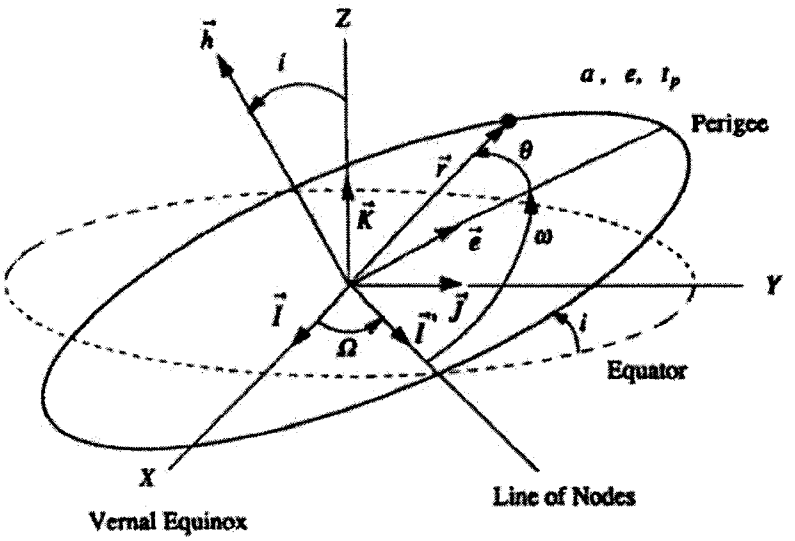

Figure 2.3: Orbital elements. (Adapted from [3]).

Figure 2.3 illustrates the elements that characterize any elliptical orbit. These elements are defined as follows:

a: Semi major axis,

e: Eccentricity,

Ω: Right ascension longitude of the ascending node,

i: Inclination of the orbit plane,

t_p: Time of perigee passage, and

ω: Argument of the perigee.

The radial position of the orbiting satellite can be determined, in terms of the eccentric anomaly (E) and the longitude of the semi major axis (a), using the expression below

$$r = a(1 - e\cos(E)) \tag{2.12}$$

where eccentric anomaly (E) can be calculated at each time, by applying the following

equation

$$\tan(\frac{\theta}{2}) = \sqrt{\frac{1+e}{1-e}}\tan(\frac{E}{2}) \tag{2.13}$$

The parameter θ in (2.13) is called *true anomaly* which represents the angle swept by the satellite from the time of passage by the perigee. To obtain the perigee passage time T_p, the *Kepler's time equation* should be used

$$\sqrt{\mu/a^3}(t-t_p) = E - e\sin(E) \tag{2.14}$$

and the position of the satellite in the orbital plane, in Cartesian coordinates is calculated as shown below

$$\begin{aligned} x &= r\sin(\theta) \\ y &= r\cos(\theta) \\ z &= 0 \end{aligned} \tag{2.15}$$

Particularly, for a circular orbit, it can be seen in (2.13) that the value of θ will be equal to the eccentric anomaly E, because the eccentricity e is equal to zero. Moreover, the semi major axis will be equal to the radius of the orbit, which in a circular orbit will be the constant $r \simeq R_E + r_s$, where R_E is the mean equatorial radius of the Earth and r_s is the altitude of the satellite above sea level.

Consequently, Kepler's time equation (2.14) will become:

$$\sqrt{\frac{\mu}{r^3}}(t-t_p) = E = \theta$$

The values obtained by applying equation (2.15) are calculated in the *Perifocal reference frame* [3]. This reference frame is also an inertial frame which is fixed to the orbital plane. Axis x points toward the perigee of the orbit, y is located in the orbital plane, and z goes out of the orbital plane, completing the orthogonal reference frame. Therefore, a *direction cosine matrix* must be used to express the position of the satellite in orbit with respect to the geocentric equatorial frame. Using $< x, y, z >$ unit vectors describing the geocentric equatorial reference frame (Earth-centered inertial frame), and $< X, Y, Z >$ as those of the Perifocal reference frame, the components of the former are related to the latter as follows:

$$\begin{bmatrix} x \\ y \\ z \end{bmatrix} = \begin{bmatrix} C_{11} & C_{21} & C_{31} \\ C_{12} & C_{22} & C_{32} \\ C_{13} & C_{23} & C_{33} \end{bmatrix} \begin{bmatrix} X \\ Y \\ Z \end{bmatrix}$$

where:

$$C_{11} = \cos(\Omega)\cos(\omega) - \sin(\Omega)\sin(\omega)\cos(i)$$

$$C_{12} = \sin(\Omega)\cos(\omega) + \cos(\Omega)\sin(\omega)\cos(i)$$

$$C_{13} = \sin(\Omega)\sin(i)$$

$$C_{21} = -\cos(\Omega)\sin(\omega) - \sin(\Omega)\cos(\omega)\cos(i)$$

$$C_{22} = -\sin(\Omega)\sin(\omega) + \cos(\Omega)\cos(\omega)\cos(i)$$

$$C_{23} = \cos(\omega)\sin(i)$$

$$C_{31} = \sin(\Omega)\sin(i)$$

$$C_{32} = -\cos(\Omega)\sin(i)$$

$$C_{33} = \cos(i)$$

Finally, to apply the position values in calculating the geomagnetic field intensity, the transformation from Cartesian to spherical coordinates is made, namely

$$r = \sqrt{X^2 + Y^2 + Z^2}$$

$$\lambda = \arctan(Y,X),\ 0 \leq \lambda \leq 2\pi$$

$$\phi = \arcsin(Z/r),\ 0 \leq \phi \leq \pi,$$

where r is the *altitude*, λ corresponds to the *longitude*, and ϕ is the *latitude* of the satellite with respect to the Earth-Centered reference frame.

2.3.2 Other Environmental Disturbances

Besides the magnetic disturbance torque, other environmental forces perturb the attitude control system. The types of disturbances that are known to be most significant for the attitude control at low Earth orbit are shown in Table 2.1, namely aerodynamic torque, gravity gradient torque, solar radiation torque, and magnetic disturbance torque [4].

Gravity Gradient Torque

Due to the non-uniformity of the gravitational field over the satellite, a gravitational torque about the body's center of mass exists. This torque is modeled by means of the equation shown below

$$T_g = 3\omega_o^2 C_b^o(3) \times J C_b^o(3), \tag{2.16}$$

where $C_b^o(3)$ is the third column of the cosine rotation matrix relating the position of the body axis with respect to the orbital frame and ω_o is the constant orbital rate.

Disturbance	Equation	Definition of Terms
ΔV Thruster Misalignment	$\mathbf{s} \times \mathbf{T}$	$\mathbf{s}$ vector distance from center of mass to thrust application point $\mathbf{T}$ vector thrust
Aerodynamic Torque	$\frac{1}{2}\rho V^2 C_d A(\mathbf{u}_v \times \mathbf{s}_{cp})$	ρ atmospheric density C_d drag coefficient (typically 2.25) A area perpendicular to $\mathbf{u}_v$ V velocity $\mathbf{u}_v$ unit vector in velocity direction $\mathbf{s}_{cp}$ vector distance from center of mass to center of pressure
Gravity Gradient Torque	$\frac{3\mu}{R_0^3}\mathbf{u}_e \times (\mathbf{I} \cdot \mathbf{u}_e)$	μ Earth's gravitational coefficient 3.986×10^{14} m^3/s^2 R_0 Distance to Earth's center (m) $\mathbf{I}$ Spacecraft inertia tensor $\mathbf{u}_e$ Unit vector toward nadir
Solar Radiation Torque	$K_s(\mathbf{u}_s \cdot \mathbf{u}_n) A \left[\begin{matrix} \mathbf{u}_s(\alpha + r_d) + \\ \mathbf{u}_n\left\{2r_s + \frac{2}{3}r_d\right\} \end{matrix} \right] \times \mathbf{s}_c$	K_s solar pressure constant 4.644×10^{-6} N/m^2 $\mathbf{s}_c$ vector from spacecraft center of mass to area A $\mathbf{u}_n$ unit vector normal to A $\mathbf{u}_s$ unit vector toward the Sun α surface absorptivity coefficient r_s surface specular reflectance coefficient r_d surface diffuse reflectance coefficient (Note: $\alpha + r_s + r_d = 1$)

Table 2.1: Disturbance torques (Adapted from [4]).

Gravity Torque constitutes as one of the most significant disturbances for the attitude control system of a satellite in LEO.

Magnetic Disturbances

This disturbance is so significant that specialized compensation is required in order to minimize its effect on the attitude control system. Permanent magnets are usually assembled to counteract the magnetic dipole of the spacecraft and care is taken in the location of the components prone to magnetization upon construction. This is done in order to reduce the residual dipole moment of the spacecraft, and thus, the presence of magnetic disturbances. More detailed information on how to determine the magnetic dipole moment of a spacecraft

can be found in [50]. Physical tests are done in order to accurately calculate the effects of the magnetism of the spacecraft.

Aerodynamic Torque

This torque is due to the effects of the atmospheric drag, which acts in the opposite direction of the velocity vector of the satellite. This type of disturbance can be calculated according to the corresponding equation in Table 2.1. However, as considered in [4] this is of more interest for the orbital control system.

Solar Radiation Torque

As a result of nuclear fusion reactions, the sun emits radiant energy that has a torque effect on the surface of the satellite facing the sun. Below 800 *Km* altitude, acceleration from drag is greater than that from solar radiation pressure and above 800 *km*, the acceleration from solar radiation pressure is greater.

In Chapter 3, it will be shown that, in the worst case, aerodynamic drag and solar radiation disturbances are smaller than the magnetic and the gravitational disturbances for the small sized satellite that is used in our simulations.

2.4 Magnetic Torquers

Magnetic torquers have commonly been used for momentum management of reaction wheels, damping augmentation in gravity gradient stabilized spacecraft, and reorientation

of the spin axis in spin-stabilized spacecraft. Moreover, it has been shown in [16], [10], [11], [51], [52], among others, that their application for 3-axis attitude control produces also satisfactory results.

The authors in [53] show that because of the sharp reduction in the geomagnetic field intensity with increasing altitude, the mechanical torques produced by magnetic torquers are small in magnitude. Hence, magnetic torquers are not suitable as primary actuators in spacecraft that are large or operate at high altitudes. Nevertheless, because of their low cost, weight and power requirements, compared to other types of actuators, magnetic torquers provide an attractive option for small satellites operating at low altitudes.

In this thesis, the study of 3-axis active attitude stabilization is brought to the application of actuator-fault recovery. For this reason, this section is dedicated to describing the operational mechanism of magnetic torquers and considerations in applying the control laws that are used for attitude stabilization.

2.4.1 Model of Magnetic Torquers

Magnetic torquers are solenoids enclosing (or not) a magnetic core which produce a magnetic moment once a current flows through the coils. In the presence of a magnetic field, the magnetic moment generated by a magnetic torquer produces a torque.

The equation describing the magnetic torque $\vec{T}_a$ as the interaction of the magnetic

moment $\vec{M}_a$ produced by three orthogonal torquers and the geomagnetic field $\vec{B}$ is given by

$$\vec{T}_a = \vec{M}_a \times \vec{B}, \tag{2.17}$$

where the output moment from the actuators $\vec{M}_a$ corresponds to:

$$\vec{M}_a = \sum_{j=1}^{3} k_j N_j A_j i_{cj} \tag{2.18}$$

For the j^{th} actuator, i_{cj} is the input current to the coil, A_j is the cross sectional area that the coil encloses, k_j represents the permeability constant of the material of the core, and N_j is the number of coils in the solenoid. It is assumed that all the parameters other than $\vec{i}_c$ are known and constant. In other words, the calculation of the control moment is interpreted as the calculation of the input currents for each one of the actuators. It is assumed, for simplicity, that the values of k_j, A_j and N_j are equal in all the magnetic torquers.

Using the operation defined in (2.17), the torque generated by each of the actuators is reflected in two directions that are perpendicular to the axis of the moment produced. The torques due to the magnetic moment from each one of the actuators are formulated in the following expressions, where T_{ai} for $i = x,y,z$ represents the torque produced due to the magnetic torquer aligned to axis i. We have

- The moment M_{ax} produced by the magnetorquer aligned with the X axis has an effect in the Y and Z directions,

$$T_{a_x} = \begin{pmatrix} 0 & 0 & 0 \\ 0 & 0 & -M_{ax} \\ 0 & M_{ax} & 0 \end{pmatrix} \begin{pmatrix} B_x \\ B_y \\ B_z \end{pmatrix} = \begin{pmatrix} 0 \\ -B_z M_{ax} \\ B_y M_{ax} \end{pmatrix}$$

- The torque produced by the magnetorquer aligned with the Y axis is

$$T_{a_y} = \begin{pmatrix} 0 & 0 & M_{ay} \\ 0 & 0 & 0 \\ -M_{ay} & 0 & 0 \end{pmatrix} \begin{pmatrix} B_x \\ B_y \\ B_z \end{pmatrix} = \begin{pmatrix} B_z M_{ay} \\ 0 \\ -B_x M_{ay} \end{pmatrix}$$

- The torque produced by the magnetorquer aligned with the Z axis is

$$T_{a_z} = \begin{pmatrix} 0 & -M_{az} & 0 \\ -M_{az} & 0 & 0 \\ 0 & 0 & 0 \end{pmatrix} \begin{pmatrix} B_x \\ B_y \\ B_z \end{pmatrix} = \begin{pmatrix} -B_y M_{az} \\ B_x M_{az} \\ 0 \end{pmatrix}$$

The total torque for each axis of the satellite's body is a result of the combined action of the torquers as presented below

$$T_a = \begin{pmatrix} B_z M_{ay} - B_y M_{az} \\ -B_z M_{ax} + B_x M_{az} \\ B_y M_{ax} - B_x M_{ay} \end{pmatrix}$$

2.4.2 Size of the Magnetic Torquers

The torque capability, as required from the actuators, is a very important sizing parameter for the selection and/or design of the magnetic torquers. This control authority must be large enough to counterbalance the disturbance torques and control the attitude during maneuvers and following the transient events such as spacecraft separation, deployment, and failure recovery [4].

The authors in [4] provide various methods to size the required capabilities from the actuators. For the purpose of this thesis, the following equations for determining the minimum required torque action are used.

- The torquing capability of an actuator may be set by an acceleration requirement such as that arising from an attitude slew maneuver (reorientation maneuver). This torque (T_{man}) can be calculated according to (2.19) or (2.20).

$$T_{man} = J \cdot a, \tag{2.19}$$

where J corresponds to the moments of inertia matrix and a is the acceleration requirement

$$T_{man} = \frac{4\theta J}{t_{dur}^2} \tag{2.20}$$

where θ is the maximum change in angle assumed and t_{dur} is the time required to reach such change.

- To cancel the disturbance torques, the norms of the worst case disturbance forces acting on the satellite's body are added.

The worst case disturbance torques and the maneuvering requirement torque is considered as the total torque required from the actuators, namely

$$T_{total} = T_{man} + T_{sp} + T_{mag} + T_{aero} + T_g, \tag{2.21}$$

where the values T_{man},T_{sr}, T_{mag}, T_{aero}, and T_g are the maneuver, solar radiation, magnetic, aerodynamic and gravity torques, respectively.

2.4.3 Magnetic Torquers and the Attitude Control Law

Upon calculation of a required control torque T_c, it is desirable to find the value of the magnetic moment that should be obtained from the magnetic torquers. Since the control

input corresponds to the magnetic moment M_c, the value of T_c, and the geomagnetic field $\overrightarrow{B}$, should be used to generate the applicable control signal.

For the purpose of fault recovery, the controller that will be implemented corresponds to the nonlinear control scheme that is presented in [19], [5], and [20]. However, the control output is the amount of torque required T_c, expressed in the body's axis, as illustrated in Figure 2.4. On account of the constraint imposed by the operation of the magnetic torquers, the control moment should be obtained such that the torque produced is as close as possible to T_c. With this in mind, the authors in [54], propose to calculate the magnetic moment using the following equation

$$\overrightarrow{M}_c = \frac{\overrightarrow{B} \times \overrightarrow{T}_c}{\| \overrightarrow{B} \|^2} \tag{2.22}$$

where $\| \overrightarrow{B} \|^2$ is the Euclidean norm of the geomagnetic field vector and the operation $\times$ corresponds to the vector cross product. By using (2.22), the best possible toque, perpendicular to the geomagnetic field is obtained.

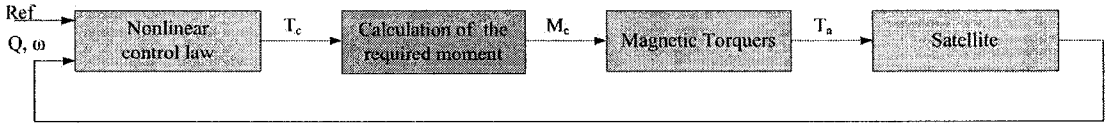

Figure 2.4: Illustration of the attitude control system using magnetic torquers

2.4.4 The Cross Product Between the Desired Torque and the Magnetic Field

The following concepts are analyzed in order to describe, in more detail, the operation that is used to calculate the magnetic moment that is to be commanded to the actuators. It is demonstrated that the torque $\overrightarrow{T}_a$ that is obtained by using the operation proposed in (2.22) is as close as possible to the control torque $\overrightarrow{T}_c$.

Definition 2.1 *([55]) Let* $\overrightarrow{U} = u_1\hat{i} + u_2\hat{j} + u_3\hat{k}$ *and* $\overrightarrow{V} = v_1\hat{i} + v_2\hat{j} + v_3\hat{k}$ *be two vectors in* $\Re^3$ *with unitary direction vectors* $\hat{i}, \hat{j}, \hat{k}$. *The* ***Cross Product*** *is a binary operation between the two vectors in the three-dimensional Euclidean space that results in another vector, perpendicular to the two input vectors, namely*

$$\overrightarrow{U} \times \overrightarrow{V} = \begin{vmatrix} \hat{i} & \hat{j} & \hat{k} \\ u_1 & u_2 & u_3 \\ v_1 & v_2 & v_3 \end{vmatrix}$$

$$= (u_2v_3 - u_3v_2)\hat{i} - (u_1v_3 - u_3v_1)\hat{j} + (u_1v_2 - u_2v_1)\hat{k} \tag{2.23}$$

From the definition of the cross product in (2.23) the triple cross product of vectors $\overrightarrow{U}$, $\overrightarrow{V}$ and $\overrightarrow{W}$ can be calculated by using (2.24), that is also known as the *Lagrange's Formula*,

$$(\overrightarrow{U} \times \overrightarrow{V}) \times \overrightarrow{W} = \overrightarrow{V}(\overrightarrow{U} \cdot \overrightarrow{W}) - \overrightarrow{U}(\overrightarrow{V} \cdot \overrightarrow{W}) \tag{2.24}$$

The following Definitions 2.2 and 2.3 will be employed to compare the vector T_c and the vector T_a that is calculated by using equation (2.22) .

Definition 2.2 *([55]) The projection (Proj) of the torque vector* $\overrightarrow{T}_c$ *on the geomagnetic field vector* $\overrightarrow{B}$ *is the vector:*

$$Proj_{\overrightarrow{T}_c}\overrightarrow{B} = \frac{\overrightarrow{T}_c \cdot \overrightarrow{B}}{\overrightarrow{B} \cdot \overrightarrow{B}}\overrightarrow{B}$$

Definition 2.3 *([55]) Let* $\overrightarrow{T} = T_1\hat{i} + T_2\hat{j} + T_3\hat{k}$ *be the torque vector and* $\overrightarrow{B} = B_1\hat{i} + B_2\hat{j} + B_3\hat{k}$ *be magnetic field vector. The* Dot Product *is the operation in* $\Re^3 \rightarrow \Re$*:*

$$\overrightarrow{T} \cdot \overrightarrow{B} = T_1B_1 + T_2B_2 + T_3B_3 \tag{2.25}$$

The following Lemma shows that by applying (2.22) , the torque obtained is the perpendicular component of the vector $\overrightarrow{T}_c$.

Lemma 2.1 *Let* $\overrightarrow{T}_c$ *and* $\overrightarrow{B}$ *be two vectors in the Eucledian space* $\Re^3$*. Let* $\overrightarrow{M}_c$*, obtained from* (2.22) *be substituted in place of* $\overrightarrow{M}_a$ *in* (2.17)*. Then, the vector* $\overrightarrow{T}_a$ *will be equal to the perpendicular component of* $\overrightarrow{T}_c$*.*

Proof: Equation (2.17) can be written by using (2.22) as

$$\overrightarrow{T}_a = \frac{(\overrightarrow{B} \times \overrightarrow{T}_c) \times \overrightarrow{B}}{\|\overrightarrow{B}\|^2} \tag{2.26}$$

Using Definitions 2.1 and 2.3 and the property from (2.24), the vector $\overrightarrow{T}_a$ can be expressed also as

$$\begin{aligned} \overrightarrow{T}_a &= \frac{\overrightarrow{T}_c(\overrightarrow{B} \cdot \overrightarrow{B}) - \overrightarrow{B}(\overrightarrow{T}_c \cdot \overrightarrow{B})}{\|\overrightarrow{B}\|^2} \\ &= \overrightarrow{T}_c - \frac{\overrightarrow{B}(\overrightarrow{T}_c \cdot \overrightarrow{B})}{\|\overrightarrow{B}\|^2} \end{aligned} \tag{2.27}$$

Based on Definition 2.2, it can be said that the parallel component ($\overrightarrow{T}_c \|$) of the vector $\overrightarrow{T}_c$, with respect to the vector $\overrightarrow{B}$, is given by

$$\overrightarrow{T}_c \| = \frac{\overrightarrow{T}_c \cdot \overrightarrow{B}}{\| \overrightarrow{B} \|^2} \overrightarrow{B} \tag{2.28}$$

Thus, the perpendicular component of $\overrightarrow{T}_c$ with respect to the vector $\overrightarrow{B}$ will be:

$$\begin{aligned} \overrightarrow{T}_c \perp &= \overrightarrow{T}_c - \overrightarrow{T}_c \| \\ &= \overrightarrow{T}_c - \frac{\overrightarrow{T}_c \cdot \overrightarrow{B}}{\| \overrightarrow{B} \|^2} \overrightarrow{B} \end{aligned} \tag{2.29}$$

Therefore, as illustrated in the Figure 2.5, it can be seen from (2.27) and (2.29) that:

$$\overrightarrow{T}_a = \overrightarrow{T}_c \perp \tag{2.30}$$

■

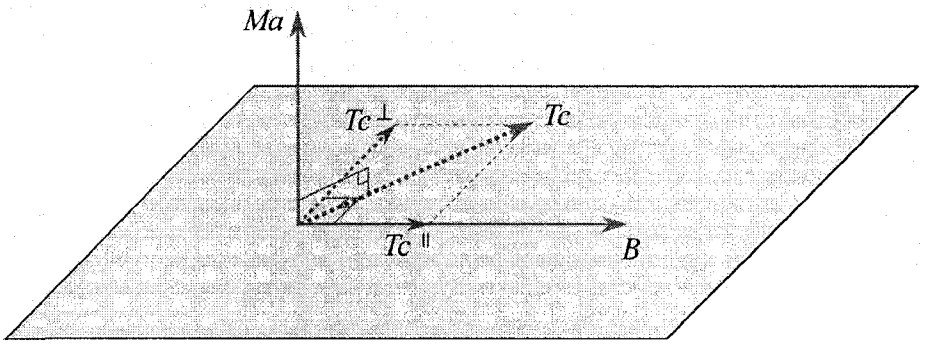

Figure 2.5: Illustration of the operation to calculate the required magnetic moment.

2.4.5 Closest Vector in Perpendicular Plane to the Geomagnetic Field

In this section, it is demonstrated that in the P_B plane, the perpendicular to the geomagnetic field is the closest vector to the desirable torque which is obtained by using equation (2.22).

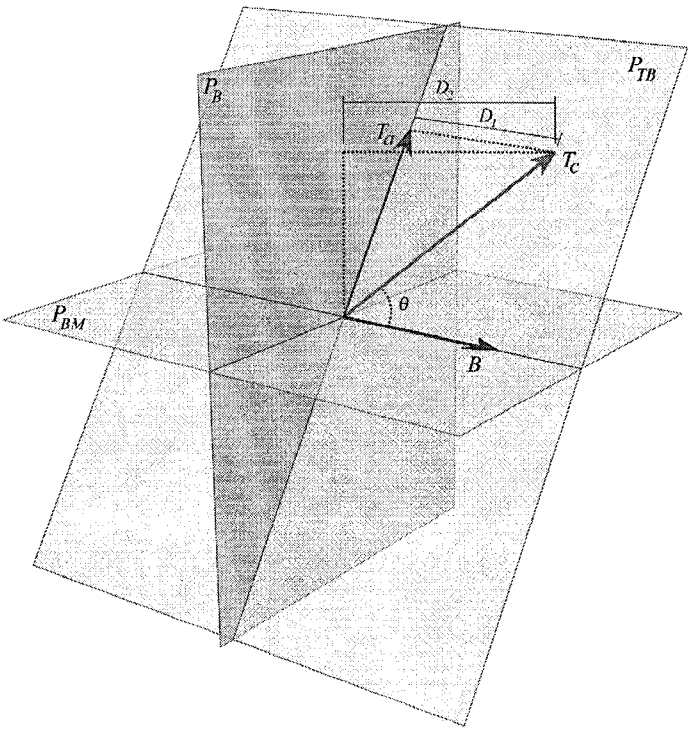

Figure 2.6: Torque and magnetic moment vectors in orthogonal planes.

Lemma 2.2 *Let* $\overrightarrow{B}$ *represents the geomagnetic field vector and* $\overrightarrow{T}_c = [T_{c1}, T_{c2}, T_{c3}]$ *be the desirable torque vector with angle* θ *with respect to the vector* $\overrightarrow{B}$ *as shown in Figure 2.6. The vector* $\overrightarrow{T}_a$ *that is closest to* $\overrightarrow{T}_c$ *in the plane perpendicular to* $\overrightarrow{B}$ *is the component of* $\overrightarrow{T}_c$ *perpendicular to* $\overrightarrow{B}$*. The vector* $\overrightarrow{T}_a$ *is obtained by substituting the vector* $\overrightarrow{M}_a$ *in* (2.17) *with* $\overrightarrow{M}_c$ *that is calculated as follows*

$$\overrightarrow{M}_c = \frac{\overrightarrow{B} \times \overrightarrow{T}_c}{\| \overrightarrow{B} \|^2} \tag{2.31}$$

Proof: The shortest distance $|D|$ between the point (T_{c1}, T_{c2}, T_{c3}) and the plane perpendicular to $\overrightarrow{B}$, is the magnitude of the projection of vector $\overrightarrow{T}_c$ to the normal to the plane. In addition, the normal to the plane perpendicular to $\overrightarrow{B}$ is defined as

$$\hat{n} = \frac{\overrightarrow{B}}{\| \overrightarrow{B} \|}$$

and the shortest distance $|D|$ is represented by

$$|D| = \vec{T}_c \cdot \hat{n}$$

Therefore, the vector $\vec{T}_a$ that is closest to $\vec{T}_c$ is

$$\vec{T}_a = \vec{T}_c - \vec{D} \tag{2.32}$$

It is known that the vector $\vec{D}$ is the component of $\vec{T}_c$ that is parallel to $\vec{B}$ and thus, the difference between $\vec{T}_c$ and $\vec{D}$ corresponds to the perpendicular component of $\vec{T}_c$ with respect to $\vec{B}$.

It was verified that with the expression

$$\vec{M}_c = \frac{\vec{B} \times \vec{T}_c}{\|B\|^2}, \tag{2.33}$$

the torque $\vec{T}_a = \vec{T}_c \perp$. Therefore, the closest vector to $\vec{T}_c$ is obtained from (2.31). ■

Using the equation (2.33), the magnetic moment $\vec{M}_c$ will be perpendicular to the desirable torque $\vec{T}_c$ and the geomagnetic field $\vec{B}$. Moreover, vector $\vec{T}_a$, in (2.17) will be the closest vector to $\vec{T}_c$ if (2.31) is used to calculate the control moment.

The conclusions that we have arrived are indicated in [10], where it is stated that by assuming that three independent control torques can be generated, an ideal torque from a control law can be applied by using equation (2.31).

It is important to note that the actuators using this control input do not always generate a torque equal to the desirable $\vec{T}_c$ due to the reasons that are listed below.

- Only the perpendicular component of $\vec{T}_c$ with respect to $\vec{B}$ is obtained by applying (2.31) to calculate the magnetic moment. This operation is illustrated in Figure 2.5.
- Only if the the angle θ between the vectors $\vec{T}_c$ and $\vec{B}$ is π, the second term of (2.27) is equal to zero, and $\vec{T}_a = \vec{T}_c$.
- If $\vec{T}_c$ is parallel to $\vec{B}$ there is no magnetic moment $\vec{M}_c$ where the magnetic torquers can produce the $\vec{T}_c$.

In [53], it is stated that in the case where the inertial direction of the ambient magnetic field is constant, the component of the spacecraft angular momentum along the direction of the magnetic filed remains constant, and hence the attitude dynamics of the spacecraft are not controllable. However, in [53] the authors show that the time-varying nature of the magnetic field along an orbit leads to the possibility of full attitude controllability. The authors also show that the time variation of a constant dipole approximation of the geomagnetic field along a closed Keplerian orbit satisfies the conditions of controllability if the orbital frame does not coincide with the geomagnetic equatorial plane and does not contain the magnetic poles.

2.5 Nonlinear Attitude Controller

This section describes the design of a baseline control law that will be used for calculating the control moment. The authors in [19], [5], and [20] propose a nonlinear control law by

using what they call, as a *"continuous-sliding condition, for the attitude stabilization of small satellites actuated by magnetic torquers only"*. The control law is designed for the purpose of aligning the body reference frame with the orbital frame. In this thesis, we have reformulated the equations so that the control objective is to track a reference trajectory by employing the following definitions.

An auxiliary vector variable is defined by the authors in [19], [5], and [20] as follows

$$S = J\omega_b^r + \Lambda_q \mathbf{q_e} \tag{2.34}$$

with $\Lambda_q = diag([L_1, L_2, L_3])$ and $L_i > 0$, $\forall i = 1,2,3$. The vector ω_b^r corresponds to the angular rate of the body axis with respect to the reference frame. Note that if the reference rate is constant this vector is equal to the angular rate of the body with respect to the inertial frame ω_b^i. Additionally, vector $\mathbf{q_e}$ is composed of the first three elements of the quaternion error, which is defined in [3] as follows

$$\begin{aligned} Q_b^r &= (Q_r^o)^{-1} \otimes Q_b^o \\ &= \begin{bmatrix} q_{4r} & q_{3r} & -q_{2r} & -q_{1r} \\ -q_{3r} & q_{4r} & q_{1r} & -q_{2r} \\ q_{2r} & -q_{1r} & q_{4r} & -q_{3r} \\ q_{1r} & q_{2r} & q_{3r} & q_{4r} \end{bmatrix} \begin{bmatrix} q_1 \\ q_2 \\ q_3 \\ q_4 \end{bmatrix} \end{aligned}$$

The operation $\otimes$ is referred to as the quaternion product, and q_{ir} and q_i, for $i = \{1, 2, 3, 4\}$ are the reference and the actual quaternion values, respectively.

For design purposes, the authors in [19], [5], and [20] assumed that the control torque

can be produced independently, in the directions of the x, y and z axes. The results of the application of this control law shows that the response of the system by using magnetic torquers is satisfactory. It will be shown in the next chapter that this control law is also effective for the recovery from faults in the actuators.

The angular velocity of the body with respect to the reference frame ω_b^r that is used in equation (2.34) can be expressed by [3]

$$\omega_b^r = \omega_b^i - C_b^r \omega_r^i \tag{2.35}$$

where ω_r^i is the angular rate of the reference frame with respect to the inertial frame. The satellite's motion in terms of the auxiliary variable (2.34) can be formulated using equation (2.35) as

$$\dot{S} = J\dot{\omega}_b^i - J\dot{C}_b^r \omega_r^i - JC_b^r \dot{\omega}_r^i + \Lambda_q \dot{\mathbf{q}}_\mathbf{e} \tag{2.36}$$

Disregarding the effects of the gravity gradient disturbance, the following expression can be derived from (2.36)

$$\dot{S} = -\omega_b^i \times J\omega_b^i - J(C_b^r \Omega_b^r)\omega_r^i - JC_b^r \dot{\omega}_r^i + \frac{1}{2} J\Lambda_q(\omega_b^r q_{e4} - \omega_b^r \times \mathbf{q}_\mathbf{e}) + T_c \tag{2.37}$$

where T_a corresponds to the applied control torque, and Ω_b^r is the skew-symmetric matrix constructed with the angular rate vector ω_b^r. Let the desirable torque be defined as

$$T_{des} = T_{eq} - \lambda S \tag{2.38}$$

where λ is a positive constant number and the equivalent torque T_{eq}, is defined as

$$T_{eq} = T_c - \dot{S} \tag{2.39}$$

$$= \omega_b^i \times J\omega_b^i + J(C_b^r \Omega_b^r)\omega_r^i + JC_b^r \dot{\omega}_r^i - \frac{1}{2} J\Lambda_q(\omega_b^r q_{e4} - \omega_b^r \times \mathbf{q}_\mathbf{e}) \tag{2.40}$$

The desired control action is resolved into two components: perpendicular and parallel to the auxiliary variable vector S. The parallel component T_{prl} is responsible for diminishing the distance of the states to the manifold defined in S, whereas the perpendicular component T_{prp} only acts to make the trajectory move on a sphere surface. Taking this into account, the parallel component of the torque in (2.38) is calculated by using the following expression

$$T_{prl} = \frac{(T_{des} \cdot S)}{\| S \|^2} S \tag{2.41}$$

The total magnetic moment to be commanded to the magnetic torquers is calculated from the following equation

$$M_c = \frac{B_b \times T_{prl}}{\| B_b \|^2} \tag{2.42}$$

and the applied control torque for a system without failure is given by

$$T_a = M_c \times B_b \tag{2.43}$$

2.6 Stability Analysis

The nature of the attitude equations of a magnetically actuated spacecraft is nonlinear and time varying. The latter is due to the variations of the geomagnetic field along a given orbit. Attitude controllability of the dynamics of a spacecraft that is actuated by magnetic torquers is discussed in detail by the authors in [53]. The authors in [53] demonstrate that the time variation of a constant dipole approximation of the geomagnetic field along a closed Keplerian orbit guarantees the strong accessibility and controllability of the attitude

dynamics. This, in the case where the orbital plane does not coincide with the geomagnetic equatorial plane and does not contain the magnetic poles.

As mentioned earlier, the system is modeled by the equations that are listed below.

$$
\begin{aligned}
J\dot{\omega}_b^i &= -\omega_b^i \times J\omega_b^i + T_c \\
\omega_b^i &= \omega_b^r - C_b^r \omega_r^i \\
\dot{\mathbf{q}}_e &= \frac{1}{2}(q_{e4}\omega_b^r - \omega_b^r \times \mathbf{q}_e) \\
\dot{q}_{e4} &= -\frac{1}{2}(\omega_b^r)^T \mathbf{q}_e \\
S &= J\omega_b^r + \Lambda_q \mathbf{q}_e \\
T_c &= \frac{(T_{eq} - \lambda)^T S}{\|S\|^2} S \\
T_{eq} &= -\dot{S} + T_c
\end{aligned}
\tag{2.44}
$$

It can be shown, following the proof that is presented by [5], that the Lyapunov function candidate in (2.45) is positive definite for all values of S if the torque T_c is the torque that is applied to the system ($T_c = T_a$ in equation (2.39)).

$$
V = \frac{1}{2} S^T S \tag{2.45}
$$

The derivative of V along the trajectories of the system described by (2.44) is

$$
\begin{aligned}
\dot{V} &= S^T \dot{S} \\
&= S^T (T_c - T_{eq}) \\
&= -\lambda \|S\|^2
\end{aligned}
\tag{2.46}
$$

which is negative definite for all values of S. This proves that the equilibrium $[\omega_b^r, \mathbf{q}_e, q_4] = [\mathbf{0}, \mathbf{0}, 1]$

is asymptotically stable [56].

However, our closed-loop system does not have the control input T_c, but instead the result of the cross product between the magnetic moment as calculated in equation (2.42) and the magnetic field B, as indicated in equation (2.43). This means that the the closed-loop equations are to be modified and the above mentioned Lyapunov function will not be useful to demonstrate asymptotic stability of the closed-loop system that is actuated by magnetic torquers.

It should be pointed out that the purpose of this thesis is not that of designing a control law for the attitude control of a satellite. It is beyond the scope of this work to present a formal proof of stability of the closed-loop system, however, we will leave indicated the closed-loop equations for future reference of the problem.

The actual control input is represented by the following equation

$$\begin{aligned} T_a &= \frac{M_c \times B}{\|B\|^2} \\ &= \frac{T_{eq}^T S}{\|B\|^2 \|S\|^2}(B \times S) \times B - \frac{\lambda}{\|B\|^2}(B \times S) \times B \end{aligned} \tag{2.47}$$

and the closed-loop equation can be expressed in terms of the variable S as follows

$$\begin{aligned} \dot{S} &= T_a - T_{eq} \\ &= \frac{T_{eq}^T S}{\|B\|^2 \|S\|^2}(B \times S) \times B - \frac{\lambda}{\|B\|^2}(B \times S) \times B - T_{eq} \end{aligned} \tag{2.48}$$

If the value of T_{eq} were sufficiently small, the derivative of the Lyapunov function

would be negative semidefinite such that

$$\begin{aligned}\dot{V} &= S^T \dot{S} \\ &= -\frac{\lambda}{\|B\|^2} S^T [(B \times S) \times B] \end{aligned} \tag{2.49}$$

by knowing that

$$S^T [(B \times S) \times B] = \|B \times S\|^2$$

The requirements for this condition to hold ($T_{eq} \equiv 0$) are not studied in the present work. However, the results of the stable system as described by equation (2.44) are presented in Section 4.2, where suitable gains λ and Λ_q are found to make the response bounded.

2.7 Chapter Summary

In this chapter fundamental concepts are introduced in modeling of the attitude control subsystem of a LEO satellite using magnetic torquers as actuators. Furthermore, the description of the coordinate systems, attitude dynamics and kinematics equations, as well as the environmental disturbances affecting the system are also presented.

The model of the magnetic actuators, the geomagnetic field and design of a nonlinear control law to meet the goal of tracking a given reference trajectory have been introduced, as well as a discussion on the stability of the closed-loop system without fault.

The next chapter will explain the fault recovery mechanism that is proposed in this thesis. It will contain the model of each type of fault to which the actuators are prone to. It will include problem formulation as well as analytical solutions to the problem of reallocating the control effort when one actuator is subject to a failure. The stability analysis of the recovery solution is also presented.

Chapter 3

Satellite Fault Recovery using Magnetic Torquers

This chapter presents the derivations that are employed to develop the recovery solution to actuator faults. The first section of the chapter will describe the general representation of the types of faults that might affect the actuators. The second section will introduce the model of each type of fault, parameterized for the specific use of magnetic torquers. Following the detection, classification and identification of faults, the proposed fault recovery mechanism and analytical solutions to the reallocation problem as well as a discussion on the stability of the closed-loop system under recovery will be presented.

3.1 Types of Faults

Dynamic control systems may be subject to faults in the actuators, sensors or abrupt changes in their physical structure. This work is focused on the study of failures in actuators. In this

section we present the parameterization of faults that is adapted from [26], which covers several different cases due to control effector faults.

First, it is assumed that three actuators are aligned to the body frame axes, thus having a direct effect in the generation of an output in three orthogonal directions, namely

$$K(t) = diag[k_1, k_2, k_3]$$

The above matrix represents in the model the gain values that characterize the efficiency of each of the actuators present in the system. According to the type of a fault, the total output from the actuators $u_a(t)$ can be classified into

$$u_a(t) = \begin{cases} K(t)u_c(t) & k_i(t) = 1, \forall t \leq t_0, i = 1,2,3 & \textit{No failure} \\ K(t)u_c(t) & 0 < \varepsilon < k_{i_f}(t) < 1, \forall t \leq t_f & \textit{LOE} \text{ (Loss of effectiveness)} \\ K(t)u_c(t) & k_i(t) = 0, \forall t \leq t_f & \textit{Float} \\ K(t)u_c + \bar{u}_{ci}(t_f) & k_i(t) = 0, \forall t \leq t_f & \textit{LIP} \text{ (Lock-in-place)} \\ K(t)u_c + \bar{u}_{ci}(t_f) & k_i(t) = 0, \forall t \leq t_f; \bar{u}_{ci}(t_f) = u_{min} \text{ or } u_{Max} & \textit{HO} \text{ (Hard over)} \end{cases} \tag{3.1}$$

where $u_a(t) = [u_{a1}(t), u_{a2}(t), u_{a3}(t)]^T$ corresponds to the actual output produced by the actuators; $u_c(t) = [u_{c1}(t), u_{c2}(t), u_{c3}(t)]^T$ is the control input commanded by the controller and $\bar{u}_{ci}(t_f)$ is a constant fault value. In case of LIP fault, $\bar{u}_{ci}(t_f)$ is a value within the range of operation of the i_{th} actuator frozen at the time of failure (t_f), whereas for the case of HO fault, $\bar{u}_{ci}(t_f)$ is either the positive (u_{max}) or negative (u_{min}) saturation value that characterizes the failing actuator.

The above mentioned representation and classification of faults will be employed to parameterize the effects of failures in the magnetic torquers. In such case, the actual output of the magnetic torquers will be presented in terms of the torque produced by the interaction of the magnetic moment with the geomagnetic field. The total torque produced will be noted by T_a and the magnetic-moment control input will be M_x, M_y and M_z for each one of the actuators.

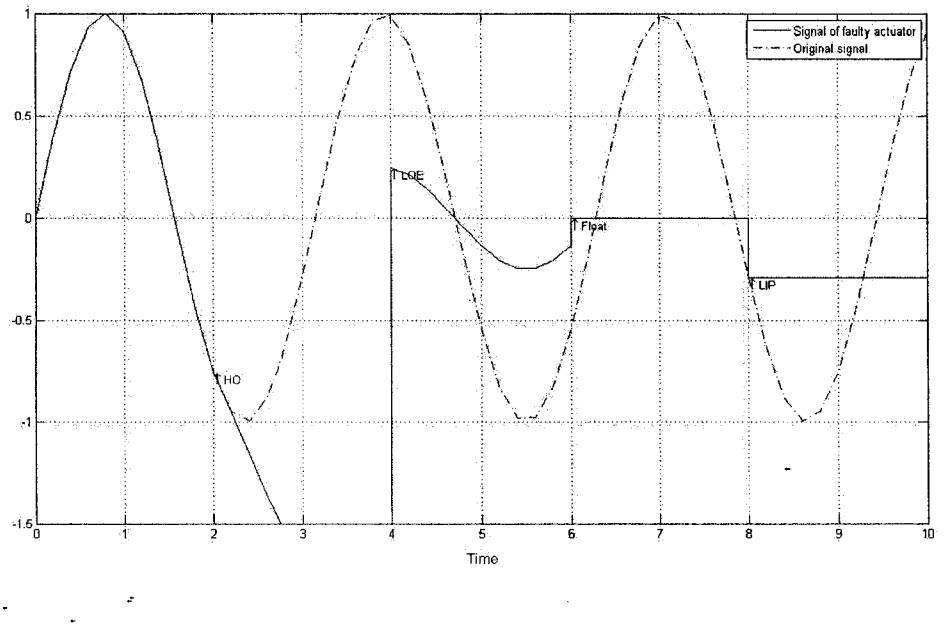

Figure 3.1: Illustration of faults in a typical control signal.

Figure3.1 shows an example of the effects of different faults on a typical control signal. At time 2 the signal is subject to an HO failure where the magnitude decreases linearly until it reaches the negative level of saturation. An HO failure may also bring the signal to the positive saturation level. The model presented for the HO fault in equation (3.1) does not make explicit the rate of change with which the output from the failing

actuator reaches the saturation. The model assumes that the saturation value is reached instantaneously. At time 4, the failure that is represented is a 75% LOE. A float type of failure is present at time 6, where the value of the signal is equal to zero and finally, an LIP failure is shown at time 8, where the signal locks in a nonzero value.

3.2 Definitions and Models of Faults in Magnetic Torquers

In Section 2.4.1 it was discussed that the total torque (T_a) produced by the actuators in the healthy condition is given by

$$T_a = \begin{pmatrix} B_z M_y - B_y M_z \\ -B_z M_x + B_x M_z \\ B_y M_x - B_x M_y \end{pmatrix} \tag{3.2}$$

where B_x, B_y, B_z are the components of the geomagnetic field in the satellite's body frame, and M_x, M_y, M_z are the magnetic moments produced by each actuator.

Following the classification that is described in (3.1), each fault in the magnetic torquers (for instance, in the torquer aligned with the X axis) can be represented as described below. The representation of faults in the actuators aligned with the Y and Z axes can be stated similarly.

- Float in the X-torquer: The magnetic moment $M_x = 0$, and

$$T_a = \left[\begin{pmatrix} 0 & 0 & 0 \\ 0 & 1 & 0 \\ 0 & 0 & 1 \end{pmatrix} \begin{pmatrix} M_x \\ M_y \\ M_z \end{pmatrix} \right] \times \begin{pmatrix} B_x \\ B_y \\ B_z \end{pmatrix}$$
$$= \begin{pmatrix} B_z M_y - B_y M_z \\ -B_x M_z \\ -B_x M_y \end{pmatrix} \tag{3.3}$$

- Loss of Effectiveness (LOE) in the X-torquer: The control magnetic moment M_x gets multiplied by a gain $0 < k < 1$, and

$$T_a = \left[\begin{pmatrix} k & 0 & 0 \\ 0 & 1 & 0 \\ 0 & 0 & 1 \end{pmatrix} \begin{pmatrix} M_x \\ M_y \\ M_z \end{pmatrix} \right] \times \begin{pmatrix} B_x \\ B_y \\ B_z \end{pmatrix}$$
$$= \begin{pmatrix} B_z M_y - B_y M_z \\ -B_z(k_x M_x) + B_x M_z \\ B_y(k_x M_x) - B_x M_y \end{pmatrix} \tag{3.4}$$

- Lock-in-place (LIP) or Hard over (HO) in the X-torquer: The representation of the HO and the LIP faults has the same structure. The parameter $\overline{M}_x$ could take the

values of M_{LIP} or M_{sat}, respectively, and

$$T_a = \left[\begin{pmatrix} 0 & 0 & 0 \\ 0 & 1 & 0 \\ 0 & 0 & 1 \end{pmatrix} \begin{pmatrix} M_x \\ M_y \\ M_z \end{pmatrix} + \begin{pmatrix} \overline{M}_x \\ 0 \\ 0 \end{pmatrix} \right] \times \begin{pmatrix} B_x \\ B_y \\ B_z \end{pmatrix}$$

$$= \begin{pmatrix} B_z M_y - B_y M_z \\ -B_z \overline{M}_x(t_f) + B_x M_z \\ B_y \overline{M}_x(t_f) - B_x M_y \end{pmatrix} \tag{3.5}$$

3.3 Recovery From Actuator Faults

The recovery mechanism proposed below corresponds to the reallocation of the control effort among the "capable" actuators, such that the torque action generated is as close as possible to the required control torque. Once the control law calculates the required torque T_c, if the actuators are faulty then the recovery mechanism is responsible and is tasked to redistribute the required moment among the remaining healthy actuators.

For the scenarios studied (faults in the actuator that is aligned with the body's X axis without loss of generality), the reallocation solution should find values for M_x^*, M_y^* and M_z^* in the case of LOE fault, and values of M_y^* and M_z^*, in all the other faulty cases, as shown in the expressions below.

- In the case of a float fault in the X-torquer, the action torque should be such that

$$T_a = \begin{pmatrix} B_z M_y^* - B_y M_z^* \\ -B_x M_z^* \\ -B_x M_y^* \end{pmatrix} \tag{3.6}$$

- In the case of a Loss of Effectiveness fault in the X-torquer, the solution will produce the action torque

$$T_a = \begin{pmatrix} B_z M_y^* - B_y M_z^* \\ -B_z(k_x M_x^*) + B_x M_z^* \\ B_y(k_x M_x^*) - B_x M_y^* \end{pmatrix} \tag{3.7}$$

- In the case of a LIP or HO fault in the X-torquer, the solution found will produce the following action torque (note that the HO fault becomes a LIP fault in one of the saturation limits)

$$T_a = \begin{pmatrix} B_z M_y^* - B_y M_z^* \\ -B_z \overline{M}_x(t_f) + B_x M_z^* \\ B_y \overline{M}_x(t_f) - B_x M_y^* \end{pmatrix} \tag{3.8}$$

3.4 Implementation of a Fault Recovery System

Figure 3.2 depicts the modules that conform the fault recovery system developed. The descriptions of each component of the attitude control subystem with fault recovery for actuator faults are provided below.

- *Attitude Control*: This corresponds to a nonlinear controller designed to guarantee stability of the system without faults.

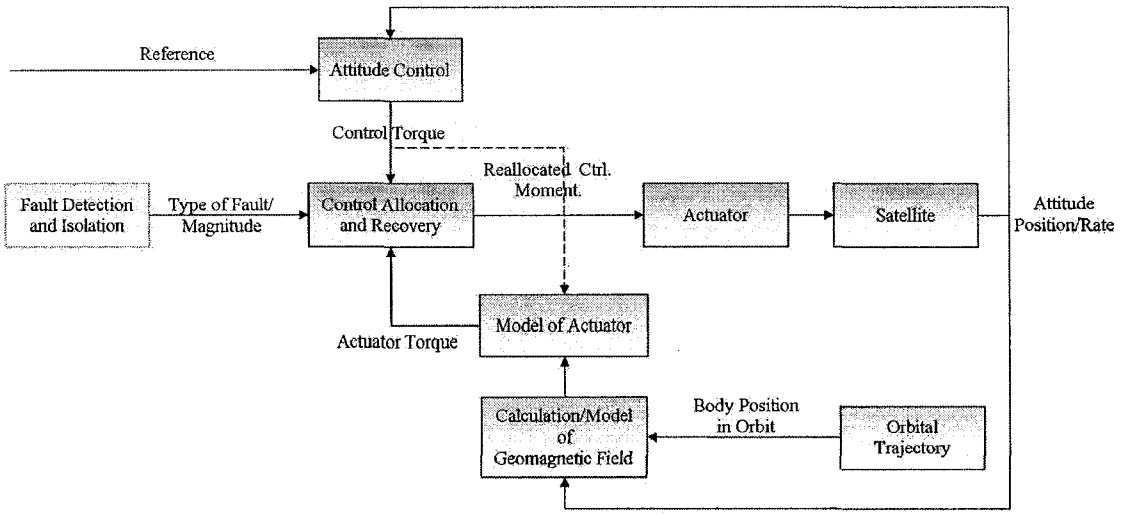

Figure 3.2: Attitude control subsystem augmented with a fault recovery for faults in the magnetic torquers.

- *Fault Detection and Isolation (FDI)*: Is in charge of generating fault alarms and information about the type and magnitude of the fault(s).

- *Control Allocation and Recovery*: Receives information from the FDI unit as well as current (measured or estimated) values of the states and attitude control. It generates the new distribution of the control effort among the magnetic torquers when the FDI system reports a fault. If no fault alarm is received, it calculates the required magnetic moment, using the cross product operation in (2.31).

- *Model of Actuators*: This block contains the model of three orthogonal magnetic torquers aligned with the body's coordinate frame. Each model of the magnetic torquer includes a model of all the possible faults. The model of faults receives information from the FDI unit and generates a signal that represents the estimated performance of each magnetic

torquer according to its current status.

- *Model of Geomagnetic Field*: This block represents the model of the geomagnetic field, calculated in the coordinates frame of the body as a function of the position of the satellite in a circular orbit.

- *Orbital Trajectory*: Contains the model of a LEO trajectory. Determines the position of the satellite with respect to the Earth-centered inertial frame in time.

- *Actuator*: Represents the set of orthogonal actuators in charge of producing magnetic moments and magnetic torques when interacting with the geomagnetic field.

- *Satellite*: Model of dynamics and kinematics equations of motion of a satellite including the effects of environmental disturbances.

It is well-known that the FDI module might provide delayed information and perhaps some level of uncertainty regarding the fault detection time. As a consequence, the system might be out of bounds at the time the FDI module generates the corresponding fault alarm and when the recovery action is initiated. Additionally, it is understood that the measurement of the magnetic field might also carry inaccuracies and delays. As shown in Chapter 4, the effects of the delays and measurement noise will be incorporated in the evaluation of the recovery system through numerical simulations. However, for the sake of simplicity in this chapter the following common assumptions are made:

- In the present work the fault identification is assumed to be accomplished instantly. Nevertheless, in the fourth chapter, it will be shown that for some finite delays, the proposed recovery mechanism still remains effective.

- It is assumed for simplicity that the values measured (or calculated) for the geomagnetic field at each time are accurate.

3.5 Control Reallocation Problem

The recovery strategy will demand the best possible magnetic moments that actuators may generate, by minimizing the error between the required torque and the torque that can be produced by the healthy magnetorquers. Towards this end, let us define the error function according to:

$$f_e(M^*) = (Tc_x - Ta_x)^2 + (Tc_y - Ta_y)^2 + (Tc_z - Ta_z)^2 \tag{3.9}$$

where T_c and T_a correspond to the desired control torque and the applicable torque, respectively. The applicable torque is defined for each type of fault from (3.6) - (3.8). The following theorems will be applied for analysis of the results that are obtained from our proposed optimization problem.

Theorem 3.1 *([57]) Let $f : \Omega \rightarrow \Re$, $f \in C^2$, be defined on an open convex set $\Omega \in \Re^n$. Then, f is convex on Ω if and only if for each $\mathbf{x} \in \Omega$, the Hessian $\mathbf{F}(\mathbf{x})$ of f at $\mathbf{x}$ is a positive semidefinite matrix.*

Theorem 3.2 *([57]) Let $f : \Omega \rightarrow \Re$ be a convex function defined on a convex set $\Omega \subset \Re^n$. Then, a point is a global minimizer of f over $\Omega \subset \Re^n$ if and only if it is a local minimizer of f.*

We can show that the cost function chosen for the reallocation problem is convex and the theorem below states this result.

Theorem 3.3 *The function $f_e(M^*)$ in* (3.9) *is convex for all the faults that are defined and for all the values of $M^* \subset \Re^3$.*

Proof: For the fault scenarios that are considered in the actuator that is aligned with the body axis X, let the variables T_{aj} with $j = \{x, y, z\}$ in (3.9) be substituted by the applicable torques from (3.6) to (3.8). The Hessian matrix corresponding to each case is computed as follows.

- **Float, HO and LIP Faults**:

  In these cases, the cost function is defined in terms of the variables M_y^* and M_z^*. Thus, the matrix F is given by

$$F(M_y^*, M_z^*) = \begin{bmatrix} 2B_z{}^2 + 2B_x{}^2 & -2B_zB_y \\ -2B_zB_y & 2B_y{}^2 + 2B_x{}^2 \end{bmatrix} \tag{3.10}$$

  The corresponding eigenvalues of the above matrix are given by

$$\lambda_1 = 2B_x^2$$

$$\lambda_2 = 2(B_x^2 + B_y^2 + B_z^2)$$

- **LOE Fault**:

  The error function (3.9) was formulated in terms of the variables M_x^*, M_y^* and M_z^* and the loss of effectiveness gain k. Therefore, the Hessian matrix is of size $3x3$ and is defined as

$$F(M_y^*, M_z^*) = \begin{bmatrix} 2k^2B_z^2 + 2k^2B_y^2 & -2B_xkB_y & -2B_xkB_z \\ -2B_xkB_y & 2B_z^2 + 2B_x^2 & -2B_yB_z \\ -2B_xkB_z & -2B_yB_z & 2B_x^2 + 2B_y^2 \end{bmatrix} \tag{3.11}$$

Furthermore, the eigenvalues of the Hessian matrix (3.11) are given by

$$\lambda_1 = 0$$

$$\lambda_2 = 2B_x^2 + 2B_z^2 + 2B_y^2$$

$$\lambda_3 = (2B_z^2 + 2B_y^2)k^2 + 2B_x^2$$

It can be seen from the eigenvalues of the Hessian matrices (3.10) and (3.11), that for all values of $M^x \in \Re^3$, the Hessian matrix of function f_e is positive semidefinite. Similar results are obtained if the analysis is carried for faults in the other two actuators. It can be concluded that the function f_e is convex for all types of faults and all values of M^*, by applying Theorem 3.1. ■

According to the results that are formulated in Theorems 3.2 and 3.3, it can also be concluded that the solutions found from the optimum reallocation of the control effort will yield a global solution to the problem considered.

The following section describes the formulation and the solution to the control reallocation problem.

3.6 Analytical Solutions to the Unconstrained Control Reallocation Problem

The problem of control reallocation was defined in the previous section in terms of an unconstrained optimization framework. Given that the cost function (3.9) is convex, the

following corollary can be employed to obtain the corresponding solutions.

Corollary 3.1 *([57]) Let $f : \Omega \rightarrow \Re$, $f \in C^1$, be a convex function defined on the convex set $\Omega \subset Re^n$. Suppose the point $\mathbf{x}^* \in \Omega$ is such that*

$$\nabla f(\mathbf{x}^*) = 0. \tag{3.12}$$

Then, $\mathbf{x}^*$ is a global minimizer of f over Ω.

Below the first order sufficient conditions under each type of fault are obtained by using the Corollary 3.1. Additionally, the solutions to the unconstrained reallocation problem are given for each fault case in the actuator that is aligned with the X body axis. The results for the faults occurring in the Y and Z magnetorquers are similar and therefore are not stated.

3.6.1 System Subject to Float Fault

The cost function for this operating condition is adapted from (3.9) and by using (3.6) we obtain

$$f_{Float}(M_y^*, M_z^*) = (T_{cx} - M_y^* B_z + M_z^* B_y)^2 + (T_{cy} - M_z^* B_x)^2 + (T_{cz} - M_y^* B_x)^2 \tag{3.13}$$

The corresponding gradient vector is given by

$$\nabla f_{Float} = \begin{bmatrix} -2B_z(T_{cx} - M_y^* B_z + M_z^* B_y) + 2B_x(T_{cz} + M_y^* B_x) \\ 2B_y(T_{cx} - M_y^* B_z + M_z^* B_y) - 2B_x(T_{cy} - M_z^* B_x) \end{bmatrix}^T \tag{3.14}$$

and by setting (3.14) equal to zero, and solving for M_y^* and M_z^*, the following solution is

obtained

$$M_y^* = \frac{(B_x B_z T_{cx} - T_{cz} B_x^2 - B_y^2 T_{cz} + B_y B_z T desy)}{B_x(B_z^2 + B_x^2 + B_y^2)}$$
$$M_z^* = \frac{(-B_z B_y T_{cz} + B_z^2 * T_{cy} + B_x^2 T_{cy} - B_x T_{cx} B_y)}{B_x(B_z^2 + B_x^2 + B_y^2)} \tag{3.15}$$

This corresponds to a unique solution for the reallocation of control effort when one actuator is subject to a Float fault.

3.6.2 System Subject to LOE Fault

Similar to the previous case, the error function from (3.9) is defined in this case by using (3.7), namely

$$f_{LE}(M_x^*, M_y^*, M_z^*) = (T_{cx} - M_y^* B_z + M_z^* B_y)^2 + (T_{cy} - M_z^* B_x + k M_x^* B_z)^2 + (T_{cz} + k M_x^* B_y - M_y^* B_x)^2 \tag{3.16}$$

The gradient vector is obtained according to

$$\nabla f_{LE} = \begin{bmatrix} 2B_z k(T_{cy} - M_z^* B_x + k M_x^* B_z) - 2B_y k(T_{cz} + k M_x^* B_y - M_y^* B_x) \\ -2B_z(T_{cx} - M_y^* B_z + M_z^* B_y) + 2B_x(T_{cz} + k M_x^* B_y - M_y^* B_x) \\ 2B_y(T_{cx} - M_y^* B_z + M_z^* B_y) - 2B_x(T_{cy} - M_z^* B_x) \end{bmatrix}^T \tag{3.17}$$

and by setting (3.17) equal to zero, and solving for M_x^*, M_y^* and M_z^* we get

$$M_x^* = M_x$$
$$M_y^* = \frac{(B_x B_z T_{cx} - T_{cz} B_x^2 - B_y^2 T_{cz} + B_y B_z T desy) + M_x^* k B_y (B_x^2 + B_y^2 + B_z^2)}{B_x(B_z^2 + B_x^2 + B_y^2)}$$
$$M_z^* = \frac{(-B_z B_y T_{cz} + B_z^2 * T_{cy} + B_x^2 T_{cy} - B_x T_{cx} B_y) + M_x^* k B_z (B_x^2 + B_y^2 + B_z^2)}{B_x(B_z^2 + B_x^2 + B_y^2)} \tag{3.18}$$

The above implies that any value for M_x could be chosen and substituted in the solution for M_y^* and M_z^*. There is no unique solution to the recovery problem. We have

determined to use M_{cx} which corresponds to the desired magnetic moment. This value is calculated by using (2.42).

3.6.3 System Subject to LIP or HO Fault

When an LIP or HO fault occurs, the magnetic moment produced by the failing actuator freezes. This happens at a value within the saturation limit for an LIP fault, and equal to the saturation moment for an HO fault. The representation for the error function derived from (3.9) and the unconstrained optimization solutions are basically the same, that is

$$f_{LIP}(M_y^*, M_z^*) = (T_{cx} - M_y^* B_z - M_z^* B_y)^2 + (T_{cy} - M_z^* B_x + \overline{M}_x B_z)^2 + (T_{cz} - \overline{M}_x B_y + M_y^* B_x)^2 \tag{3.19}$$

Therefore, the gradient vector is defined as

$$\nabla f_{LIP} = \begin{bmatrix} -2B_z(T_{cx} - M_y^* B_z + M_z^* B_y) + 2B_x(T_{cz} - \overline{M}_x B_y + M_y^* B_x) \\ 2B_y(T_{cx} - M_y^* B_z + M_z^* B_y) - 2B_x(T_{cy} - \overline{M}_x B_y + M_z^* B_x) \end{bmatrix}^T \tag{3.20}$$

and the solution for M_y^* and M_z^*, when (3.20) is set to zero is given by

$$\begin{aligned} M_y^* &= \frac{(B_y^3 \overline{M}_x + B_x^2 \overline{M}_x B_y - B_x^2 T_{cz} + B_y B_z^2 \overline{M}_x + B_x B_z T_{cx} + B_y B_z T_{cy} - B_y^2 T_{cz})}{B_x(B_x^2 + B_y^2 + B_z^2)} \\ M_z^* &= \frac{(B_z B_y^2 \overline{M}_x + B_z B_x^2 \overline{M}_x + B_z^3 \overline{M}_x + B_z^2 T_{cy} - B_z B y T_{cz} + B_x^2 T_{cy} - B_x T_{cx} B_y)}{B_x(B_x^2 + By^2 + B_z^2)} \end{aligned} \tag{3.21}$$

As stated in Theorem 3.3, due to the convexity of the cost function (3.9), the solution that is obtained for the reallocation of the control moment in case of each fault is global.

3.7 Analytical Solutions to the Constrained Control Reallocation Problem

The solution to the unconstrained control allocation problem in the event of a fault in any of the actuators requires a division by the value of the magnetic field in the axis of the fault as shown in equations (3.15), (3.18) and (3.21). It is also known that as the position of the satellite approaches the poles or the equator the behavior of the magnetic field changes so that the strength of the yaw (B_z) and pitch (B_y) components diminish, respectively. This implies that the solution to reallocate the control effort will generate very large torques, which may not be physically possible for a magnetic torquer. It should be noted that each actuator is capable of producing control only up to its saturation moment.

Consequently, a constrained formulation of the reallocation problem is necessary. The results are obtained for each type of fault as shown below. This constrained optimization problem is formulated as follows:

$$\text{Min} \qquad f_e = (T_{cx} - T_{ax})^2 + (T_{cy} - T_{ay})^2 + (T_{cz} - T_{az})^2$$

Subject to:

$$M_{sat,x,1} \leq M_x^* \leq M_{sat,x,2}$$

$$M_{sat,y,1} \leq M_y^* \leq M_{sat,y,2}$$

$$M_{sat,z,1} \leq M_z^* \leq M_{sat,z,2} \tag{3.22}$$

where $M_{sat,x,2}$, for example, is the upper saturation (positive) moment for the torquer aligned with the X body axis, and $M_{sat,x,1}$ is the lower saturation (negative) moment. It

is assumed, for simplicity and without loss of generality, that the upper and lower saturation moments are equal in magnitude. In addition, T_{cj} and T_{aj}, for $j = \{x, y, z\}$ are the desired and applicable controls, respectively.

The concepts applied to solve the constrained reallocation problem are first introduced below.

Definition 3.1 *([57]) An inequality constraint $g_j(x) \leq 0$ is said to be **active** at x^* if $g_j(x^*) = 0$. It is **inactive** at x^* if $g_j(x^*) < 0$.*

This amounts to defining $g_j = 0$ (an active constraint), when the hypothesis of the solution is that the corresponding actuator is saturated.

Definition 3.2 *([57]) Let x^* satisfy $g(x^*) \leq 0$, and let $J(x^*)$ be the index set of active inequality constraints, that is,*

$$J(x^*) \triangleq \{j : g_j(x^*) = 0\}.$$

*Then, we say that x^* is a **regular point** if the vectors*

$$\nabla g_j(x^*), 1 \leq j \leq m, j \in J(x^*)$$

are linearly independent.

Theorem 3.4 *([57]) Let $f : \Re^n \rightarrow \Re$, $f \in C^1$, be a convex function on the set of feasible points*

$$\Omega = \{\mathbf{x} \in \Re^n : \mathbf{g}(\mathbf{x}) \leq \mathbf{0}\},$$

where $g : \Re^n \to \Re^p$, $g \in C^1$, *and* Ω *is convex. Suppose there exist* $\mathbf{x}^* \in \Omega$, $\mu^* \in \Re^p$, *such that*

1. $\mu^* \geq 0$
2. $Df(\mathbf{x}^*) + \mu^{*\mathbf{T}} D\mathbf{g}(\mathbf{x}^*) = \mathbf{0}^T$; *and*
3. $\mu^{*\mathbf{T}}\mathbf{g}(\mathbf{x}^*) = 0$.

Then, $\mathbf{x}^*$ *is a global minimizer of* f *over* Ω.

Let us now define the following matrix

$$\mathbf{L}(\mathbf{x}, \mu) = \mathbf{F}(\mathbf{x}) + [\mu \mathbf{G}(\mathbf{x})], \tag{3.23}$$

where $\mathbf{F}(\mathbf{x})$ is the Hessian matrix of f at x, and the notation $[\mu G(x)]$ represents

$$[\mu \mathbf{G}(\mathbf{x})] = \mu_1 \mathbf{G_1}(\mathbf{x}) + \cdots + \mu \mathbf{G_p}(\mathbf{x}),$$

where $\mathbf{G_i}(\mathbf{x})$ is the Hessian of the constraint $g_i(x)$ at $\mathbf{x}$ that is given by

$$\mathbf{G_i}(\mathbf{x}) = \begin{bmatrix} \frac{\partial^2 g_1}{\partial x_1 \partial x_1} & \cdots & \frac{\partial^2 g_1}{\partial x_1 \partial x_m} \\ \frac{\partial^2 g_2}{\partial x_2 \partial x_1} & \cdots & \frac{\partial^2 g_2}{\partial x_2 \partial x_m} \\ \cdots & \cdots & \cdots \\ \frac{\partial^2 g_p}{\partial x_n \partial x_1} & \cdots & \frac{\partial^2 g_p}{\partial x_n \partial x_m} \end{bmatrix}$$

Define also the set

$$\tilde{T}(x^*, \mu^*) = \{y : Dg_j(x^*)y = 0, j \in \tilde{J}(x^*, \mu^*)\}, \tag{3.24}$$

where $\tilde{J}(x^*, \mu^*) = \{j : g_j = 0, \mu^* > 0\}$.

The second order sufficient conditions are stated in the next theorem to identify the solutions to the optimization problem.

Theorem 3.5 ***Second-order Sufficient Conditions.*** *([57])*

Suppose $f, g \in C^2$ *and there exist a feasible point* $x^* \in \Re^n$ *and vector* $\mu^* \in \Re^p$ *such that:*

1. $\mu^* \geq 0$, $Df(\mathbf{x}^*) + \mu^{*T} Dg(x^*) = \mathbf{0}^T$, $\mu^{*\mathbf{T}}\mathbf{g}(\mathbf{x}^*) = 0$; *and*

2. *For all* $y \in \tilde{\mathbf{T}}(\mathbf{x}^*, \mu^*)$, $y \neq 0$, *we have* $y^T \mathbf{L}(\mathbf{x}^*, \mu^*) y > 0$.

Then, $\mathbf{x}^*$ *is a strict local minimizer of* f *subject to* $\mathbf{g}(\mathbf{x}) \leq 0$.

For the problem under study, the inequality constraints g_i, for $i = 1, 2, \cdots, 6$, are defined as follows.

$$\begin{aligned} g_1 &= |M_{sat,x}| - M_x^* \quad ; \quad & g_2 &= -|M_{sat,x}| - M_x^* \\ g_3 &= |M_{sat,y}| - M_y^* \quad ; \quad & g_4 &= -|M_{sat,y}| - M_y^* \\ g_5 &= |M_{sat,z}| - M_z^* \quad ; \quad & g_6 &= -|M_{sat,z}| - M_z^* \end{aligned} \tag{3.25}$$

where $|M_{sat,j}|$, $j = \{x, y, z\}$ is the magnitude of the saturation moment for the actuator along the corresponding body axis. For simplicity, it is assumed that this value is equal for all the magnetic torquers (e.g. $M_{sat,i,1} = -M_{sat,i,2}$,for $i = x, y, z$ in equation (3.22)) and it is referred to as M_{sat}.

For each type of fault, the second order sufficient conditions in Theorem 3.5 are applied in order to find a solution to the problem in (3.22).

3.7.1 System Subject to a Float Fault

In presence of a float fault (in the actuator that is aligned with the body axis X), the gradient vector is obtained in terms of the variable moments M_y^* and M_z^*. The corresponding performance index for this case was given in (3.13) and its gradient in (3.14). The first order necessary conditions for this faulty operating mode are governed by

$$-2(T_{cx}+M_zB_y-M_y^*B_z)B_z+2(T_{cz}+M_y^*B_x)B_x+\mu_3^*-\mu_4^*=0 \quad (3.26)$$

$$2(T_{cx}+M_z^*B_y-M_y^*B_z)B_y-2(T_{cy}-M_z^*B_x)B_x+\mu_5^*-\mu_6^*=0 \quad (3.27)$$

$$\mu_3^*(M_y^*-M_{sat})+\mu_4^*(-M_y^*-M_{sat})+\mu_5^*(M_z^*-M_{sat})+\mu_6^*(-M_z^*-M_{sat})=0 \quad (3.28)$$

$$\mu_i^*\geq 0,\ \forall\ i=3,4,5,6 \quad (3.29)$$

The function $L(M^*,\mu^*)$ defined in (3.23) is equal to the Hessian matrix H of f_{Float} given in (3.13), since G_i, $i=\{1,2,\cdots,6\}$ is identically zero. The Hessian matrix is given by

$$H(f_{Float}(M^*))=\begin{bmatrix} 2{B_z}^2+2{B_x}^2 & -2B_zB_y \\ -2B_zB_y & 2{B_y}^2+2{B_x}^2 \end{bmatrix} \quad (3.30)$$

The set of constraints, from (3.25), is reduced to g_3,g_4,g_5 and g_6, since the value of $M_x=0$ lies within the saturation values ($g1$ and g_2 are always inactive constraints).

The solution to the constrained problem should be obtained by evaluating different combinations of assumed active and inactive constraints. For the present problem, it is only possible to leave one constraint active at a time, so that the number of equations is equal to the number of variables to solve for, namely, M_y,M_z and μ_i^* such that $g_i(M^*)=0$ (for the active constraint).

- **All constraints are inactive**

  The solution for M^* is the same as that in the unconstrained case as given by (3.15). This solution will be valid only if the values for M^* are smaller than the saturation moment M_{sat}.

- **Constraint g_3 or g_4 is active**

  With this hypothesis, it is assumed that M_y^* is equal to $-|M_{sat}|$ or $|M_{sat}|$, the negative or the positive saturation values, respectively. The solution is presented in the following form

$$M^* = \left\{ \begin{bmatrix} 0 & 0 & 0 \\ 0 & 0 & 0 \\ -B_y & B_x & 0 \end{bmatrix} \begin{bmatrix} T_{cx} \\ T_{cy} \\ T_{cz} \end{bmatrix} + M_{sat} \begin{bmatrix} 0 \\ (B_x^2 + B_y^2) \\ B_y B_z \end{bmatrix} \right\} / (B_x^2 + B_y^2) \tag{3.31}$$

  From the first order conditions, the values of μ_3 and μ_4, namely the multipliers corresponding to the active constraint for the candidate solution are also found. By assuming saturation of the Y magnetorquer, μ_3 is obtained to be

$$\mu_3^* = \frac{-2B_x(M_{sat}B_x^3 + M_{sat}B_xB_z^2 + M_{sat}B_xB_y^2 - B_xB_zT_{cx} + T_{cz}Bx^2 + B_y^2T_{cz} - B_yB_zT_{cy})}{B_y^2 + B_x^2} \tag{3.32}$$

  It follows that determining analytically the sign of μ_3^* and identifying the feasibility of the hypothetical solution according to the condition (3.29) is not trivial due to the time varying nature of the magnetic field vector $\overrightarrow{B}$. For implementation purposes, this hypothetical solution should be verified by evaluating the multipliers at each time.

Let us assume that this value is positive ($\mu_3^* > 0$), which corresponds to a possible solution to the optimization problem. Hence, the second order condition from Theorem 3.5 should also be satisfied. Toward this end, first, the set $\tilde{T}$ is defined

$$\begin{aligned}\tilde{T} &= \{y : Dg_3 y = 0\} = \{y : [1,0]y = 0\} \\ &= \{[0,\alpha]^T, \forall \alpha \in \Re\}\end{aligned} \tag{3.33}$$

We now have

$$y^T L(f_{Float})Y = 2\alpha^2(B_x + B_y)^2. \tag{3.34}$$

This implies that the matrix $L(f_{Float})$ is positive definite for all $y \in \tilde{T}$ and that if the solution (assuming that the actuator in the Y axis is saturated in the positive value) is feasible ($\mu_3^* > 0$), it will be a strict local minimum. Furthermore, according to Theorem 3.4, this will be a global minimizer of problem (3.22).

Similarly, the solution by saturating the actuator in the Y axis corresponding to the negative saturation moment is obtained as shown below

$$\mu_4^* = \frac{-2B_x(M_{sat}B_x^3 + M_{sat}B_xB_z^2 + M_{sat}B_xB_y^2 + B_xB_zT_{cx} - T_{cz}B_x^2 - B_y^2Tcz + B_yB_zT_{cy})}{B_y^2 + B_x^2} \tag{3.35}$$

$$\tilde{T} = \{y : [-1,0]y = 0\} = \{[0,\alpha]^T, \forall \alpha \in \Re\}$$

which is the same vector that is used to obtain (3.34).

- **Constraint g_5 or g_6 is active**

This implies that M_z^* is made equal to $-|M_{sat}|$ or $|M_{sat}|$, that is

$$M^* = \left\{ \begin{bmatrix} 0 & 0 & 0 \\ B_z & 0 & -B_x \\ 0 & 0 & 0 \end{bmatrix} \begin{bmatrix} T_{cx} \\ T_{cy} \\ T_{cz} \end{bmatrix} + M_{sat} \begin{bmatrix} 0 \\ B_y B_z \\ (B_x^2 + B_z^2) \end{bmatrix} \right\} / (B_x^2 + B_z^2) \tag{3.36}$$

The values for μ_5 and μ_6 are given by

$$\mu_5^* = \frac{-2B_x(M_{sat}B_x^3 + M_{sat}B_xB_z^2 + M_{sat}B_xB_y^2 + B_zB_yT_{cz} - B_z^2T_{cy} - B_x^2T_{cy} + B_xT_{cx}B_y)}{B_z^2 + B_x^2}$$

$$\mu_6^* = \frac{-2B_x(M_{sat}B_x^3 + M_{sat}B_xB_z^2 + M_{sat}B_xB_y^2 - B_zB_yT_{cz} + B_z^2T_{cy} + B_x^2T_{cy} - B_xT_{cx}B_y)}{B_z^2 + B_x^2}$$

As mentioned earlier, it is assumed that for some values of B_x, B_y and B_z, we have $\mu_5 > 0$ or $\mu_6 > 0$. For these to be feasible solutions to the constrained optimization problem, the second order sufficient condition should be satisfied for all $y \in \tilde{T} = \{y : Dg_j = 0, j \in \tilde{J}\}$, namely

$$\begin{aligned} \tilde{T} &= \{y : Dg_5 y = 0\} & \tilde{T} &= \{y : Dg_6 y = 0\} \\ &= \{y : [0,1]y = 0\} & &= \{y : [0,-1]y = 0\} \\ &= \{[\alpha, 0]^T\} & &= \{[\alpha, 0]^T\} \end{aligned}$$

It can be verified that in these two cases, $y^T L(f_{Float})y > 0$ is satisfied. Therefore, both solutions, if feasible, are global minimizers, as discussed in the previous case.

3.7.2 System Subject to an LIP Fault

In presence of an LIP fault, moments M_y^* and M_z^* and the multipliers μ_3^*, μ_4^*, μ_5^*, μ_6^* should be found from the system of equations provided below

$$-2(T_{cx}+M_z^*B_y-M_y^*B_z)B_z+2(T_{cz}+M_y^*B_x-\overline{M}_xB_y)B_x+\mu_3^*-\mu_4^*=0 \quad (3.37)$$

$$2(T_{cx}+M_z^*B_y-M_y^*B_z)B_y-2(T_{cy}-M_z^*B_x+\overline{M}_xB_z)B_x+\mu_5^*-\mu_6^*=0 \quad (3.38)$$

$$\mu_3^*(M_y^*-M_{sat})+\mu_4^*(-M_y^*-M_{sat})+\mu_5^*(M_z^*-M_{sat})+\mu_6^*(M_z^*-M_{sat})=0 \quad (3.39)$$

$$\mu_i^*\geq 0 \forall i\in J=\{i:g_i(M^*)=0\} \quad (3.40)$$

The Hessian matrix $L(M^*,\mu^*)=H(f_{LIP})$, since for all $i=1,2,\cdots,6$, $G_i(M^*)=0$. This matrix is equal to the matrix defined in (3.30) corresponding to the float fault.

The solutions, under the hypothesis of μ_i^*, where only one constraint is active at a time are presented below.

- **All constraints are inactive**

  The result for M^* is the same as in the unconstrained case as presented in (3.21). As mentioned earlier, this will be a feasible solution only if the result satisfies all of the constraints $g(M^*)$.

- **Constraint g_3 or g_4 is active**

  The hypothesis implies that M_y^* is equal to $-|M_{sat}|$ or $|M_{sat}|$, the negative or positive

saturation moments, respectively. The following minimum candidate was obtained

$$M^* = \left\{ \begin{bmatrix} 0 & 0 & 0 \\ 0 & 0 & 0 \\ -B_y & B_x & 0 \end{bmatrix} \begin{bmatrix} T_{cx} \\ T_{cy} \\ T_{cz} \end{bmatrix} + \begin{bmatrix} \overline{M}_x(B_x^2+B_y^2) \\ M_{sat}(B_x^2+B_y^2) \\ B_z(M_{sat}B_y+\overline{M}_xB_x) \end{bmatrix} \right\} /(B_x^2+B_y^2) \quad (3.41)$$

From the set of equations (3.40), the result for the multipliers μ_3^* (for saturation in the positive value of M_{sat}) and μ_4^* (for saturation in the negative value of M_{sat}) are obtained as

$$\mu_3^* = \{ -2B_x(M_{sat}B_x^3 + M_{sat}B_xB_z^2 + M_{sat}B_xB_y^2 - B_yB_x^2\overline{M}_x$$
$$- B_y^3\overline{M}_x - B_yB_z^2\overline{M}_x - B_yB_zT_{cy} + B_y^2T_{cz} + T_{cz}B_x^2 - B_xB_zT_{cx})\}/(B_y^2+B_x^2),$$

and

$$\mu_4^* = \{ -2B_x(M_{sat}B_x^3 + M_{sat}B_xB_z^2 + M_{sat}B_xB_y^2 + B_yB_x^2\overline{M}_x$$
$$+ B_y^3\overline{M}_x + B_yB_z^2\overline{M}_x + B_yB_zT_{cy} - B_y^2T_{cz} - T_{cz}B_x^2 + B_xB_zT_{cx})\}/(B_y^2+B_x^2).$$

It can be verified that if either g_3 or g_4 is considered active and $\mu_3^* > 0$ or $\mu_4^* > 0$, the second order sufficient conditions are satisfied. This can be achieved by finding the set $\tilde{T}$ for each case of active constraints and by determining if $y^T L(f_{LIP})y > 0$, which was already obtained in the analysis of the float fault.

In the case of an LIP fault, the Hessian matrix, as defined by (3.30), is positive definite for all $y \in \tilde{T}$ and all values of $\alpha \in \Re$, such that,

$$y = [\alpha, 0]^T$$

Therefore, for the values of B_x, B_y, B_z such that $\mu_3^* > 0$ or $\mu_4^* > 0$ (in the case of an LIP fault), the solution with saturation of the actuator in the Y axis, is a strict global minimum.

- **Constraint g_4 or g_5 is active**

This corresponds to assigning $M_z^* = -|M_{sat}|$ or $M_z^* = |M_{sat}|$. The solution for M^* will be now

$$M^* = \left\{ \begin{bmatrix} 0 & 0 & 0 \\ B_z & 0 & -B_x \\ 0 & 0 & 0 \end{bmatrix} \begin{bmatrix} T_{cx} \\ T_{cy} \\ T_{cz} \end{bmatrix} + \begin{bmatrix} \overline{M}_x(B_x^2 + B_z^2) \\ B_z(M_{sat}B_y + \overline{M}_x B_x) \\ M_{sat}(B_x^2 + B_z^2) \end{bmatrix} \right\} / (B_x^2 + B_z^2) \quad (3.42)$$

The multipliers will have the following values for each case ($g_4 = 0$ or $g_5 = 0$, respectively), that is

$$\mu_5^* = \{ -2B_x(M_{sat}B_x^3 + M_{sat}B_xB_z^2 + M_{sat}B_xB_y^2 + B_xT_{cx}B_y - B_x^2\overline{M}_xB_z$$
$$- B_x^2T_{cy} - B_y^2B_z\overline{M}_x - B_z^3\overline{M}_x - B_z^2T_{cy} + B_zB_yT_{cz})\}/(B_z^2 + B_x^2),$$

and

$$\mu_6^* = \{ -2B_x(M_{sat}B_x^3 + M_{sat}B_xB_z^2 + M_{sat}B_xB_y^2 - B_xT_{cx}B_y + B_x^2\overline{M}_xB_z$$
$$+ B_x^2T_{cy} + B_y^2B_z\overline{M}_x + B_z^3\overline{M}_x + B_z^2T_{cy} - B_zB_yT_{cz})\}/(B_z^2 + B_x^2)$$

The same analysis as that conducted for the multipliers for the float fault can be applied in the case of an LIP fault, since the matrix $L(f_{LIP}) = L(f_{Float})$. In the case that it is assumed the actuator in the Z axis is saturated, the positive definiteness of $L(f_{LIP})$ is guaranteed for all $y \in \tilde{T} : y = [0, \alpha]^T, \forall \alpha \in \Re$. This allows us to conclude that if the saturation of the actuator in the Z axis is a feasible solution, it is also a strict global minimum.

3.7.3 System Subject to an HO Fault

The HO fault is a special case in which the constraints associated to the faulty actuator ($g_1(M^*)$ or $g_2(M^*)$ for positive or negative saturation, respectively) are always active. The system of equations corresponding to the first order necessary conditions is given by

$$\mu_1^* - \mu_2^* = 0 \tag{3.43}$$

$$-2B_z(T_{cx} - M_y^* B_z + M_z^* B_y) + 2B_x(T_{cz} + M_{sat} B_y + M_y^* B_x) + \mu_3^* - \mu_4^* = 0 \tag{3.44}$$

$$2B_y(T_{cx} - M_y^* B_z + M_z^* B_y) - 2B_x(T_{cy} - M_z^* B_x + M_{sat} B_z) + \mu_5^* - \mu_6^* = 0 \tag{3.45}$$

If the HO fault is in the positive value of M_{sat}, the following equation should be used

$$\begin{aligned} -\mu_2^*(2M_{sat}) + \mu_3^*(M_y^* - M_{sat}) + \mu_4^*(-M_y^* - M_{sat}) \\ + \mu_5^*(M_z^* - M_{sat}) + \mu_6^*(-M_z^* - M_{sat}) = 0 \end{aligned}$$

Otherwise, if the saturation of M_x occurs in the negative value of M_{sat} we use

$$\begin{aligned} -\mu_1^*(2M_{sat}) + \mu_3^*(M_y^* - M_{sat}) + \mu_4^*(-M_y^* - M_{sat}) \\ + \mu_5^*(M_z^* - M_{sat}) + \mu_6^*(-M_z^* - M_{sat}) = 0, \end{aligned} \tag{3.46}$$

and to complete the first order necessary conditions we set

$$\mu_i^* \geq 0, \ \forall \ i = 1, 2, \cdots, 6 \tag{3.47}$$

It can be shown that under the hypothesis of saturation of one more actuator, there will be no solution to the constrained optimization problem for the HO fault in one actuator. The only possible solution when $M_i^* < M_{sat}$, is the unconstrained solution that is also obtained in (3.18). However, it is known that for some values of B_x, B_y, B_z, the constraints $g_i(M^*) < 0$

will not be satisfied. Therefore, it is concluded that the HO fault can be recovered as a float fault only if the faulty actuator is shut down.

3.7.4 System Subject to an LOE Fault

The faulty actuator will generate a response that is governed by

$$M_{xf} = kM_x^*$$

where $0 < k < 1$ is the loss of effectiveness gain and M_x^* is the control moment for the torquer in the X axis. The performance index is formulated by expression (3.16) and the gradient is given by (3.17). Hence, the first order conditions are defined according to

$$2B_z k(T_{cy} - M_z^* B_x + kM_x^* B_z) - 2B_y k(T_{cz} + kM_x^* B_y - M_y^* B_x) + \mu_1 - \mu_2 = 0 \tag{3.48}$$

$$-2B_z(T_{cx} - M_y^* B_z + M_z^* B_y) + 2B_x(T_{cz} + kM_x^* B_y - M_y^* B_x) + \mu_3 - \mu_4 = 0 \tag{3.49}$$

$$2B_y(T_{cx} - M_y^* B_z + M_z^* B_y) - 2B_x(T_{cy} - M_z^* B_x) + \mu_5 - \mu_6 = 0 \tag{3.50}$$

$$\mu_1^*(M_x^*) - \mu_2^*(-M_x^*) + \mu_3^*(M_y^* - M_{sat}) + \mu_4^*(-M_y^* - M_{sat}) + \mu_5^*(M_z^* - M_{sat}) + \mu_6^*(-M_z^* - M_{sat}) = 0 \tag{3.51}$$

$$\mu_i^* \geq 0, \ \forall \ i = 1, 2, \cdots, 6 \tag{3.52}$$

The only solution that satisfies the constraints (3.48) through (3.52) are those results that are obtained for the unconstrained case which assumes that all the constraints are inactive (no saturation of the healthy actuators is required). This solution was given in (3.18) and it follows that it does not provide a unique solution for M^*. In the unconstrained

optimization problem it was determined that the value $M_x^* = M_{cx}$ would be used for the purpose of analysis. However, if M_x^* is left as a parameter of optimization, it will be possible to find values for M^* such that the saturation constraints $g_i(M^*), \forall i = \{1,2,\cdots,6\}$, are satisfied. This property will be verified through numerical simulations in Section 4.4.

3.8 System Subject to Concurrent Faults

It was described earlier that the magnetic moment of one actuator has effects in two directions of the torque produced. In view of this fact it is possible to consider that as long as two of the three magnetic torquers remain functional, the reallocation of the control effort can still be achieved. This is possible even if one of the actuators (for example the X torquer) is subject to a fault such as an LIP, Float, or HO (fixed values for M_x), and a second or third actuator is subject to an LOE fault (regardless of the gain value), a value for M_y^* and M_z^* can be found.

By following the derivations that are similar to those presented above for a single actuator fault, the reallocation algorithm is developed to enable the recovery from certain types of concurrent faults. The corresponding results are shown in the next chapter.

The next section will describe the constrained optimization algorithm that is implemented in simulations of the fault recovery in the attitude control system of a satellite with magnetic torquers.

3.8.1 Constrained Optimization Algorithm

The constrained optimization algorithm implemented for simulations is adapted from the algorithm that is presented in [58]. This algorithm combines the Lagrange and the penalty function methods, known for formulating the constrained optimization problem as an unconstrained problem.

The Augmented Lagrangian function is defined as follows

$$L(\mathbf{x},\lambda,\rho) = f(\mathbf{x}) + \sum_{i=1}^{m}[max(\frac{1}{2}\lambda_i + \rho g_i, 0)]^2$$

with λ as the Lagrange multiplier and ρ as the adjustable penalty parameter. The values of λ_i are found iteratively by using the expression

$$\lambda^* \cong \lambda_{k+1} = max(\lambda_k + 2\rho_k g(\mathbf{x_k^*}), 0)$$

Algorithm 3.1 *[58]*

1. *Choose a tolerance ε, the maximum number of iterations N, an initial search point $\mathbf{X_0}$, an initial penalty parameter $\rho_0 = 1$, and an initial value for the Lagrange multipliers $\lambda_0 = 0$. Set k=0;*

2. *Perform unconstrained optimization (linear search) on the augmented Lagrangian function $L(\mathbf{X_0}, \lambda_k, \rho_k)$ to obtain $\mathbf{X_k^*}$.*

3. *Update the value of $\lambda_{k+1} = max(\lambda_k + 2\rho_k g(\mathbf{x_k^*}), 0)$.*

4. *Update the value of $\rho_{k+1} = 2\rho_k$ if $\|\lambda_k - \lambda_{k+1}\| < 0.5$.*

5. *Check the tolerance criteria: if* $\|\mathbf{X_k} - \mathbf{X_{k+1}}\| < \varepsilon$, *stop the algorithm, otherwise set* $\mathbf{X_0} = \mathbf{X_k^*}$ *and return to step 2.*

6. *Check the number of iterations. If* $k \geq n$, *stop the algorithm, otherwise set* $k = k+1$ *and return to step 2.*

Upon detection and identification of a fault, it is now possible that using the current status of the actuators we can find a solution to the reallocation problem. In other words, one checks if the types of faults are within the set of faults that can be recovered from. The recovery function then assigns the cost function that should be used according to the type of fault and uses the above algorithms to obtain the optimal solution. Finally, the results obtained from the reallocation algorithm are assigned as inputs to the magnetic torquers.

3.9 Stability Analysis of System Recovered From Fault

In this section, the stability of the system that is recovered from each type of fault is analyzed and investigated. The stability analysis will be based on the analytical solutions to the unconstrained optimization problem, and the torque commanded by the nonlinear control law obtained in Section 2.5.

Knowing that the reallocation of the control effort among the non-faulty actuators has similar expressions to the faulty cases of the magnetic torquers that are aligned to the x, y or z axes, only the failure in one of the axes will be studied. without loss of generality, the recovery in the event of a fault in one of the magnetorquers that is aligned with the satellite's X axis will be analyzed.

3.9.1 Float and HO Faults

As presented in Section 3.6, the solution to the unconstrained optimization problem for the reallocation of the control effort among torquers Y and Z directions due to a float fault, is obtained according to (3.15). It was noted that the HO fault would be treated as a float fault by disabling the faulty actuator from producing a moment. Therefore, the stability analysis presented in this section, is valid for the system under both types of faults (i.e. float and HO). The following theorem states that under the recovery mechanism, the equilibrium point of the system subject to float (or HO) fault in one of the actuators is stable.

Theorem 3.6 *Let the system represented by* (2.44) *be subject to a float (or HO) fault in the actuator that aligned to the X axis of the satellite's body, and let*

$$M^* = \left\{ \begin{bmatrix} 0 & 0 & 0 \\ B_x B_z & B_y B_z & -(B_x 2 + B_y^2) \\ -B_x B_y & (B_x^2 + B_z^2) & -B_y B_z \end{bmatrix} \begin{bmatrix} T_x \\ T_y \\ T_z \end{bmatrix} \right\} / B_x \|B\|^2$$
$$= \frac{R[B \times (B \times T_c)]}{B_x \|B\|^2}$$

with

$$R = \begin{bmatrix} 0 & 0 & 0 \\ 0 & 0 & 1 \\ 0 & -1 & 0 \end{bmatrix} \tag{3.53}$$

be the control input moment to the healthy actuators.

Furthermore, assume that the fault occurs when the system is in steady state. Namely, $T_{eq} \approx 0$. *Then, the equilibrium point of the closed-loop system*

$$\omega_b^r = \mathbf{0}, \mathbf{q_e} = \mathbf{0}, q_{4e} = 1$$

is stable.

Proof: The torque generated by applying the control moment given in (3.53) is

$$T_a = \frac{\{R[B \times (B \times T_c)]\} \times B}{B_x \|B\|^2}.$$

If the Lyapunov function candidate V is defined according to

$$V = \frac{1}{2} S^T S,$$

it can then be shown that

$$S^T \{R[B \times ((B \times S) \times B)] \times B\} = B_x \|B\|^2 \|B \times S\|^2.$$

Furthermore, the derivative of V along the trajectories of the system can be expressed as

$$\dot{V} = S^T T_a$$

and if we assume that the fault occurs when the system is in steady state with $T_{eq} \approx 0$ (this is quite a realistic and practical assumption that for all practical purposes faults do not occur during the initial transients of the mission), it can be concluded that

$$\dot{V} = -\lambda_s \|B \times S\|^2 \tag{3.54}$$

Equation (3.54) is negative semidefinite for all values of S provided that the assumption of $T_{eq} \approx 0$ holds. This proves that the system recovered from a float (or HO) fault has a stable equilibrium point. Similar proofs can be derived for the case of fault in the other two orthogonal actuators. ■

3.9.2 LOE Fault

The unconstrained optimization problem has a solution that is presented by expression (3.18). It will be shown that by using the recovery solution that was proposed the system subject to an LOE fault has a stable equilibrium point.

Theorem 3.7 *Let the system represented as* (2.44) *be subject to an LOE fault in the actuator that is aligned to the X axis of the satellite's body, and let*

$$M^* = \frac{R[B \times (B \times T_c)] + M_{cx}\|B\|^2 h}{B_x \|B\|^2}$$

with M_{cx}*, the desired moment calculated from* (2.31),

$$R = \begin{bmatrix} 0 & 0 & 0 \\ 0 & 0 & 1 \\ 0 & -1 & 0 \end{bmatrix}, \text{ and } h = \begin{bmatrix} B_x \\ B_y k \\ B_z k \end{bmatrix}$$

be the control input moments to the actuators.

Furthermore, assume that the fault occurs when the system is in steady state. Namely, $T_{eq} \approx 0$*. Then, the equilibrium point of the closed-loop system*

$$\omega_b^r = \mathbf{0}, \mathbf{q_e} = \mathbf{0}, q_{4e} = 1$$

is stable.

Proof: The torques that the actuators generate are given by

$$T_a = \frac{\{R[B \times (B \times T_c)]\} \times B + M_{cx}\|B\|^2 h \times B}{B_x \|B\|^2}$$

If the Lyapunov function candidate $V = S^T JS$ is chosen by assuming that the fault occurs in the steady state operation of the satellite (so that $T_{eq} \rightarrow 0$), it can be shown that

$$S^T \{(R[B \times (B \times [(B \times S) \times B]) \times B\} = B_x \|B\|^2 \|B \times S\|^2.$$

It is also true that

$$M_{cx} = \frac{-\lambda(S_3 B_y - S_2 B_z)}{\|B\|^2}$$

In addition, the cross product between the vectors h and B are

$$h \times B = \begin{bmatrix} -B_y k B_z + B_y k B_z \\ B_x k B_z - B_x B_z \\ -B_x k B_y + B_y B_x \end{bmatrix} = \begin{bmatrix} 0 \\ B_z(k-1) \\ -B_y(k-1) \end{bmatrix}.$$

Therefore,

$$S^T (h \times B) = (1-k)(B_y S_3 - B_z S_2)$$

By substituting these results into the derivative of the Lyapunov function one gets

$$\begin{aligned} \dot{V} &= S^T (T_a - T_{eq}) \\ &= -\frac{\lambda}{\|B\|^2} \left[\|B \times S\|^2 + (1-k)(B_y S_3 - B_z S_2)^2 \right] \end{aligned}$$

which shows that the equilibrium $S = 0$ is stable for all $0 \leq k < 1$. ■

3.9.3 LIP Fault

The solution that is obtained in (3.21) will be shown to guarantee that the equilibrium point is stable when the system is subject to an LIP fault in the actuator that is aligned with the satellite's X body axis.

Theorem 3.8 *Let the system that is represented by* (2.44) *be subject to an LIP fault in the actuator that is aligned to the X axis of the satellite's body, and let*

$$M^* = \frac{R[B \times (B \times T_c)] + \overline{M}_x \|B\|^2 B}{B_x \|B\|^2} \tag{3.55}$$

with

$$R = \begin{bmatrix} 0 & 0 & 0 \\ 0 & 0 & 1 \\ 0 & -1 & 0 \end{bmatrix},$$

be the control input moments to the healthy actuators.

Furthermore, assume that the fault occurs when the system is in steady state. Namely, $T_{eq} \approx 0$. *Then, the equilibrium point of the closed-loop system*

$$\omega_b^r = \mathbf{0}, \mathbf{q_e} = \mathbf{0}, q_{4e} = 1$$

is stable.

Proof: The torque that is applied by generating the moment in (3.55) is given by

$$T_a = \frac{\{R[B \times (B \times T_c)]\} \times B + \overline{M}_x \|B\|^2 (B \times B)}{B_x \|B\|^2}$$

The operation $B \times B = 0$ simplifies the above expression so that it becomes equal to the result that was obtained for the float fault case. Consequently, the proof of stability is the same as the one described for Theorem 3.6. ■

3.10 Chapter Summary

This chapter first presented the effects of different types of faults in the magnetic actuators. A mechanism is proposed to reallocate the control effort among the healthy magnetic torquers in the event of a given fault in one of the torquers. The analytical solutions to the unconstrained and constrained control reallocation problem have been developed. In addition, the stability property of the equilibrium point of the closed-loop recovered system when the recovery input is applied has been demonstrated formally. The results and theorems presented in this chapter are verified and validated through a number of simulations that are presented in the next chapter.

Chapter 4

Simulation Results

The parameters, specifications, and constraints of the simulated system are described in the first section of this chapter. In the second section, the response of the system under each type of fault followed by the results of the corresponding recovery system using our proposed constrained reallocation solutions will be included. Furthermore, the simulation results that also include finite delays in the application of the recovery after occurrence of a fault will be presented. Finally, the response of the recovery system from two concurrent faults are presented.

4.1 System Parameters, Specifications and Constraints

The scenarios under study in this chapter correspond to a LEO satellite that is equipped with three magnetic torquers that are perpendicularly aligned. The attitude control design was addressed by taking into account that the actuators operate on the basis of interactions

between magnetic moments from a set of three orthogonal current-driven coils and the geomagnetic field.

4.1.1 Satellite Model Parameters

The values indicated in Table 4.1 are parameters that define the shape and size of the satellite that is used in this chapter for numerical simulations. It is assumed that the satellite has a shape of a rectangular prism and that its center of mass is located at the geometric center of the satellite. The moments of inertia and weight of the satellite that are used in the simulations correspond to the Ørsted satellite as identified in [5], which is equipped with magnetic torquers as main actuators for attitude control.

Ørsted qualifies as a micro satellite, characterized for having a weight that is less than $100 Kg$.

SYMBOL	VALUE	NAME
m_s	61 [Kg]	Total mass of the satellite
l_x	340[mm]	Length along the x body axis
l_y	450[mm]	Length along the y body axis
l_z	680[mm]	Length along the z body axis
J_x	2.904 $[Kg/m^2]$	First principal moment of inertia
J_y	3.428 $[Kg/m^2]$	Second principal moment of inertia
J_z	1.275 $[Kg/m^2]$	Third principal moment of inertia

Table 4.1: Physical characteristics of a typical satellite [5].

4.1.2 Orbital Trajectory and Geomagnetic Field

The geomagnetic field is a variable of interest in the application of magnetic torquers for attitude control. Because the field is a function of the orbital position of the satellite, the model of a circular orbit is chosen for simulation purposes. The parameters in Table 4.2 are used in the simulated model.

ORBITAL ELEMENTS	VALUES
Semi-Mayor Axis (Km)	7,063.27
Eccentricity	0.00115
Inclination (deg)	98.127
Right Ascension of Ascending Node (deg)	81.108
Argument of Perigee (deg)	90.0

Table 4.2: Orbital elements for a typical simulation ([6] and [7]).

The type of the orbit that is modeled is shown in Figure 4.1. The values of the orbital parameters are extracted from [6] and [7], which describe the orbital trajectory followed by a real satellite. Figure 4.2 shows the variation of the geomagnetic field as the satellite orbits around the Earth on a LEO with the parameters as given in Table 4.2. This figure is produced by using equations (2.5) to (2.7) and the values are calculated in nano Teslas.

It should be noted that the orbital position of the satellite is controlled independently from its attitude. Orbital perturbations are neglected as it is assumed that the orbital trajectory controller compensates for them.

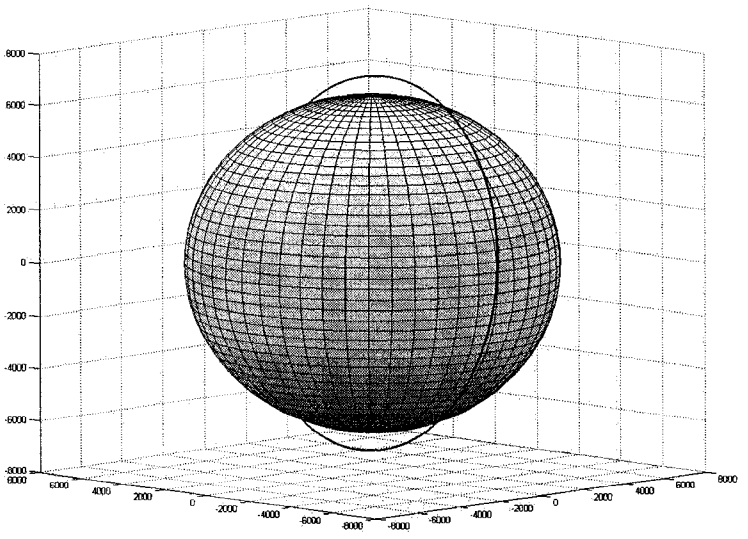

Figure 4.1: Circular LEO to be used in the simulation results.

4.1.3 Size and Limitations of the Magnetic Torquers

In order to utilize the applicable disturbance torques to the model, their worst case values are calculated as indicated in this section. The maximum values of the environmental perturbations are determined by using the equations given in Table 4.3.

Table 4.4 shows the additional parameters that are used in calculation of the disturbance torques. The results for the numerical simulation example that is implemented are shown as follows:

- Using equation (2.20), a maneuvering torque $T_{man} = [0.1310, 0.1547, 0.0575]^T x10^{-6}\,[Nm]$ is required to demand the satellite to reach its steady state in 2 orbits, or about 11,800 seconds from a maximum angle of $\theta = \pi/2$.

- The worst-case disturbance torques that are calculated according to Table 4.3, and

Distur-bance	Type	Influenced Primarily by	Formula
Gravity-gradient	Constant torque for Earth-oriented vehicle, cyclic for inertially oriented vehicle	• Spacecraft inertias • Orbit altitude	$T_g = \frac{3\mu}{2R^3}\lvert I_z - I_y \rvert \sin(2\theta)$ where T_g is the max gravity torque; μ is the Earth's gravity constant (3.986×10^{14} m^3/s^2); R is orbit radius (m), θ is the maximum deviation of the Z-axis from local vertical in radians, and I_z and I_y are moments of inertia about z and y (or x, if smaller) axes in kg·m^2.
Solar Radiation	Cyclic torque on Earth-oriented vehicle, constant for solar-oriented vehicle or platform	• Spacecraft geometry • Spacecraft surface reflectivity • Spacecraft geometry and cg location	Solar radiation pressure, T_{sp}, is highly dependent on the type of surface being illuminated. A surface is either transparent, absorbent, or a reflector, but most surfaces are a combination of the three. Reflectors are classed as diffuse or specular. In general, solar arrays are absorbers and the spacecraft body is a reflector. The worst case solar radiation torque is $T_{sp} = F(c_{ps} - cg)$ where $F = \frac{F_s}{c} A_s (1+q)\cos i$ and F_s is the solar constant, 1,367 W/m^2, c is the speed of light, 3×10^8 m/s, A_s is the surface area, c_{ps} is the location of the center of solar pressure, cg is the center of gravity, q is the reflectance factor (ranging from 0 to 1, we use 0.6), and i is the angle of incidence of the Sun.
Magne-tic Field	Cyclic	• Orbit altitude • Residual spacecraft magnetic dipole • Orbit inclination	$T_m = DB$ where T_m is the magnetic torque on the spacecraft; D is the residual dipole of the vehicle in amp·turn·m^2 (A·m^2), and B is the Earth's magnetic field in tesla. B can be approximated as $2M/R^3$ for a polar orbit to half that at the equator. M is the magnetic moment of the Earth, 7.96×10^{15} tesla·m^3, and R is the radius from dipole (Earth) center to spacecraft in m.
Aerody-namic	Constant for Earth-oriented vehicles, variable for inertially oriented vehicle	• Orbit altitude • Spacecraft geometry and cg location	Atmospheric density for low orbits varies significantly with solar activity. $T_a = F(c_{pa} - cg) = FL$ where $F = 0.5\,[\rho\, C_d A V^2]$; F being the force; C_d the drag coefficient (usually between 2 and 2.5); ρ the atmospheric density; A, the surface area; V, the spacecraft velocity; c_{pa} the center of aerodynamic pressure; and cg the center of gravity.

Table 4.3: Simplified disturbance torques ([4]).

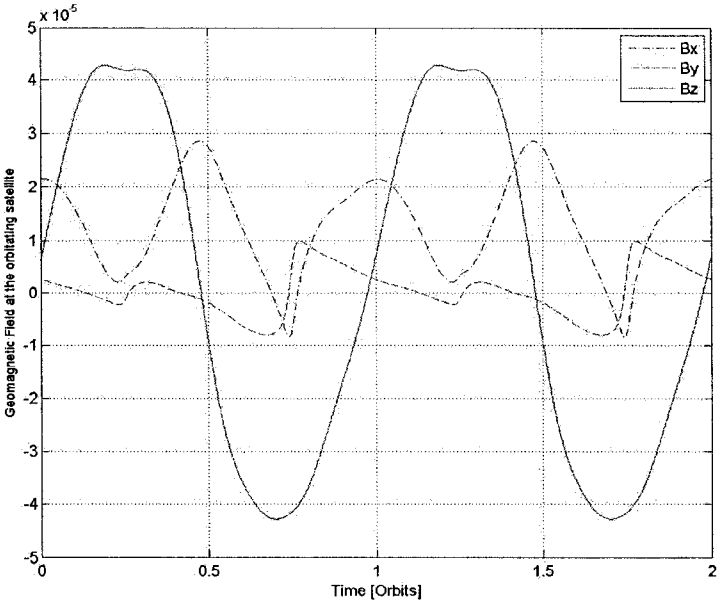

Figure 4.2: Geomagnetic field during two orbits as calculated in the geocentric coordinates.

PARAMETER	VALUE
Altitude ASL (r_s)	650[Km]
Atmospheric Density (ρ)	2.64×10^{-13} $[Kg/m^3]$
Drag Coefficient (C_d)	2
Reflectance Factor (q)	0.6
Residual Dipole Moment (D)	$0.001[Am^2]$
Velocity of Satellite in Orbit	$7,531$ $[m/s]$
Magnetic Moment of the Earth (M_e)	7.96×10^{15} $[Tm^3]$

Table 4.4: The environmental parameters that are defined for a typical satellite.

the values given in Tables 4.1 and 4.4 are:

$$\text{Gravity Gradient Torque:} 7.42x10^{-6}\,[Nm]$$

$$\text{Aerodynamic Torque: } 5.79x10^{-7}\,[Nm]$$

$$\text{Magnetic Disturbance Torque: } 4.58x10^{-8}\,[Nm]$$

$$\text{Solar Radiation Torque: } 6.38x10^{-8}\,[Nm]$$

$$T_{total} \leq 8.67x10^{-6}\,[Nm]$$

The most important disturbances correspond to the gravity gradient torque and the aerodynamic drag, followed by the magnetic disturbance torque (if the residual moment is small enough) and the solar radiation impingement. These results are obtained by using Table 4.3 that is extracted from [4] which also introduces the simplified equations for estimating the upper bounds of the environmental disturbance forces.

As mentioned in Section 2.3.2, the magnetic dipole of the satellite is one of the important disturbances that one needs to take into account. However, special methods for compensating this particular disturbance are considered to be out of the scope of this thesis. In this thesis it is assumed that the magnetic dipole of the satellite is already compensated for, leaving a residue of $0.001Am^2$.

The maximum value of the magnetic moment is calculated as detailed below

$$B_{max} = \frac{2M_e}{R_E^3}$$

$$= 4.5861x10^{-5}\,[Tm^3] \tag{4.1}$$

where M_e is the magnetic moment of the Earth and R is the distance from the center of the Earth to the center of the satellite.

Now, by using the values above and the average value of the geomagnetic field from (4.1), for a non-faulty system, the minimum moment that the torquers should produce in each direction is approximately given by

$$M_{min} = \frac{T_{total}}{B_{max}}$$
$$= 0.19Am^2$$

In [5] it is mentioned that the magnetic torquers on board of the Ørsted satellite are sized to produce a maximum amplitude moment of $20Am^2$, which in theory is sufficient to compensate for the above mentioned disturbances and maneuver torques. The saturation value used in the simulation results that will be presented in this chapter was set to $\pm 10Am^2$.

4.2 Response of Satellite Without Fault

The behavior of the satellite under normal conditions has been evaluated through numerical simulations by commanding the attitude control system to follow a zero reference with respect to the inertial frame, and the time varying trajectories shown in figures 4.3 and 4.4.

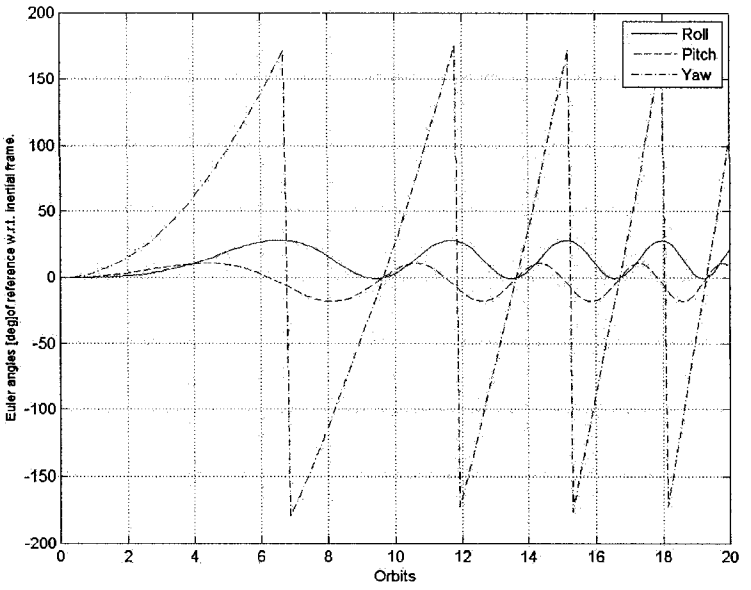

Figure 4.3: Time varying trajectory. Reference with respect to the inertial frame.

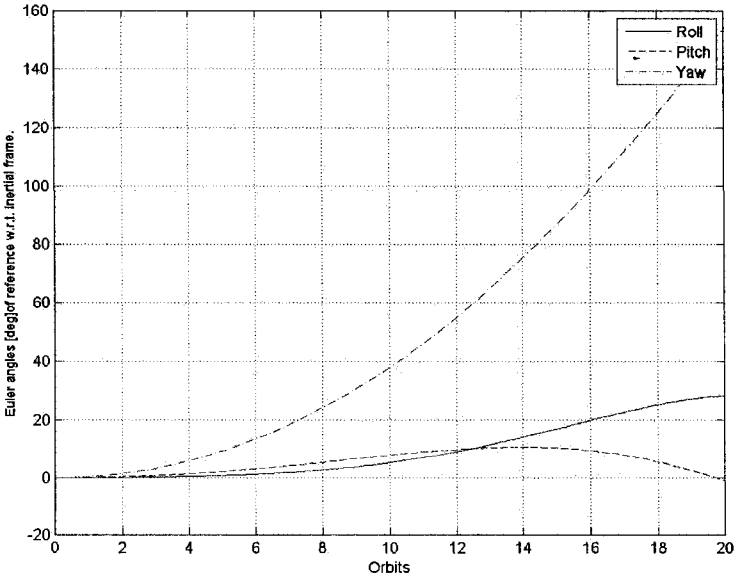

Figure 4.4: Slow time varying trajectory. Reference with respect to the inertial frame.

The Figures 4.3 and 4.4 show the Euler angles for the time varying reference trajectories used in the simulations. In the first trajectory the angles follow sinusoidal paths with frequencies of the order of $10^{-7}\,rad/s$, while the latter has lower frequencies of $10^{-8}\,rad/s$ as indicated in expressions (4.2) and (4.3).

$$\begin{aligned}
\omega_{xr}^{i} &= 0.015\sin(1.5\times 10^{-7}t)\ rad/s \\
\omega_{yr}^{i} &= 0.025\sin(0.4\times 10^{-7}t)\ rad/s \\
\omega_{zr}^{i} &= 0.05\sin(0.8\times 10^{-7}t)\ rad/s
\end{aligned} \tag{4.2}$$

$$\begin{aligned}
\omega_{xr}^{i} &= 0.015\sin(1.5\times 10^{-8}t)\ rad/s \\
\omega_{yr}^{i} &= 0.025\sin(0.4\times 10^{-8}t)\ rad/s \\
\omega_{zr}^{i} &= 0.05\sin(0.8\times 10^{-8}t)\ rad/s
\end{aligned} \tag{4.3}$$

In steady state, as it can be seen in the upper Figure 4.5, the response of the attitude control system following the zero reference results in Euler angles that are bounded within ± 9 degrees. This satisfies the precision requirements of the mission for the sample satellite Ørsted according to [5], where the control design criteria is to obtain a maximum error of 10 degrees for roll and pitch, and 20 degrees for the yaw angle. The Ørsted satellite has been designed to map the Earths magnetic field, measure the charged particle environment, and study auroral phenomena [59]. It is also shown in the lower Figure 4.5 that the applied magnetic moments lay within $\pm 0.1\ [Am^2]$, far below the saturation level of the magentorquers ($\pm 10 Am^2$).

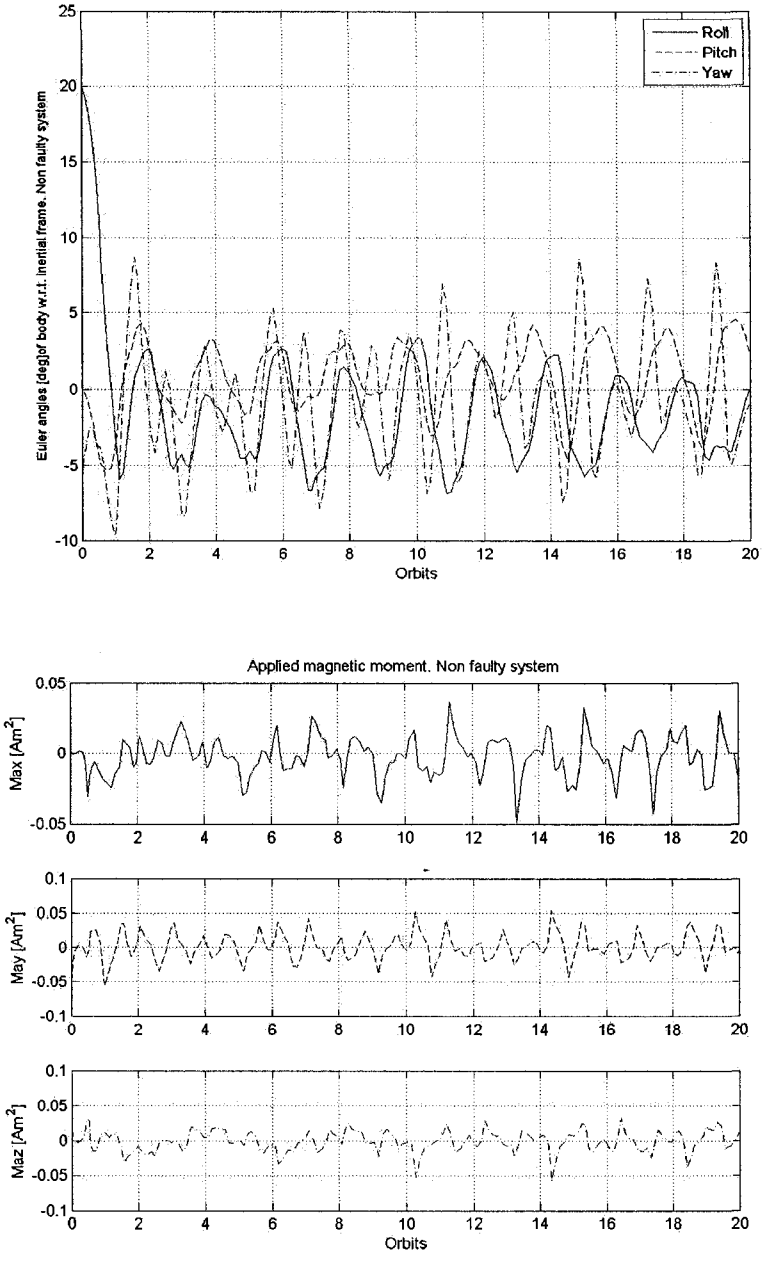

Figure 4.5: Response of the satellite without fault following a zero reference with respect to the inertial frame.

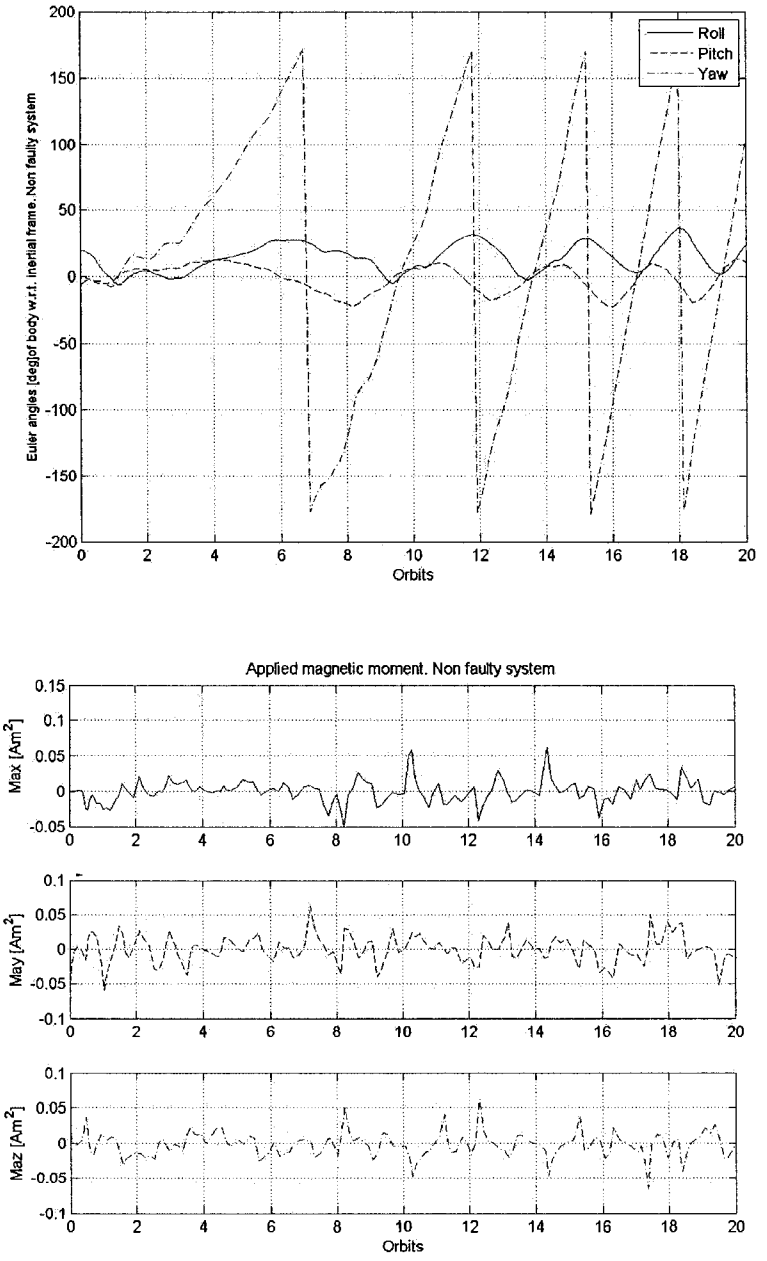

Figure 4.6: Response of the satellite without fault following the time varying reference in Figure 4.3.

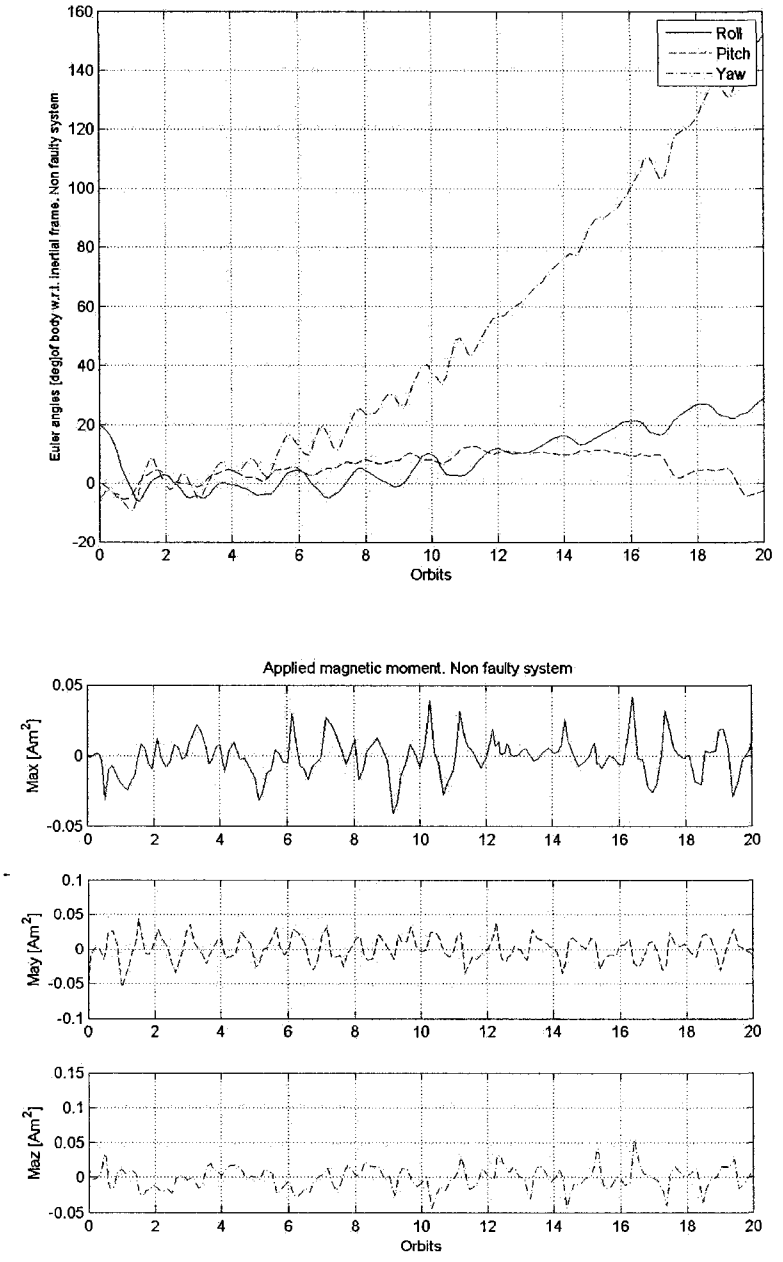

Figure 4.7: Response of the satellite without fault following the time varying reference in Figure 4.4.

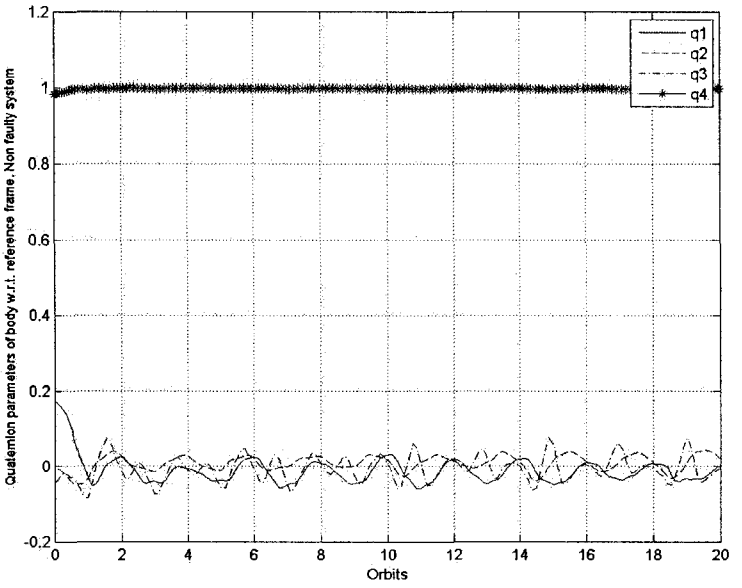

(a) Zero reference trajectory

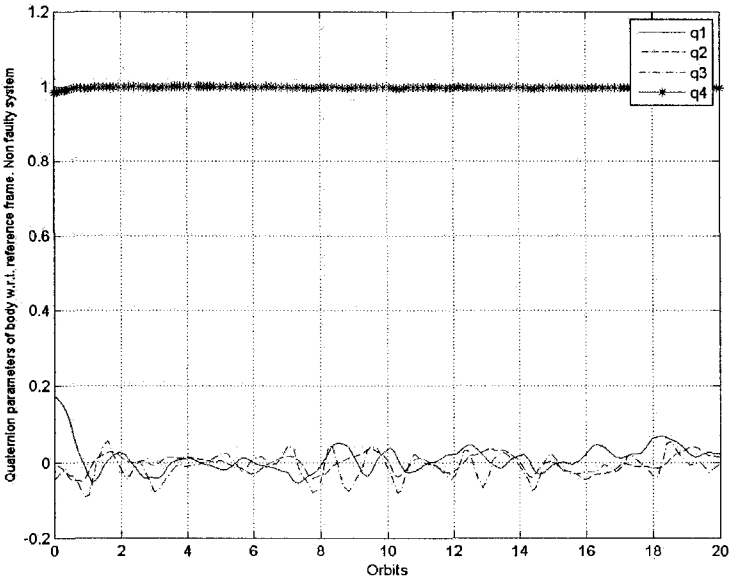

(b) Trajectory from Figure 4.3

Figure 4.8: Quaternion errors. Responses from the system without a fault.

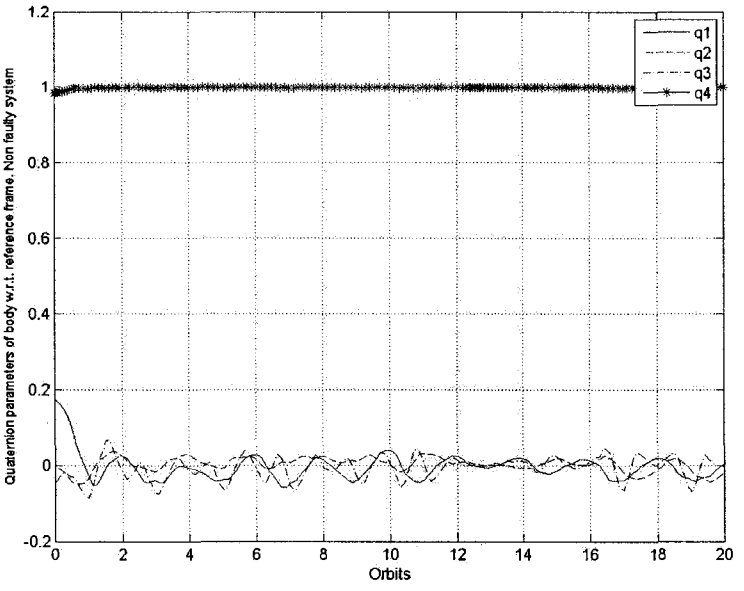

Figure 4.9: Quaternion errors. Response from the system without a fault following the trajectory of Figure 4.4.

The Figures 4.6 and 4.7 show the response of the attitude control system that follows the time varying trajectories (4.2) and (4.3), respectively. In steady state the relative errors of the Euler angles are comparable to those obtained in the zero reference scenario. The quaternion errors presented in Figures 4.8 and 4.9 confirm this similarity.

4.3 Satellite Response Under Actuator Faults

The following simulation results show the response of the satellite that is subject to the different faults that are described in Section 3.2, and without invoking a recovery action. The behavior of the Euler angles, the applied magnetic moment and the quaternion errors are shown for the zero and the time varying references from Figures 4.3 and 4.4. As can be

seen in Figures 4.10 to 4.12, the degradation of the relative errors is more significant when the system is commanded with a time varying trajectory. Also, a faster rate of change of the command reference results in larger steady state errors at earlier times.

The response of the system subject to an LIP fault is shown in Figures 4.15 and 4.16. The effect of the constant input of $0.02\,Am^2$ from the faulty magnetorquer is very significant and the Figure 4.17 shows that the quaternion errors are larger when the trajectory that is followed is time varying.

The simulations of the LOE faults presented in Figures 4.18 and 4.20 were carried out for 90% and 75% of loss of effectiveness, respectively, for the actuator alligned to the X axis of the body frame and following a zero reference. The results to the time varying reference in Figures 4.19 and 4.21 correspond to the reference input in Figure 4.4. Although the fault does not lead the system to instability, the quaternion errors shown in Figures 4.22 and 4.23 indicate the effect of the fault in proportion to the loss of effectiveness gain, which is larger when the trajectory to follow is time varying.

The HO fault was evaluated for the zero trajectory and the time varying trajectory in Figure 4.4 with a saturation level of $\pm 10 Am^2$ reached at a rate of $0.001 Am^2/s$. It is evident that the most critical fault is the HO, which leads the system to complete instability. However, although the response of the system remains bounded in the presence of float, LIP and LOE faults, the effects in the performance of the system are important, particularly when the reference trajectory is time varying.

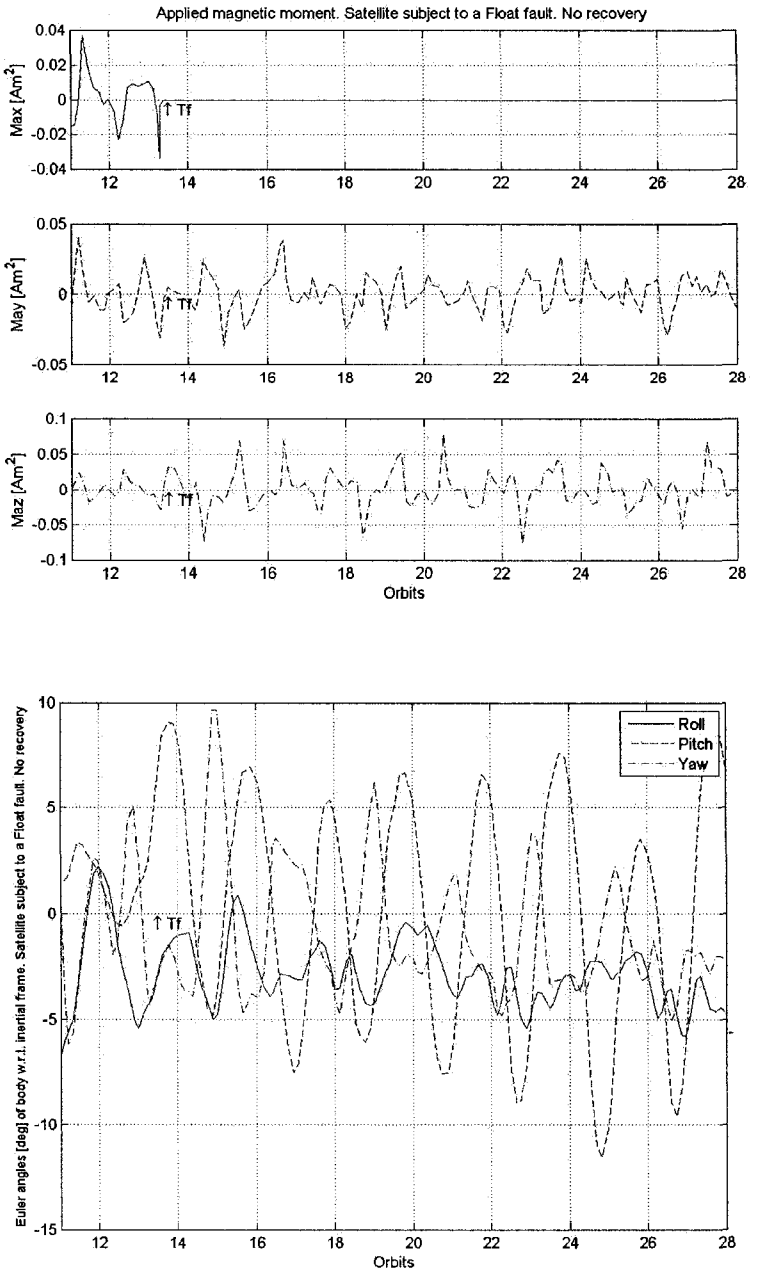

Figure 4.10: Response of the satellite following a zero reference trajectory. System is subject to a float fault that is applied at time $T_f = 13$ oribts.

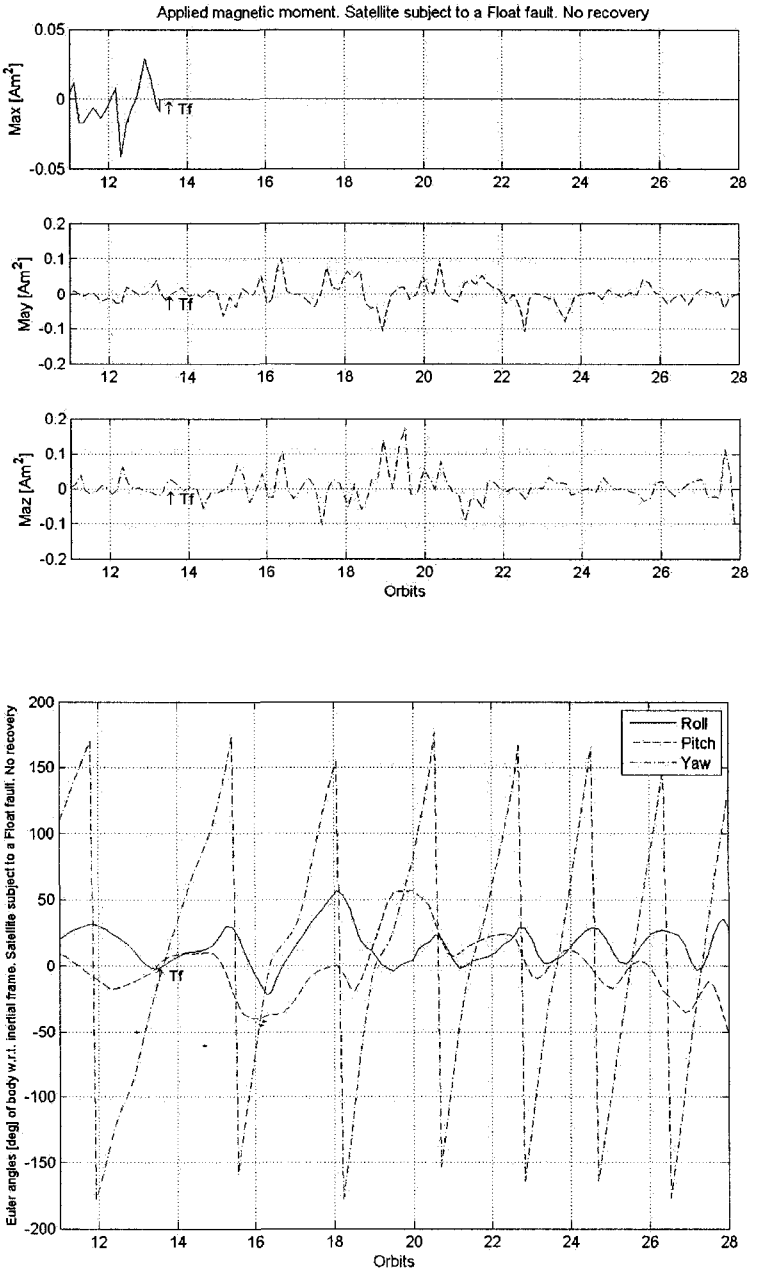

Figure 4.11: Response of the satellite following the time varying reference in Figure 4.3. System is subject to a float fault that is applied at time $T_f = 13$ orbits.

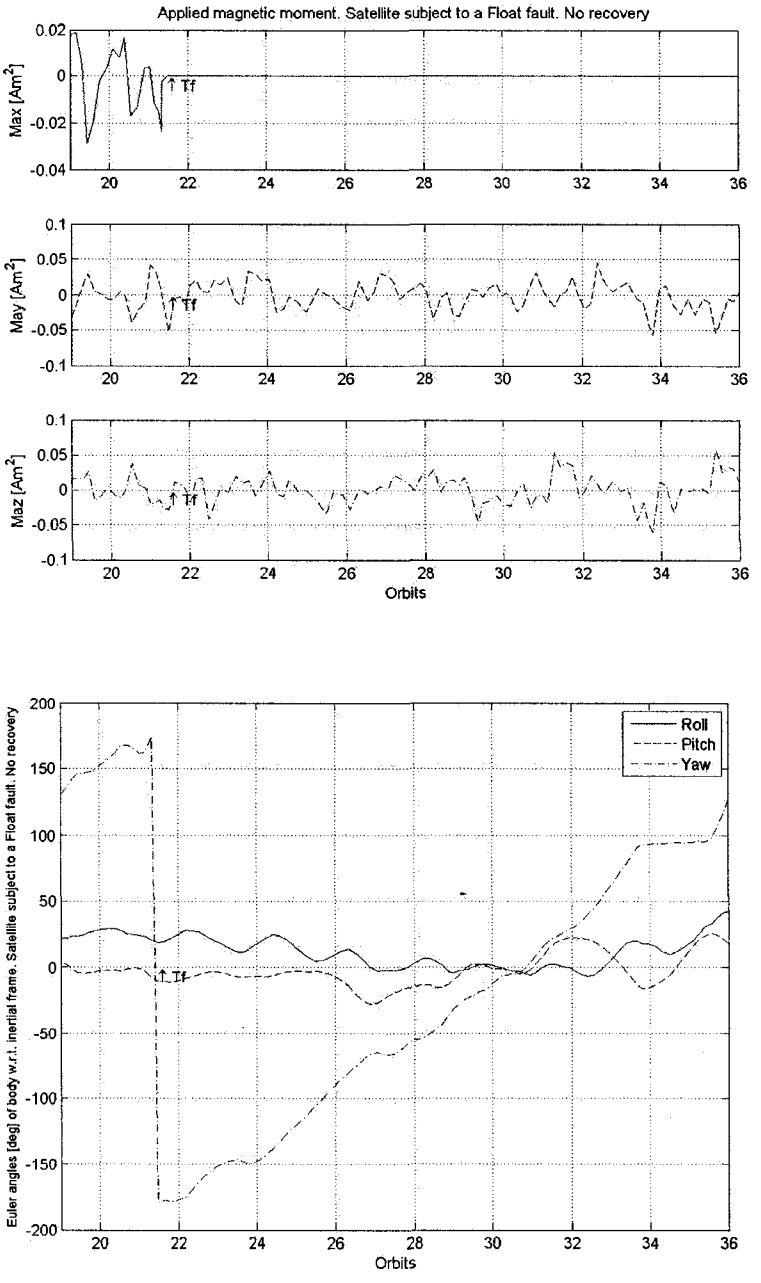

Figure 4.12: Response of the satellite following the time varying reference in Figure 4.4. System is subject to a float fault that is applied at time $T_f = 21$ orbits.

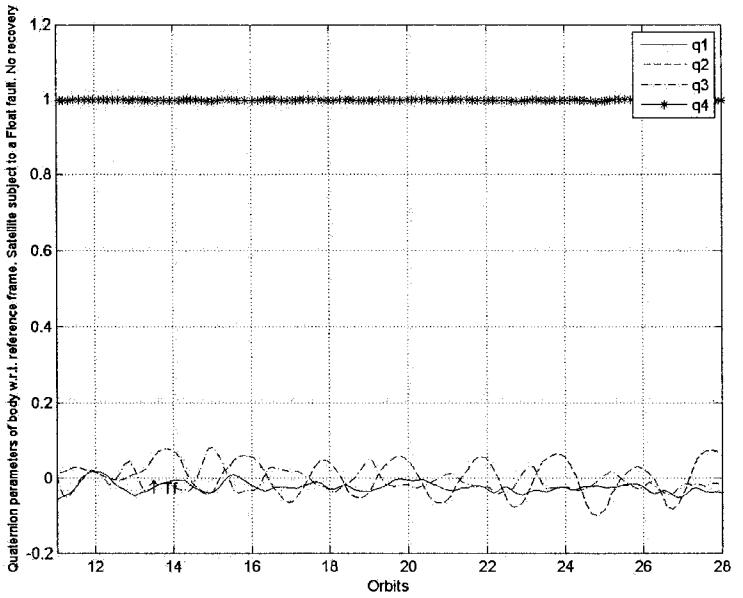

(a) Zero reference trajectory

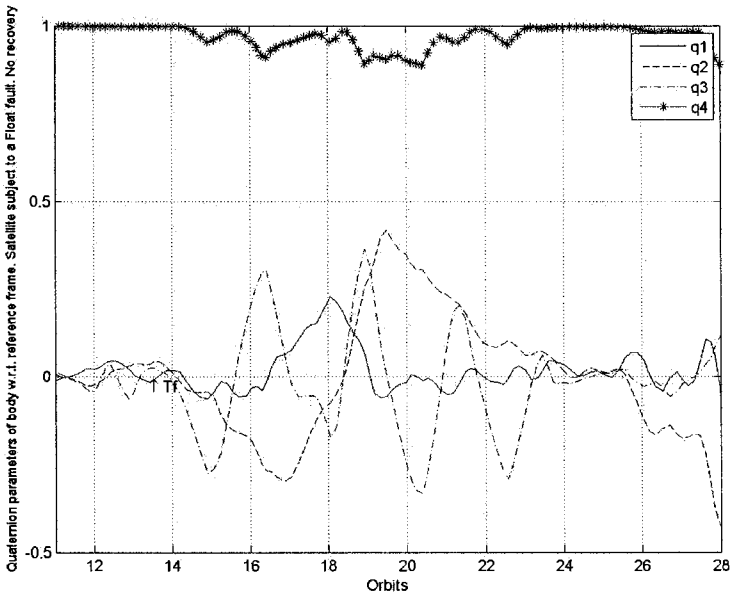

(b) Trajectory from Figure 4.3

Figure 4.13: Quaternion errors. System is subject to a float fault that is applied at time $T_f = 13$ orbits.

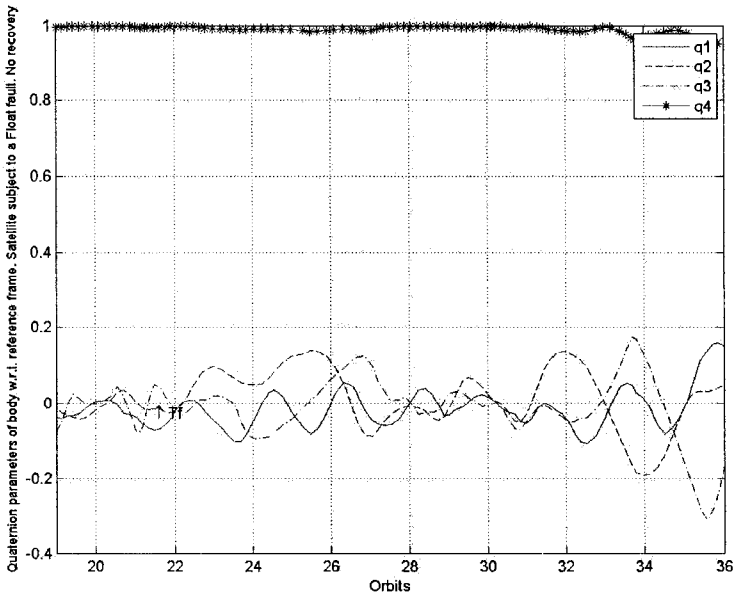

Figure 4.14: Quaternion errors. Response from the system following the trajectory in Figure 4.4. The system is subject to a float fault that is applied at time $T_f = 21$ orbits.

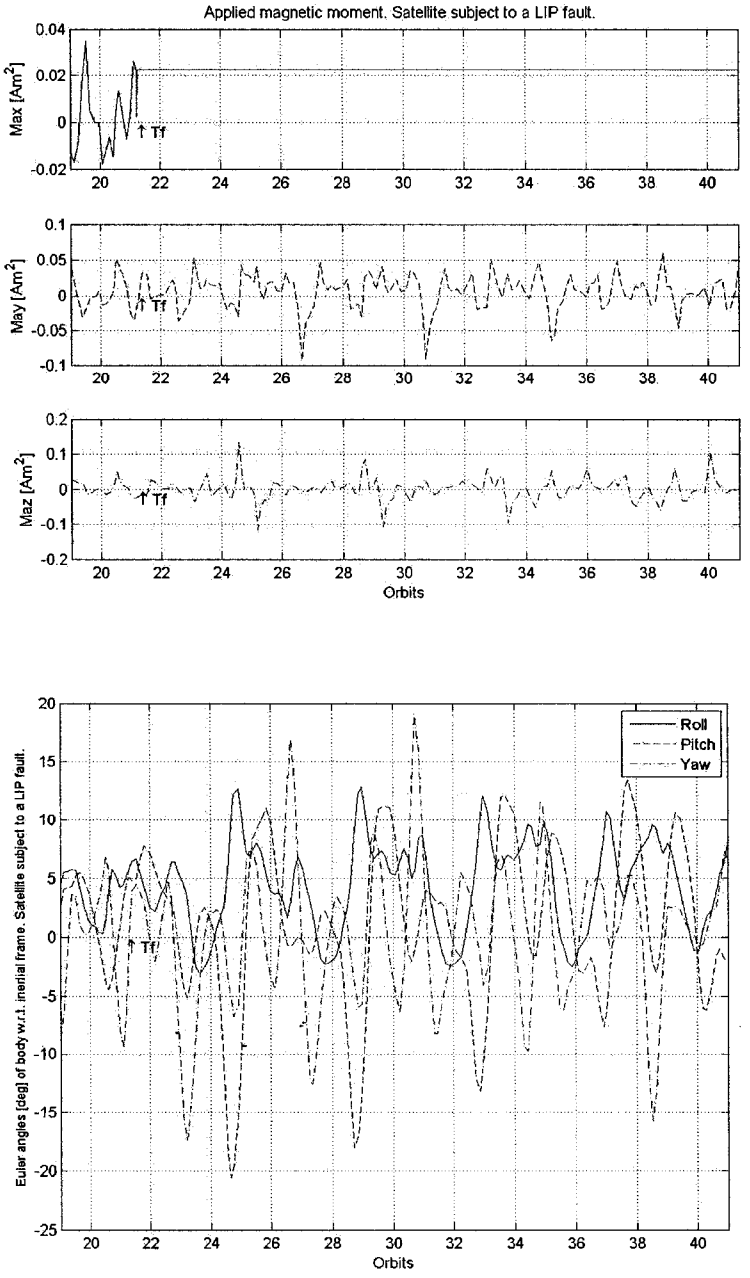

Figure 4.15: Response of the satellite following a zero reference with respect to the inertial frame. System is subject to a LIP fault that is applied at time $T_f = 21$ orbits.

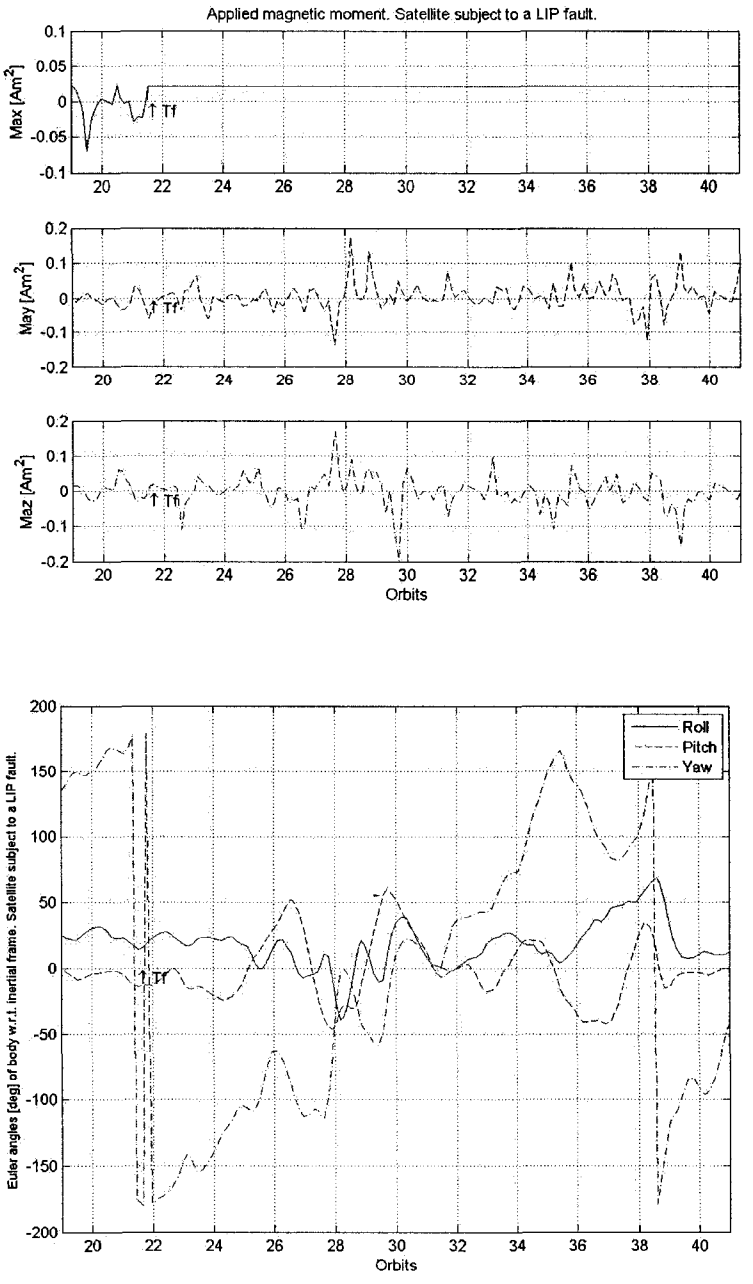

Figure 4.16: Response of the satellite following the time varying reference in Figure 4.4. System is subject to a LIP fault that is applied at time $T_f = 21$ orbits.

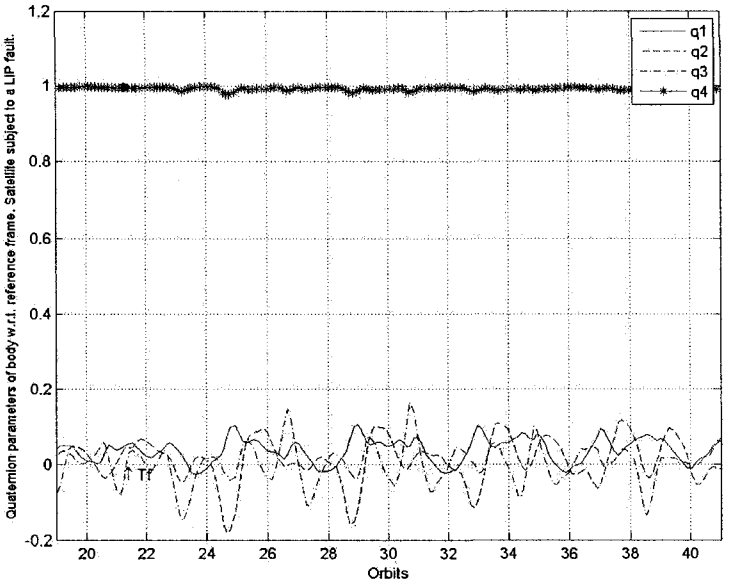

(a) Zero reference trajectory

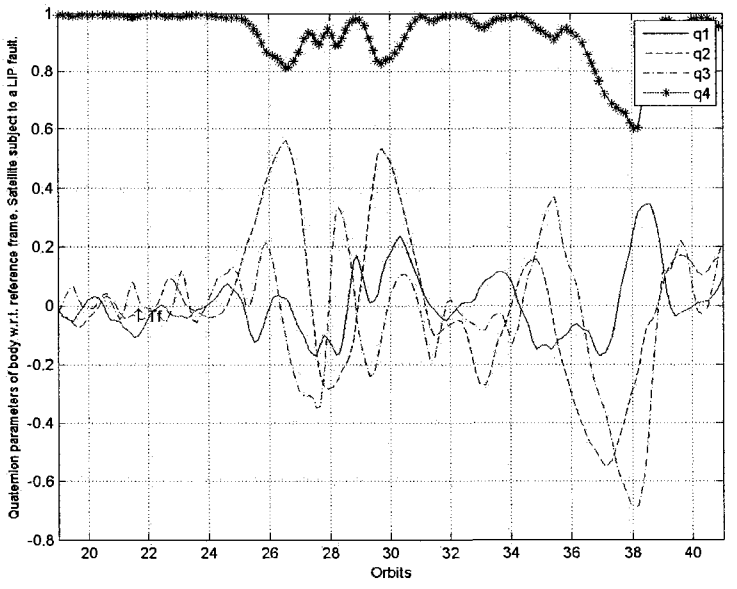

(b) Trajectory from Figure 4.4.

Figure 4.17: Quaternion errors. System is subject to a LIP fault that is applied at time $T_f = 21$ orbits.

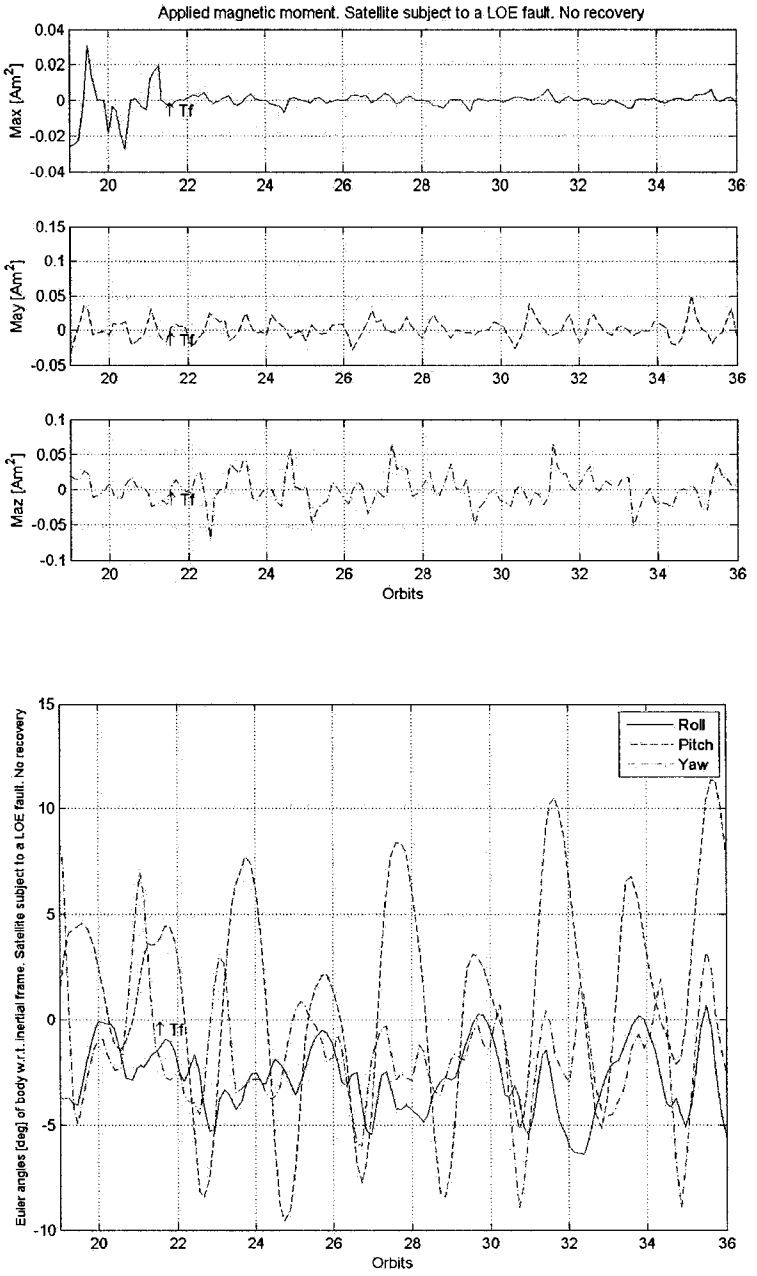

Figure 4.18: Response of the satellite following a zero reference. System is subject to a 90% LOE fault that is applied at time $T_f = 21$ orbits.

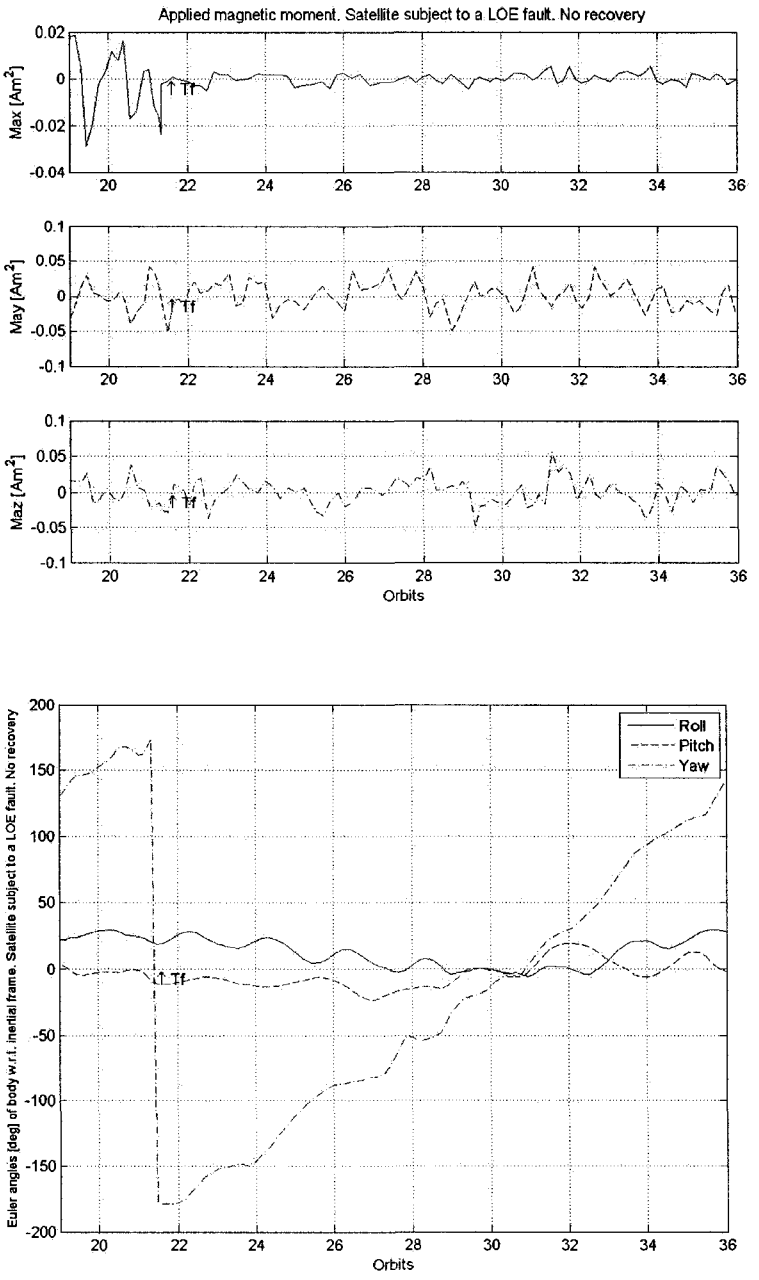

Figure 4.19: Response of the satellite following the time varying reference in Figure 4.4. System is subject to a 90% LOE fault that is applied at time $T_f = 21$ orbits.

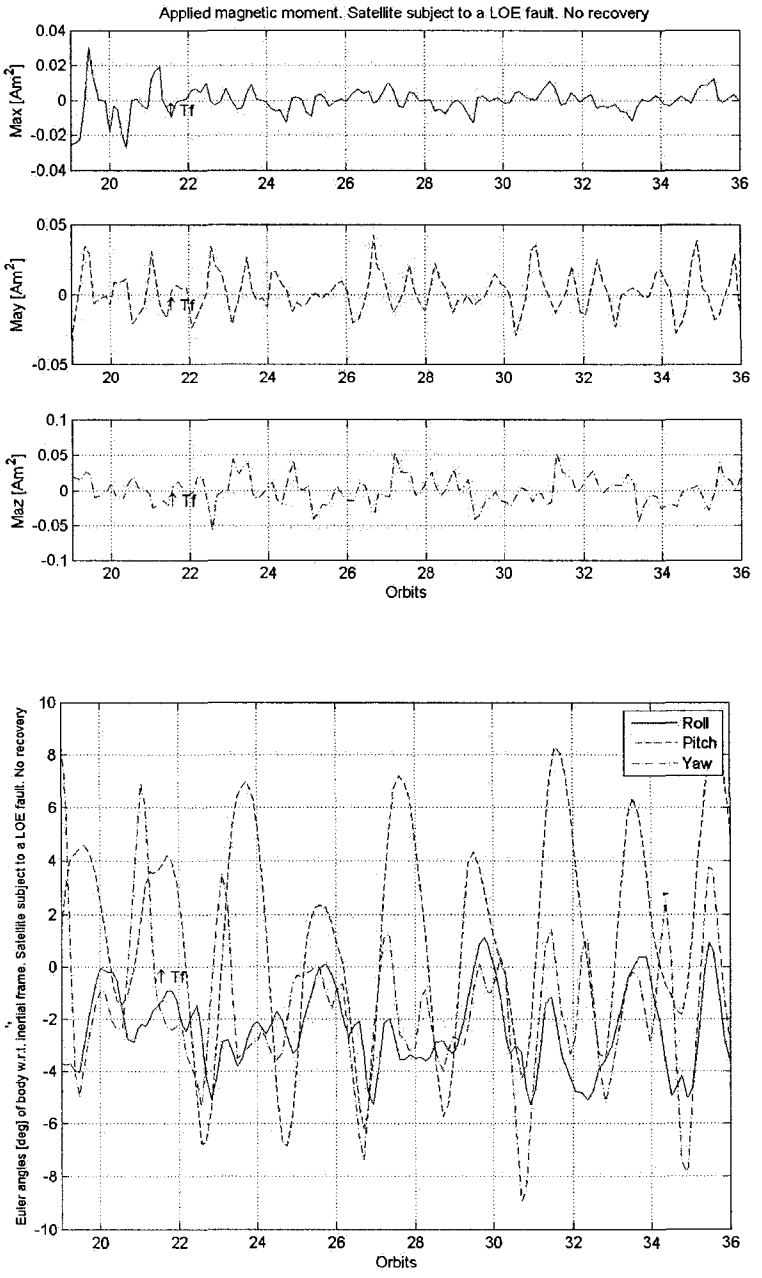

Figure 4.20: Response of the satellite following a zero reference. System is subject to a 90% LOE fault that is applied at time $T_f = 21$ orbits.

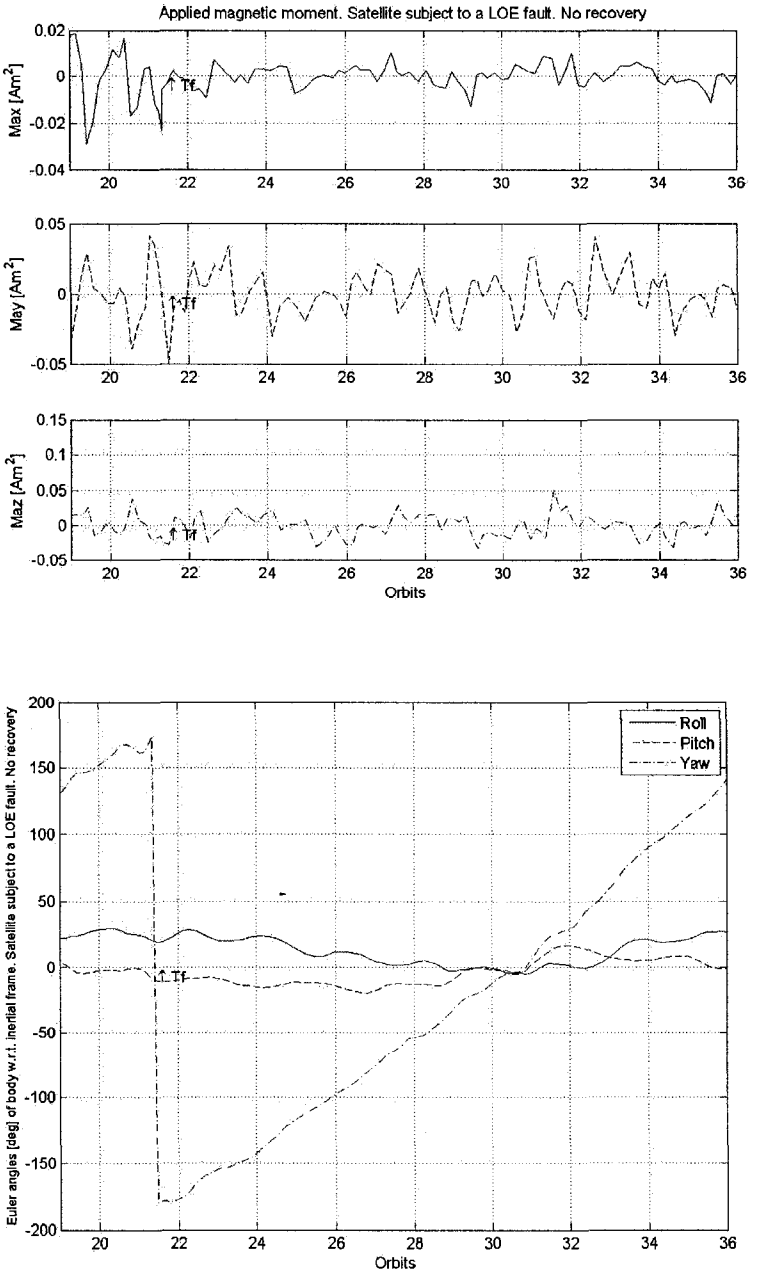

Figure 4.21: Response of the satellite following the time varying reference in Figure 4.4. System is subject to a 75% LOE fault that is applied at time $T_f = 21$ orbits.

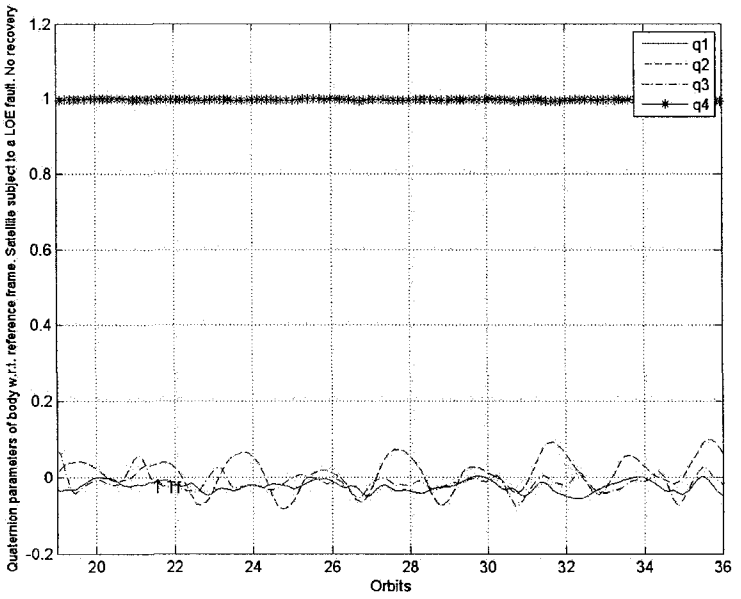

(a) Zero reference trajectory

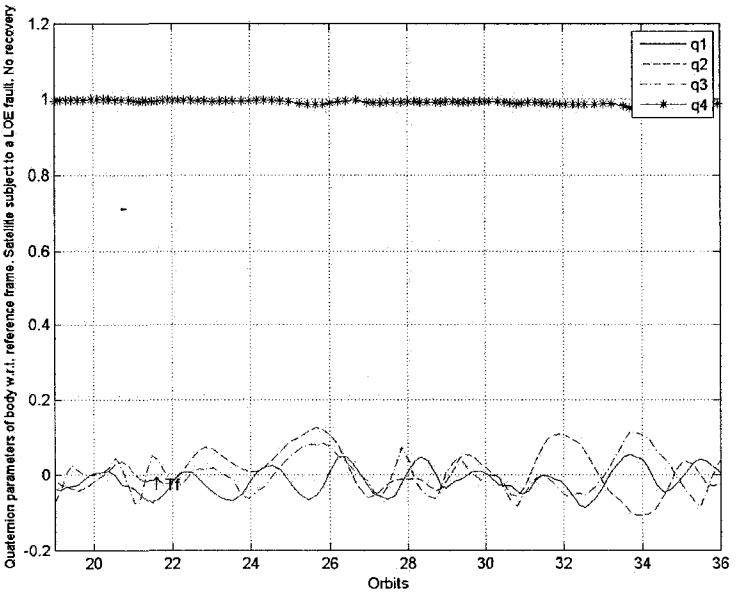

(b) Trajectory from Figure 4.4

Figure 4.22: Quaternion errors. System is subject to a 90% LOE fault that is applied at time $T_f = 21$ orbits.

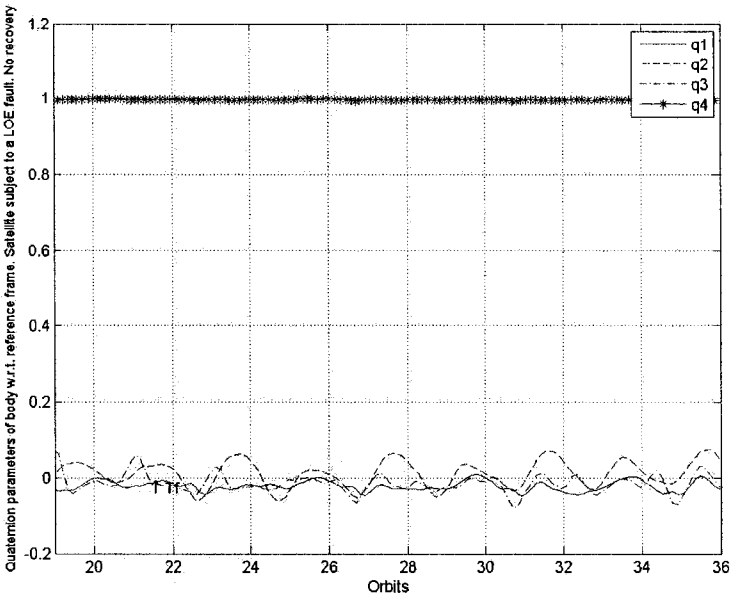

(a) Zero reference trajectory

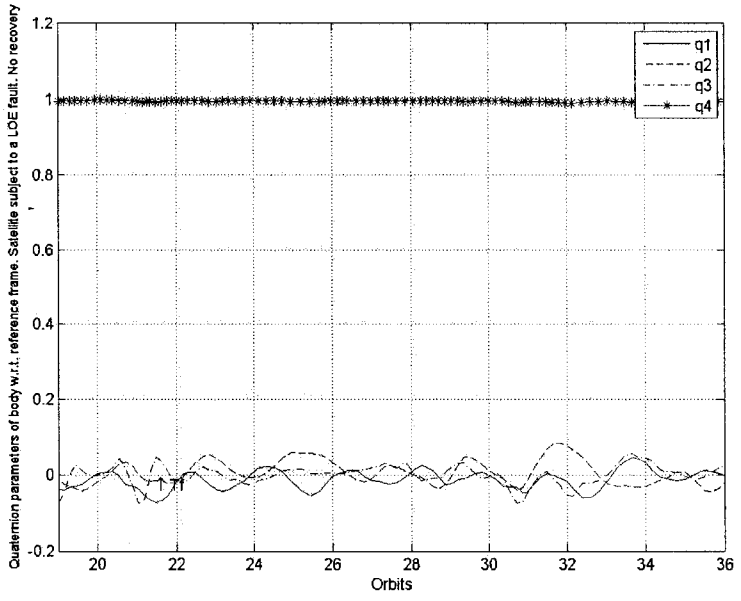

(b) Trajectory from Figure 4.4

Figure 4.23: Quaternion errors. System is subject to a 75% LOE fault that is applied at time $T_f = 21$ orbits.

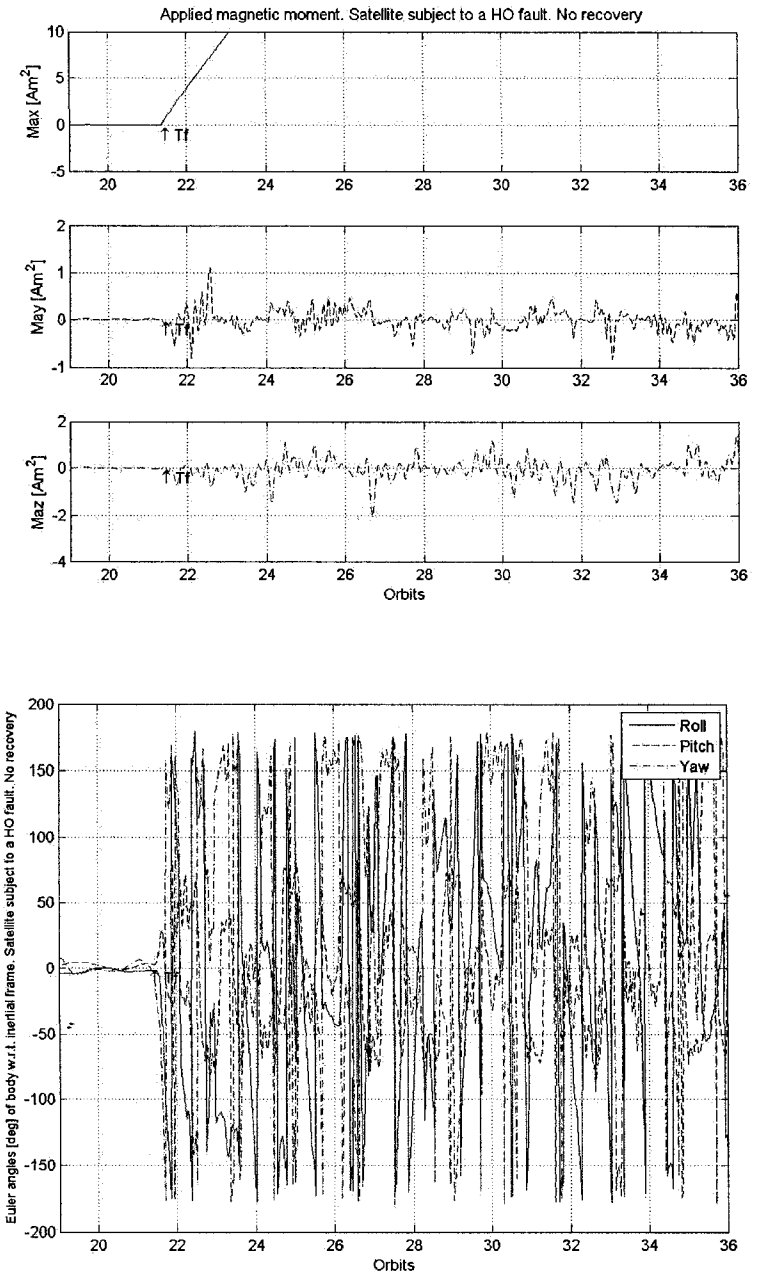

Figure 4.24: Response of the satellite following a zero reference with respect to the inertial frame. System is subject to an HO fault that is applied at time $T_f = 21$ orbits.

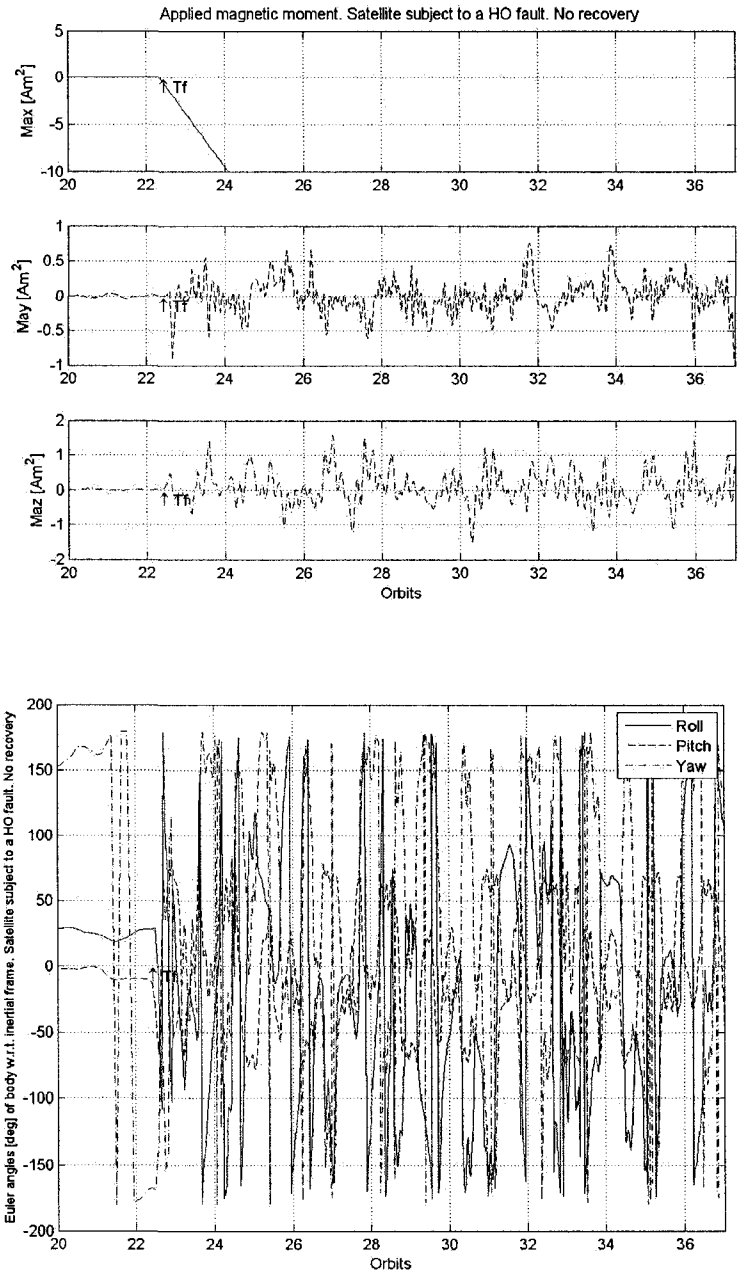

Figure 4.25: Response of the satellite following the time varying reference in Figure 4.4. System is subject to an HO fault that is applied at time $T_f = 22$ orbits.

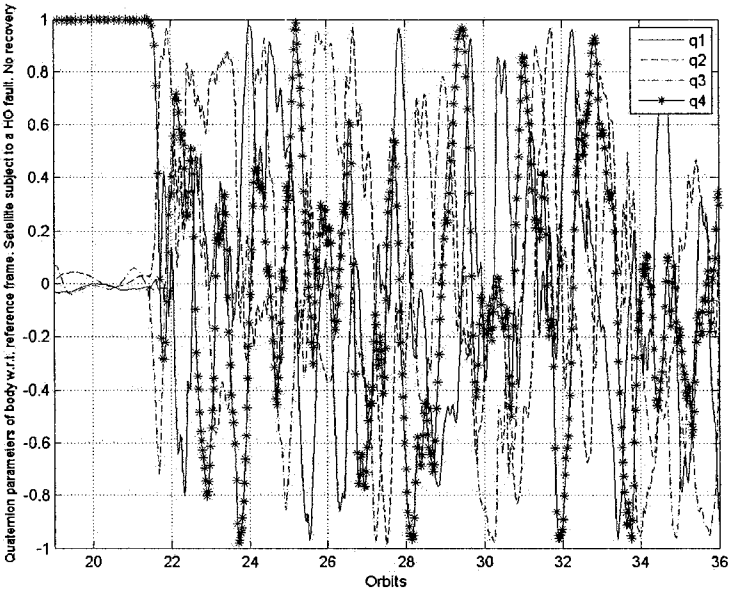

(a) Zero reference trajectory

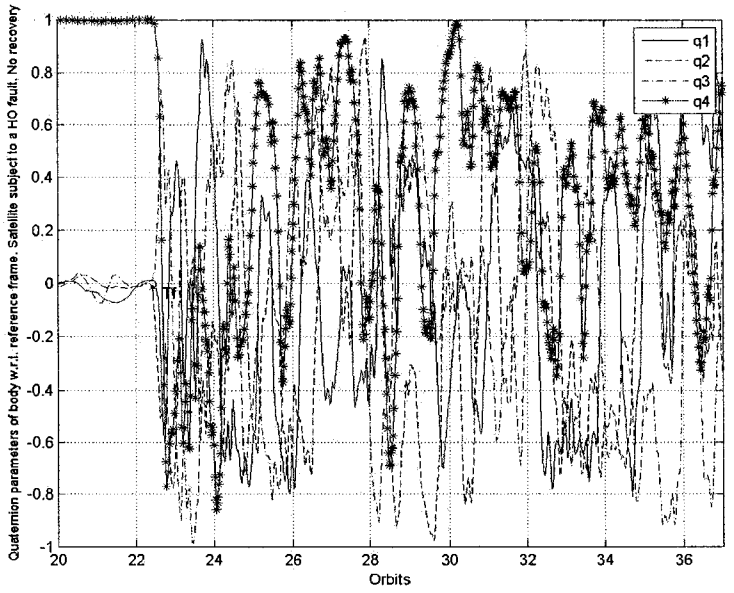

(b) Trajectory from Figure 4.4

Figure 4.26: Quaternion errors. System is subject to an HO fault that is applied at time $T_f = 21$ and $T_f = 22$ orbits.

A qualitative comparison is performed for the response of the satellite with and without fault (except for the HO fault). The data correspond to the estimated mean and standard deviation of the three main quaternion parameters. These values are calculated from the results of the simulations of the system in steady state as indicated in Figure 4.27. The statistical results are shown in Table 4.5 and Figure 4.28 for zero reference trajectory and Table 4.6 and Figure 4.29 for the time varying trajectory shown in Figure 4.4.

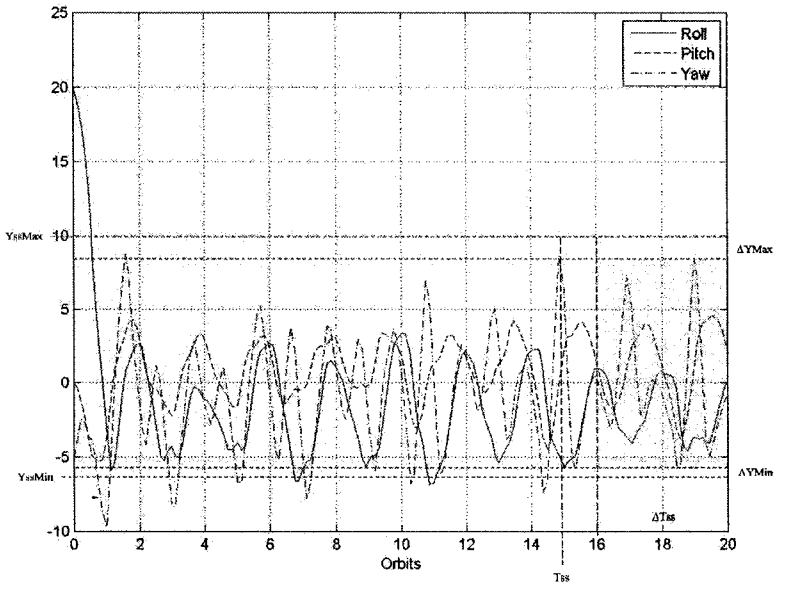

Figure 4.27: A typical calculation of the settling time and the steady state values.

The settling time of the response was calculated within the band that form the 10% of the upper and lower bounds of the signal in the last four orbits of the simulations. These are the values that are registered in the tables for comparison of the response among the different scenarios.

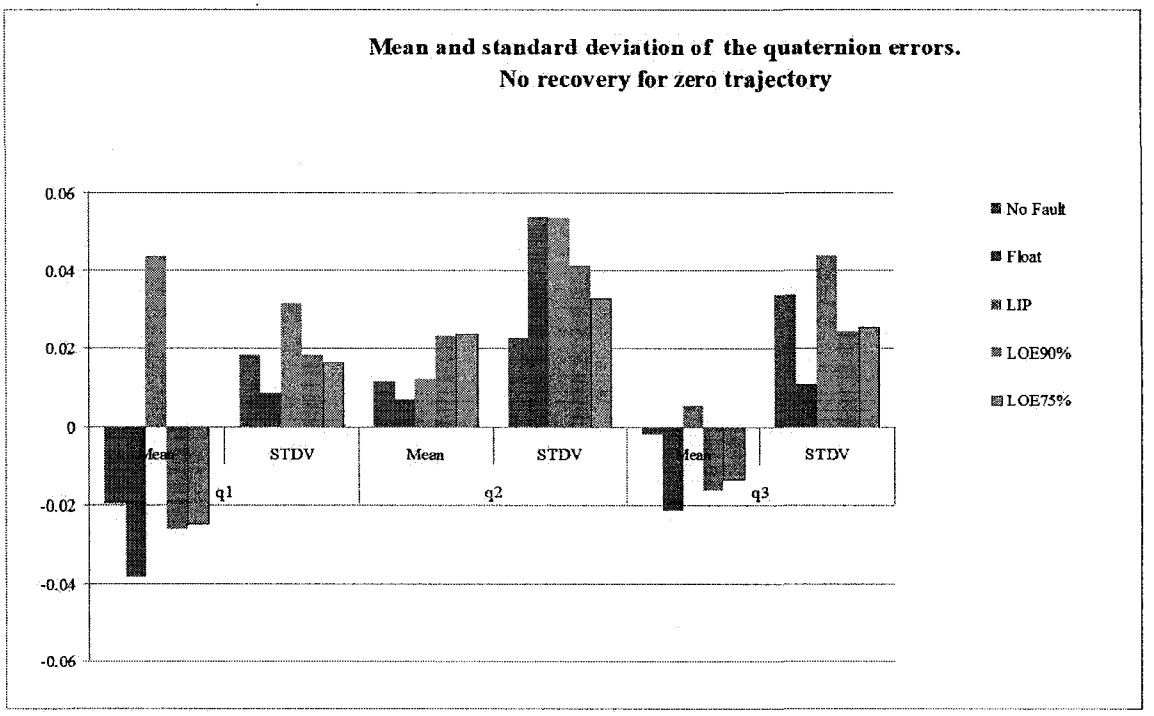

Figure 4.28: Mean and standard deviation of the quaternion errors according to Table 4.5. Satellite is following a zero reference and subject to faults without recovery.

Mean and standard deviation (Stdv) of the quaternion errors						
	q_1 **Mean**	q_1 **Stdv**	q_2 **Mean**	q_2 **Stdv**	q_3 **Mean**	q_3 **Stdv**
No Fault	-0.0198	0.0181	0.0114	0.0226	-0.0021	0.0336
Float	-0.0384	0.0086	0.0069	0.0536	-0.0213	0.0108
LIP	0.0433	0.0314	0.0121	0.0533	0.0052	0.0435
LOE 90%	-0.0261	0.0182	0.0232	0.0409	-0.0165	0.0242
LOE 75%	-0.0249	0.0164	0.0235	0.0327	-0.0137	0.0255

Table 4.5: Mean and standard deviation of quaternion errors in steady state. Healthy and faulty system following a zero reference trajectory.

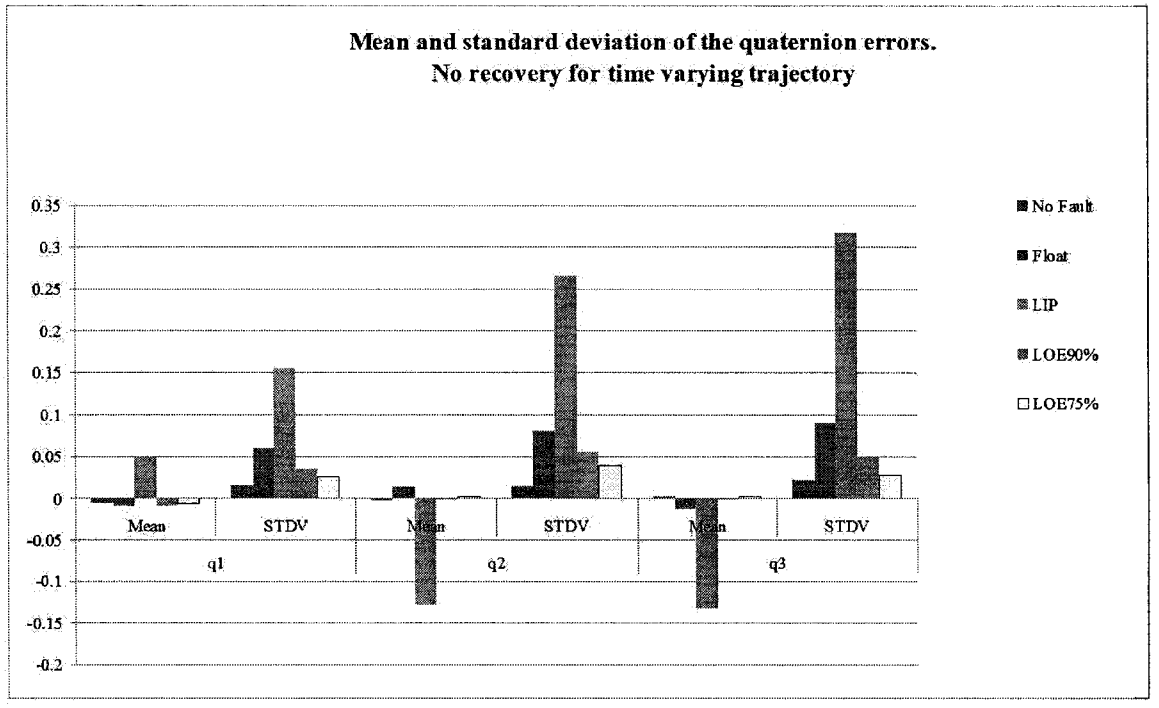

Figure 4.29: Mean and standard deviation of the quaternion errors according to Table 4.6. Satellite is following a time varying trajectory subject to faults without recovery.

Mean and standard deviation (Stdv) of the quaternion errors						
	q_1 Mean	q_1 Stdv	q_2 Mean	q_2 Stdv	q_3 Mean	q_3 Stdv
No Fault	-0.0058	0.0168	-0.0031	0.0159	0.0014	0.0217
Float	-0.0094	0.0587	0.0145	0.0804	-0.0123	0.0898
LIP	0.0501	0.1548	-0.1295	0.2649	-0.1342	0.3173
LOE 90%	-0.0095	0.0354	-0.0020	0.0561	-0.0013	0.0506
LOE 75%	-0.0061	0.0259	0.0017	0.0388	0.0018	0.0282

Table 4.6: Mean and standard deviation of the quaternion errors in steady state. Healthy and faulty satellite following a time varying trajectory.

The faults applied occur due to a failure in the magnetic torquer aligned with the X axis of the satellite's body frame. Because the impaired magnetic moment affects the total torque in orthogonal directions, this fault has a clear effect in the steady state error of the angles associated with the orthogonal to the X axis (namely q1 and q3). The largest impact in the attitude position is caused by the LIP and HO faults, followed by float and LOE. The HO fault has not been included in the figures above because an unstable behavior does not constitute a point for comparison.

4.4 Response of the Recovered Satellite From Faults

Taking into account the saturation limits that are reflected in the magnetic moment that the torquer is able to produce, the optimization solution to the control reallocation problem is constrained to lie within allowable values. For the simulation results shown below this saturation limit is calculated according to the sizing of the magnetic torquers that are explained in Sections 2.4.1 and 4.1.3.

This section presents the results for the application of the recovery mechanism that we have proposed in the previous chapter as well as a quantitative comparison that is conducted between the simulations for the system with and without the recovery scheme.

4.4.1 Constrained Recovery

By using the recovery mechanism that was proposed, the following figures are obtained from the simulations of the system that is subject to each one of the faults. It can be seen in Figures 4.30 and 4.32 that the recovery from the float fault is successful for the zero reference and the time varying reference in Figure 4.4. It is shown in Figure 4.31 that the result of the recovery action when the satellite is following the trajectory in Figure 4.3 does not lead to a bounded equilibrium.

The system has been recovered from the LIP faults for zero and time varying references. Figures 4.36 and 4.37 show that as in the case of a float, the recovery from a LIP fault when the reference is that of Figure 4.4 is successful, whereas for the input of Figure 4.3 the response is not bounded.

LOE faults have been simulated for 90% and 75% following the time varying trayectory in Figure 4.4 as shown in Figures 4.40 and 4.41, respectively. Recovery from HO faults are not shown since the recovery action is to shut down the failing actuator and to treat the system as if it were subject to a float fault.

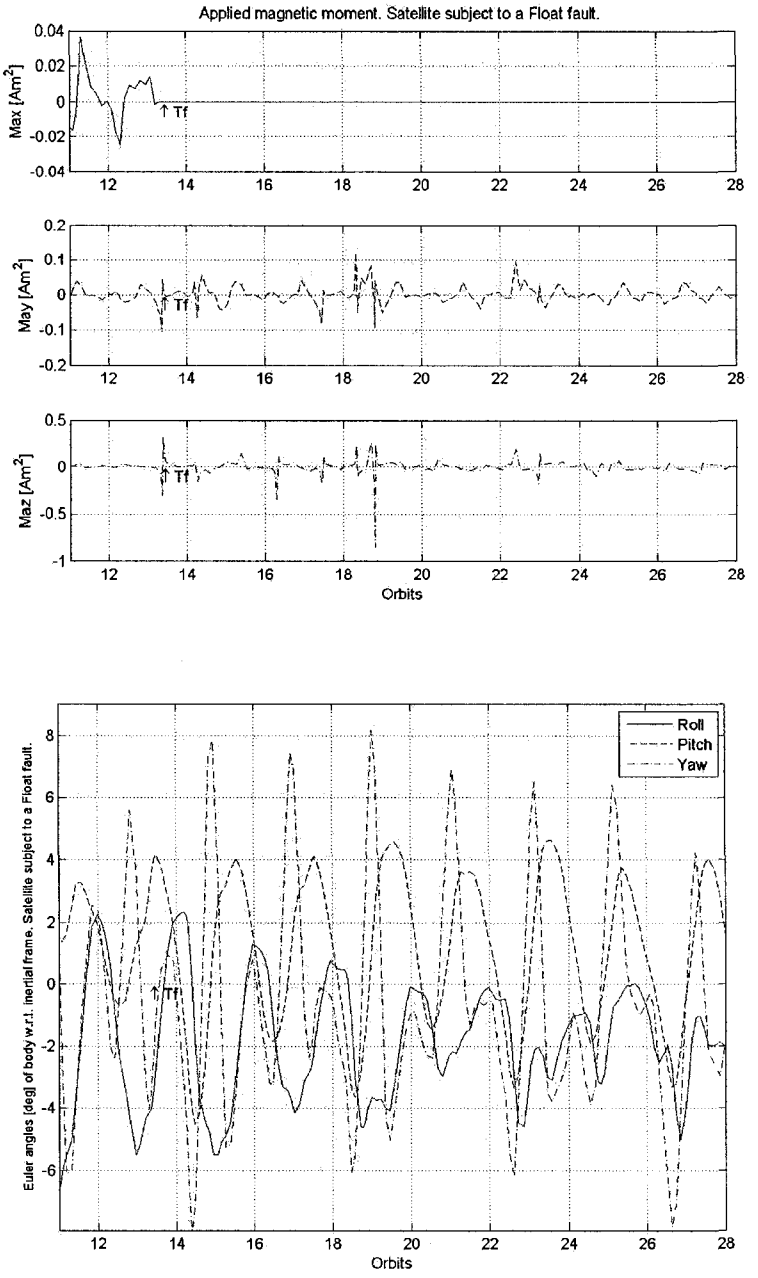

Figure 4.30: Response of the satellite following a zero reference with respect to the inertial frame. System is recovered from a float fault that is applied at time $T_f = 13$ orbits.

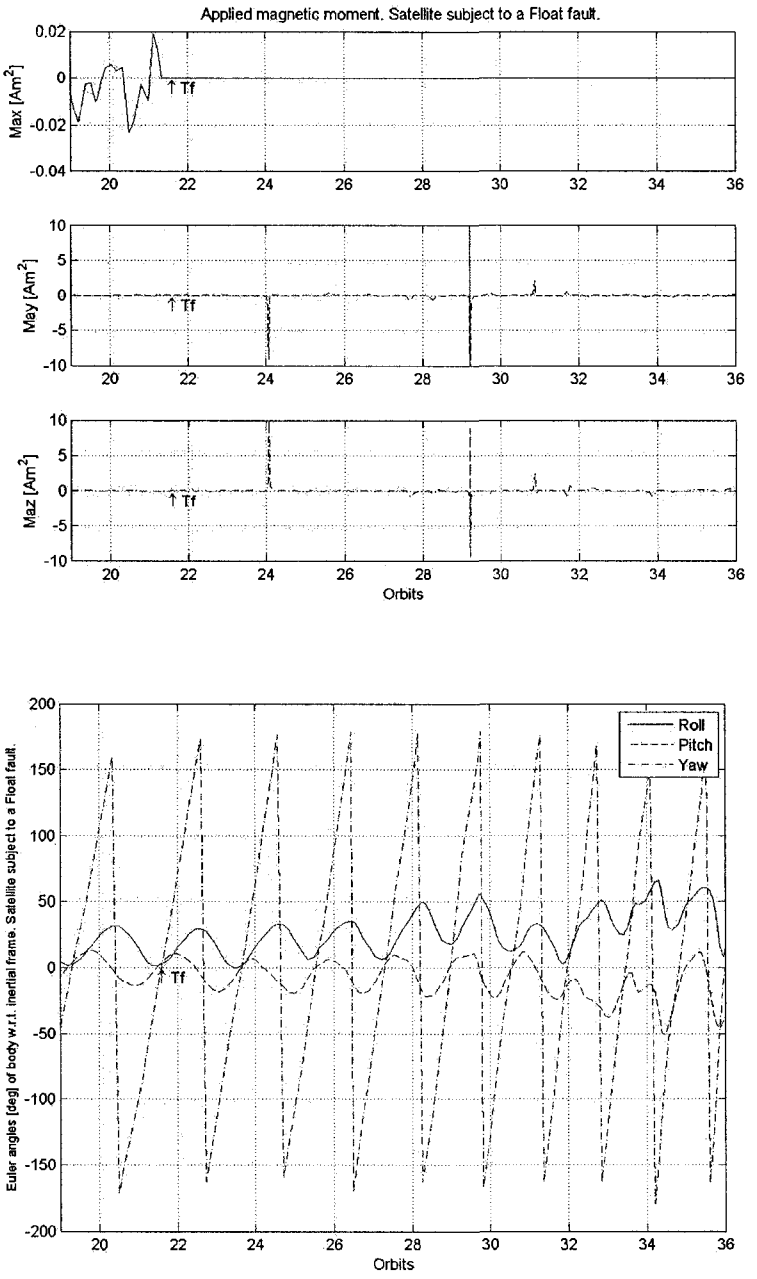

Figure 4.31: Response of the satellite following the time varying reference in figure 4.3. System is recovered from a float fault that is applied at time $T_f = 21$ orbits.

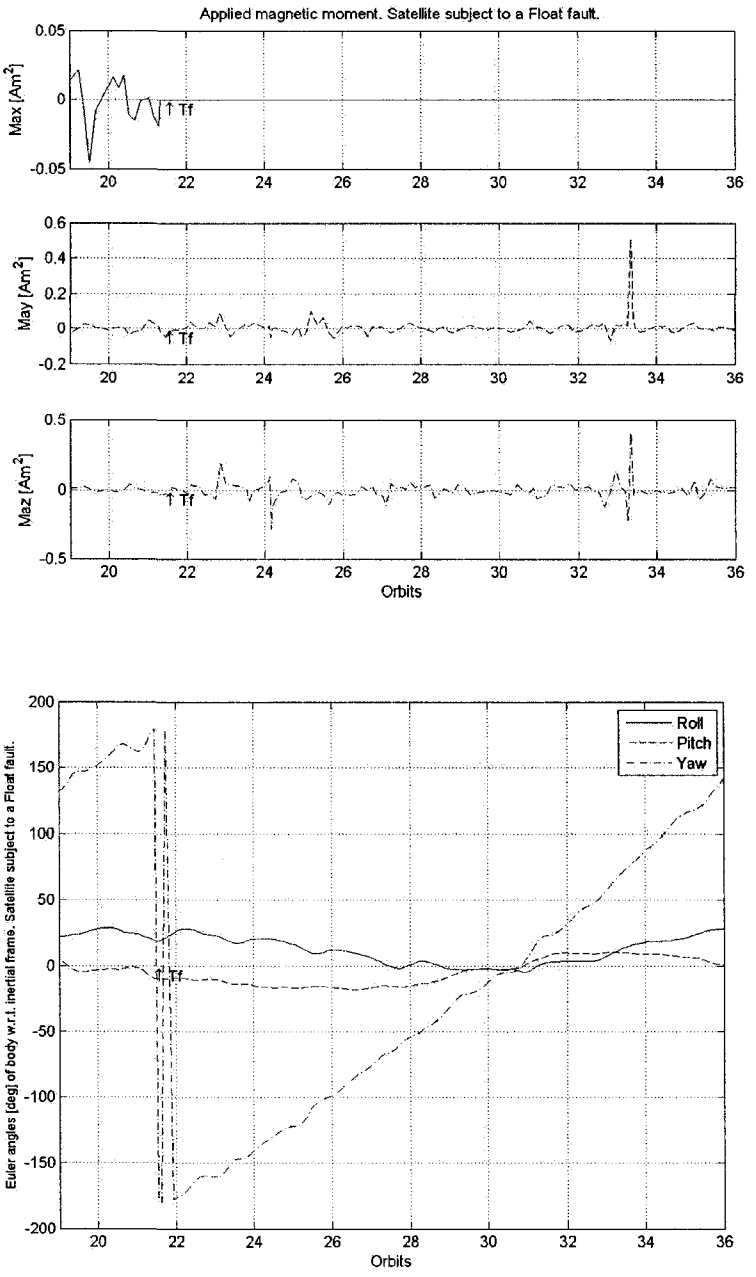

Figure 4.32: Response of the satellite following the time varying reference in Figure 4.4. System is recovered from a float fault that is applied at time $T_f = 21$ orbits.

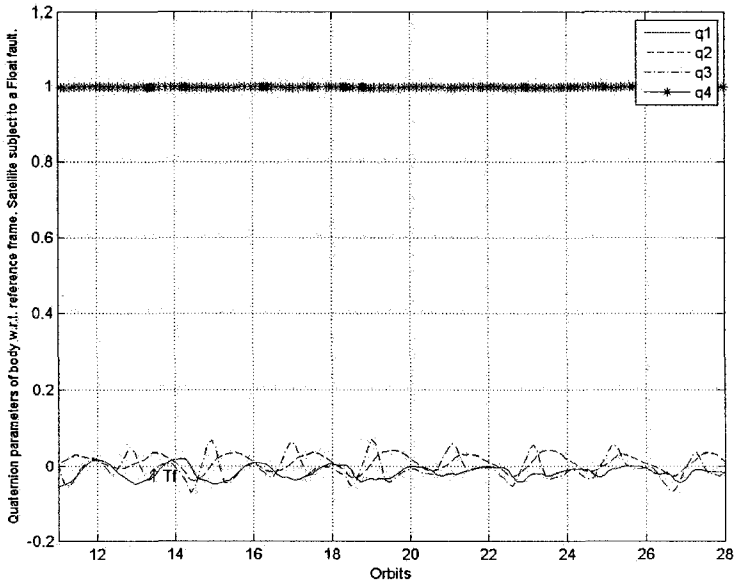

(a) Zero reference trajectory

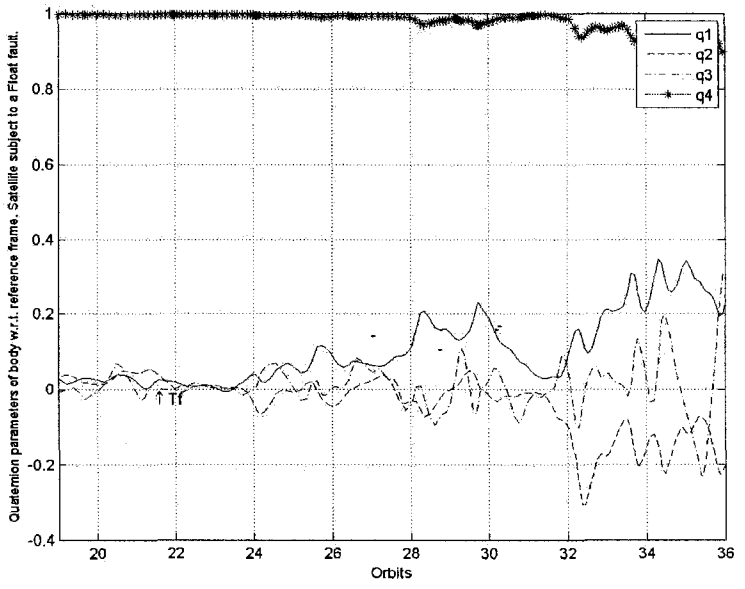

(b) Trajectory from Figure 4.3

Figure 4.33: Quaternion errors. System is recovered from a float fault that is applied at time $T_f = 13$ and $T_f = 21$ orbits, respectively.

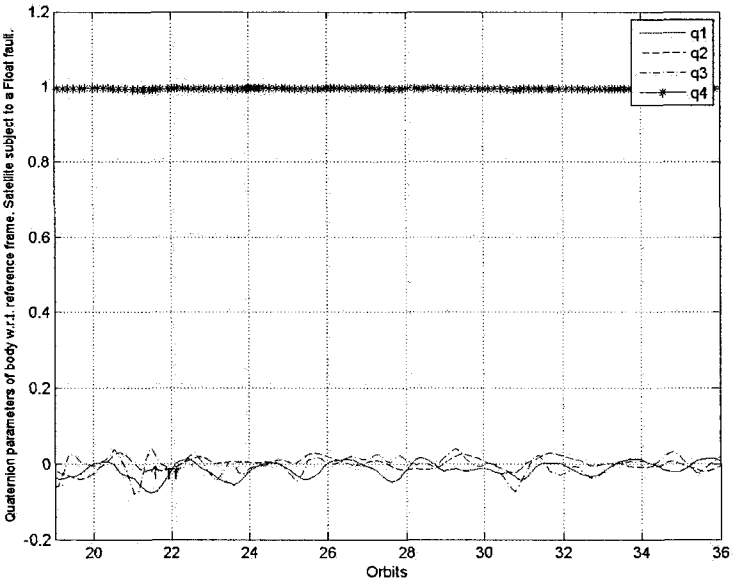

Figure 4.34: Quaternion errors of system following the trajectory from Figure 4.4. System is recovered from a float fault that is applied at time $T_f = 21$ orbits.

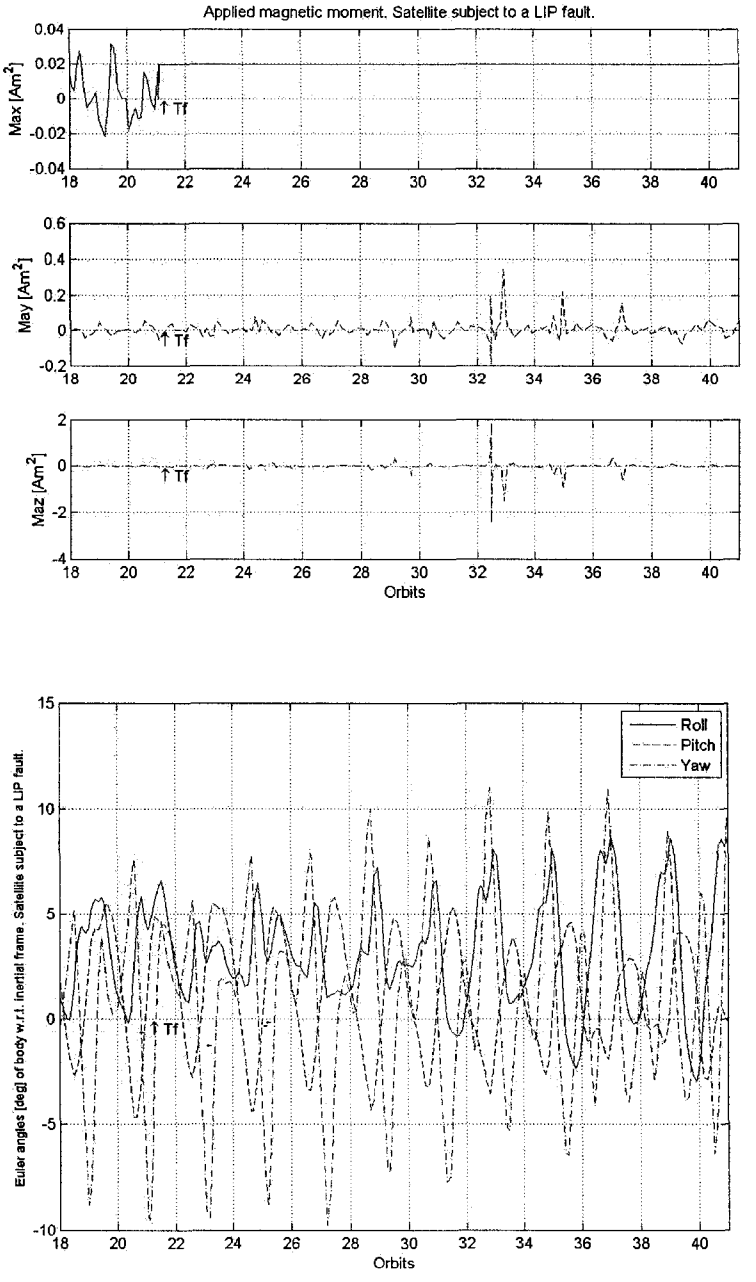

Figure 4.35: Response of the satellite following a zero reference. System is recovered from a LIP fault that is applied at time $T_f = 21$ orbits.

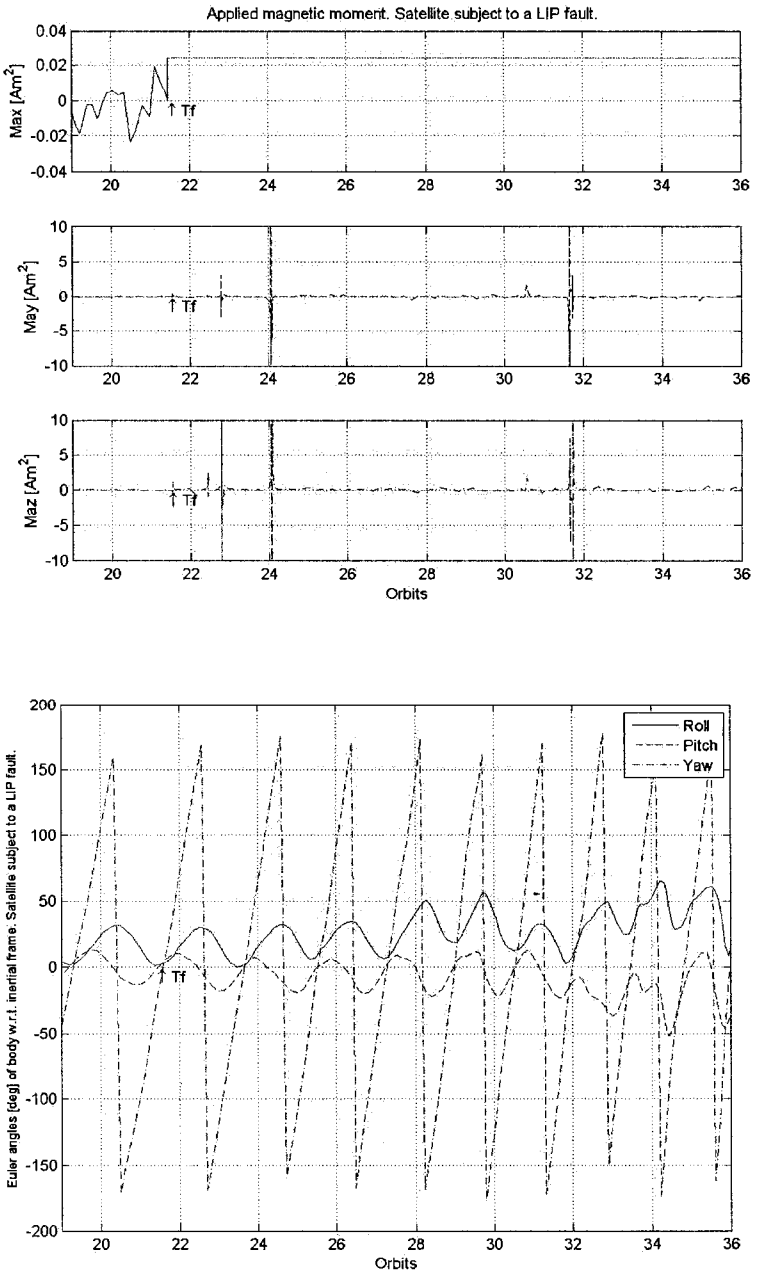

Figure 4.36: Response of the satellite following the time varying reference in Figure 4.3. System is recovered from a LIP fault that is applied at time $T_f = 21$ orbits.

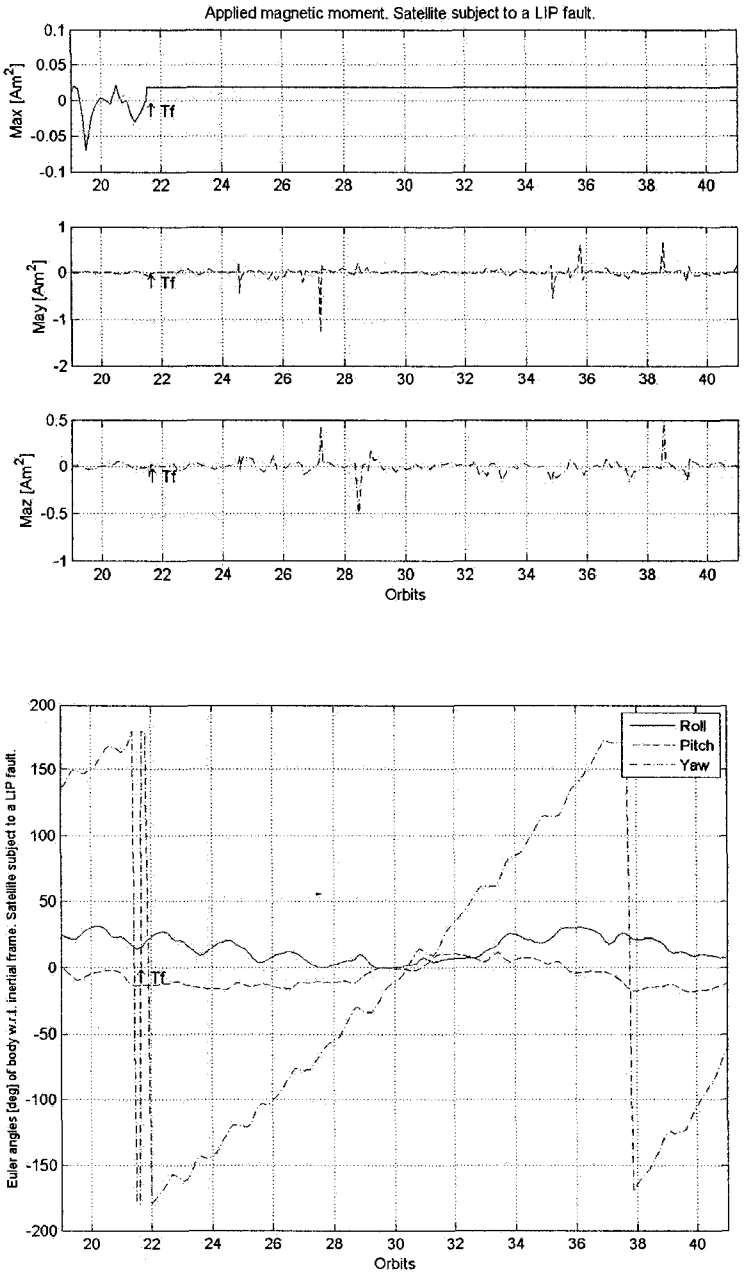

Figure 4.37: Response of the satellite following the time varying reference in Figure 4.4. System is recovered from a LIP fault that is applied at time $T_f = 21$ orbits.

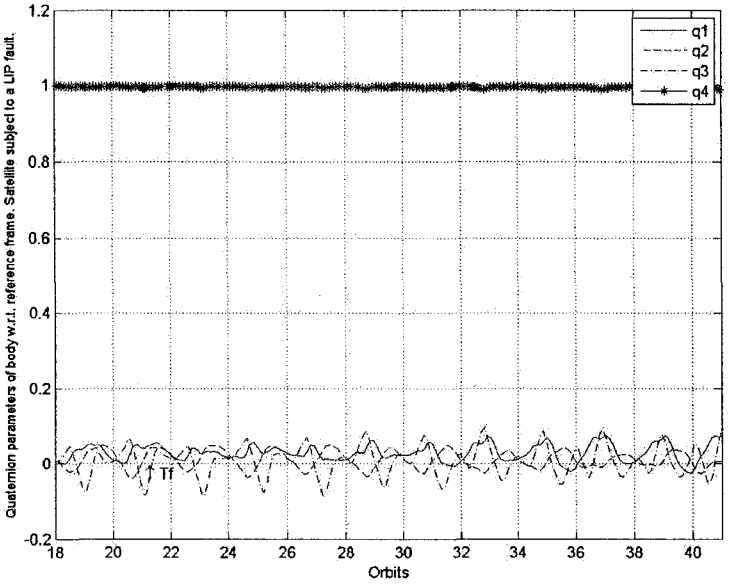

(a) Zero reference trajectory

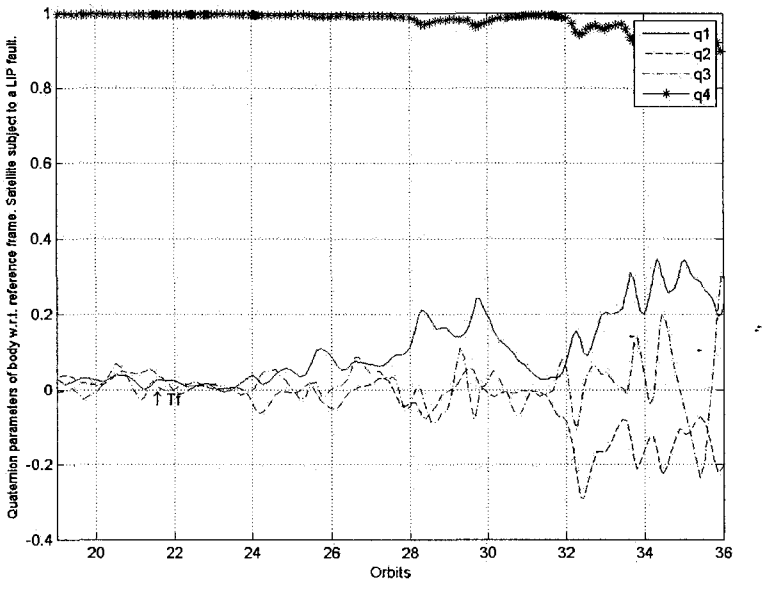

(b) Trajectory from Figure 4.3

Figure 4.38: Quaternion errors. System is recovered from a LIP fault that is applied at time $T_f = 21$ orbits.

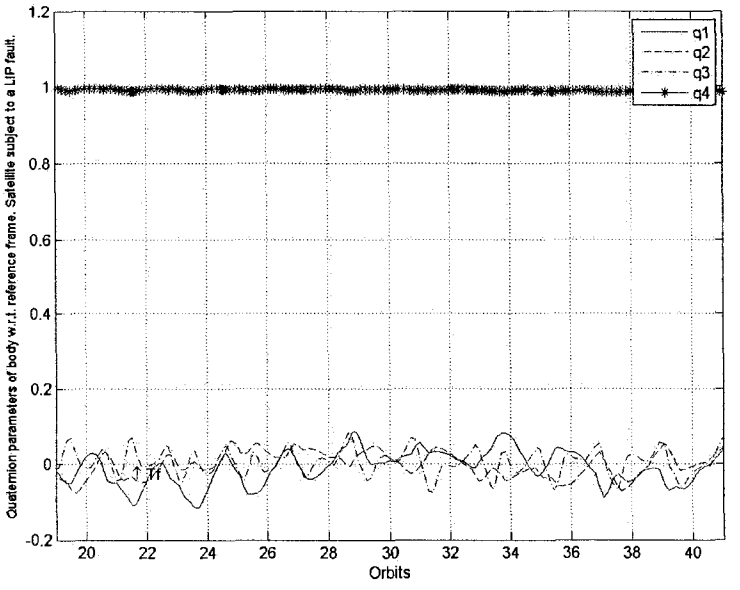

Figure 4.39: Quaternion errors of system following the trajectory from Figure 4.4. System is recovered from a LIP fault that is applied at time $T_f = 21$ orbits.

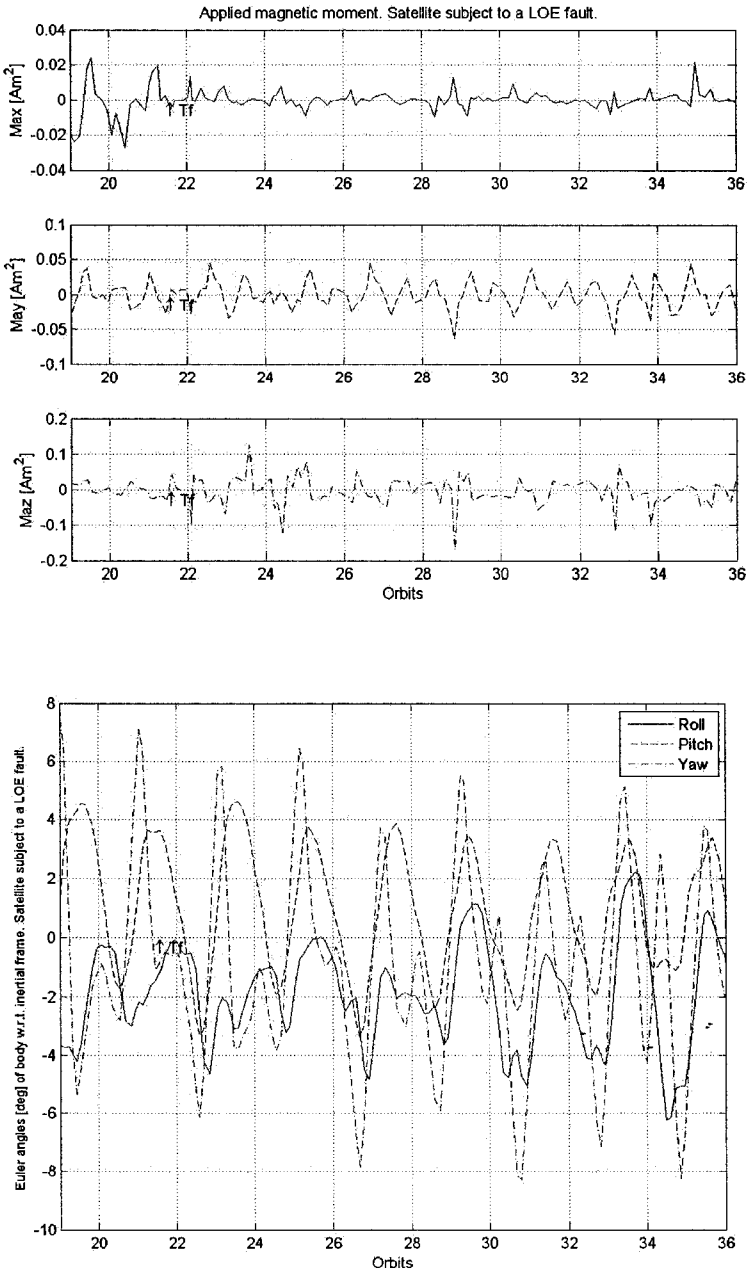

Figure 4.40: Response of the satellite following a zero reference. System is recovered from a 90% LOE fault that is applied at time $T_f = 21$ orbits.

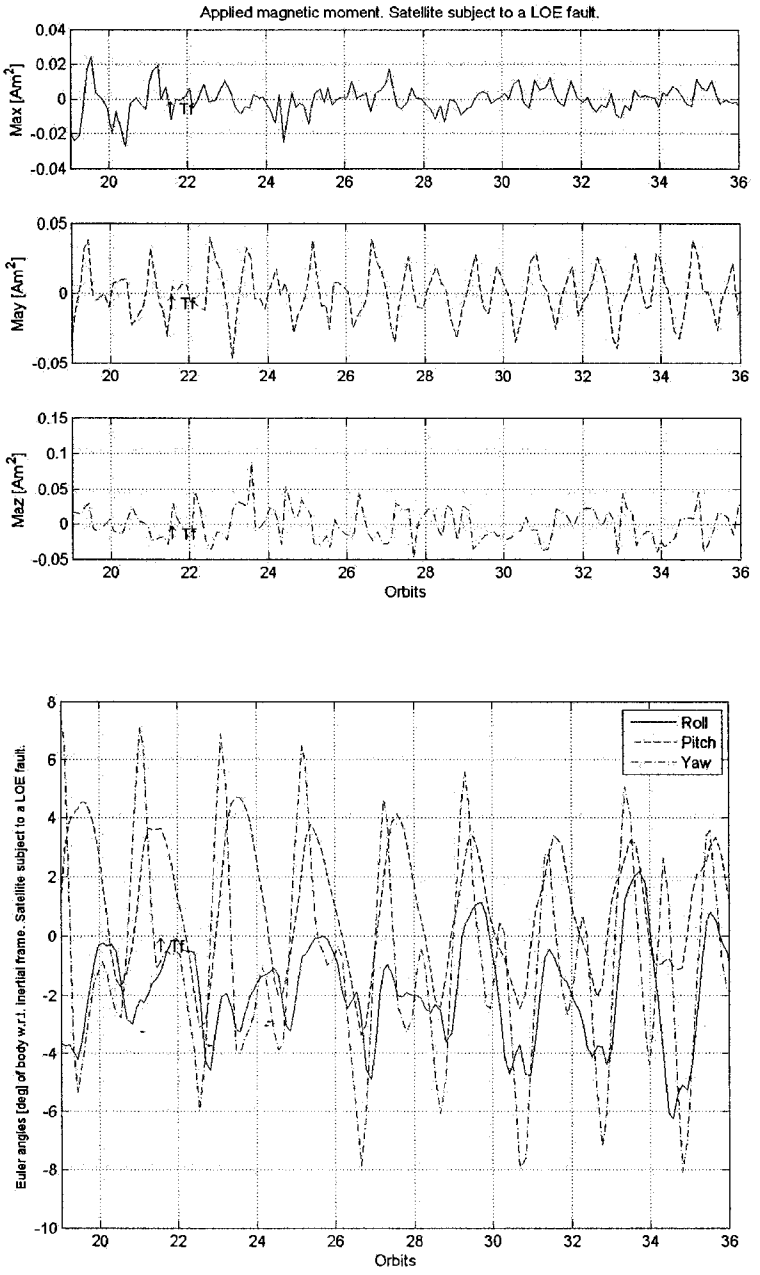

Figure 4.41: Response of the satellite following a zero reference. System is recovered from a 75% LOE fault that is applied at time $T_f = 21$ orbits.

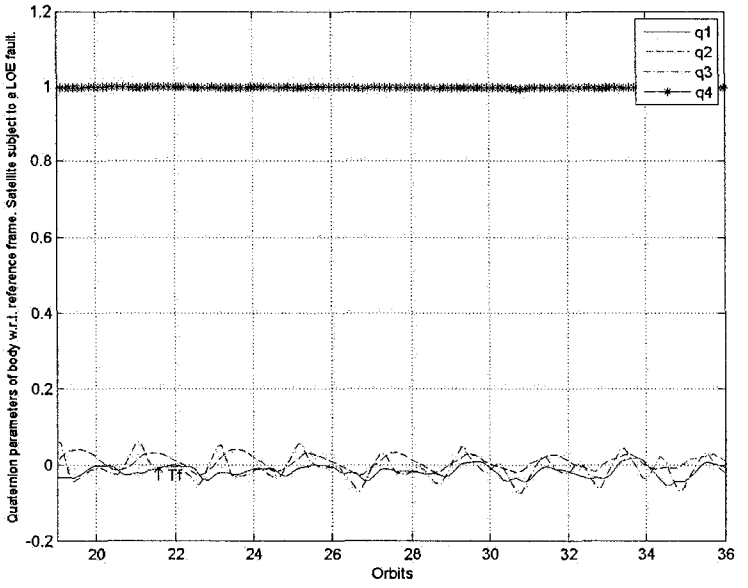

(a) System recovered from a 90% LOE fault.

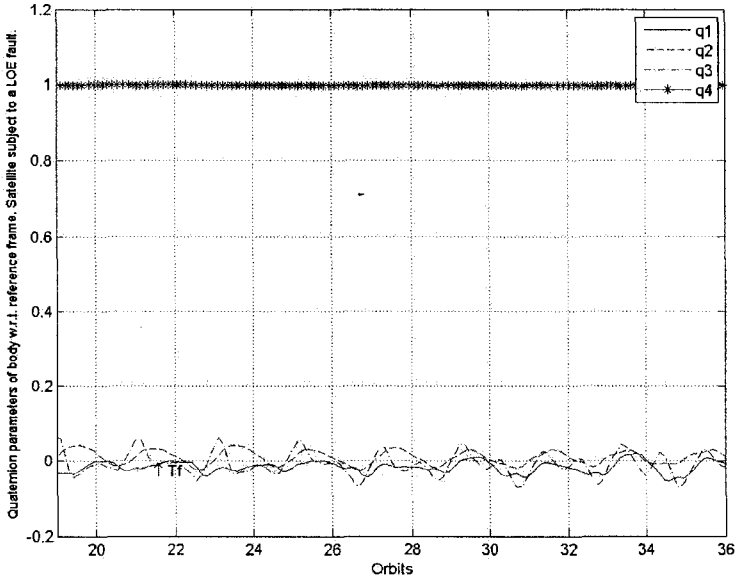

(b) System recovered from a 75% LOE fault.

Figure 4.42: Quaternion errors of system following a zero reference trajectory. System is recovered from LOE faults that are applied at time $t_f = 21$ orbits.

Tables 4.7 and 4.8 and Figures 4.44 and 4.45 show the mean and standard deviation values of the quaternion errors in steady state for zero and time varying trajectories, respectively. The results indicate, in general, that the system recovered from fault presents quaternion errors with smaller mean values for the zero and the time varying trajectories when we compare Figures 4.44 and 4.45 with the Figures 4.28 and 4.29 presented in the previous section.

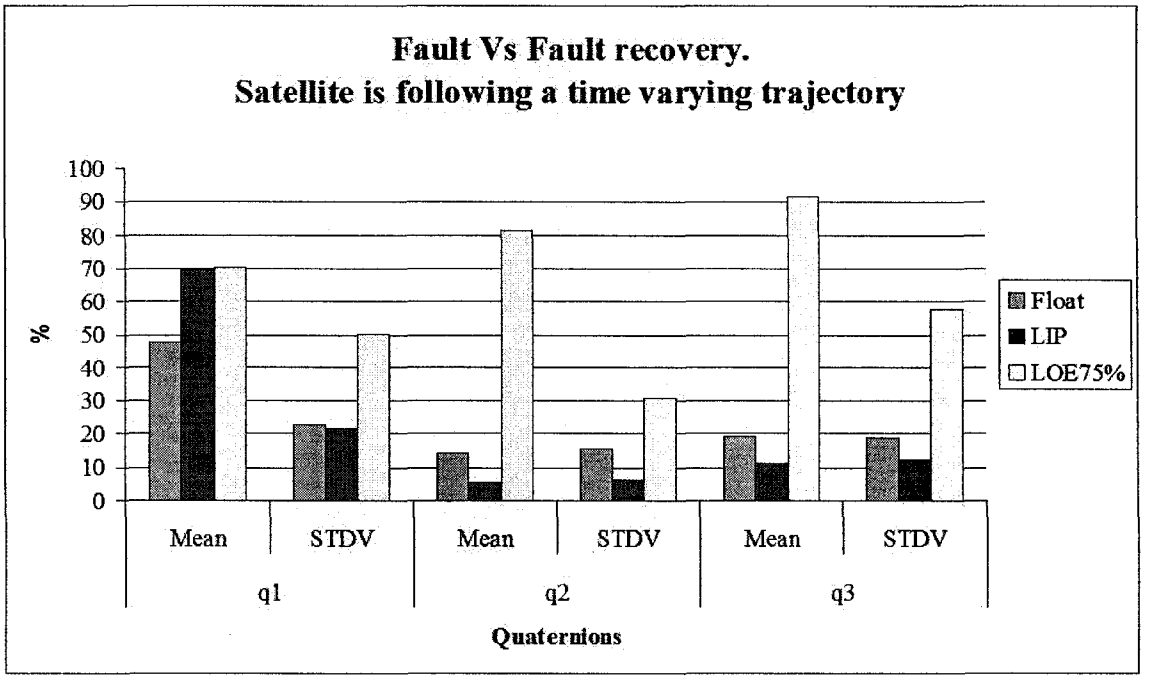

Figure 4.43: Comparison of response of the system with fault and recovered from fault. System is following a time varying reference.

The Standard deviation values in Figure Figure 4.44 are also smaller than those shown

in Figure 4.28 for the system following a zero reference trajectory. However, the performance improvement of the recovered system with respect to the faulty system is better evidenced when we compare the results in Figures 4.29 and 4.45 for the system commanded with a time varying trajectory.

Figure 4.43 shows the ratio of the response of the system that is recovered from fault and the system that is subject to fault without recovery when the system follows a time varying trajectory. In other words, the output of the system recovered from fault corresponds to the percentage of the output of the faulty system that is shown in the . The Figure allow us to see that the performance of the system recovered from fault is improved with respect to the faulty system.

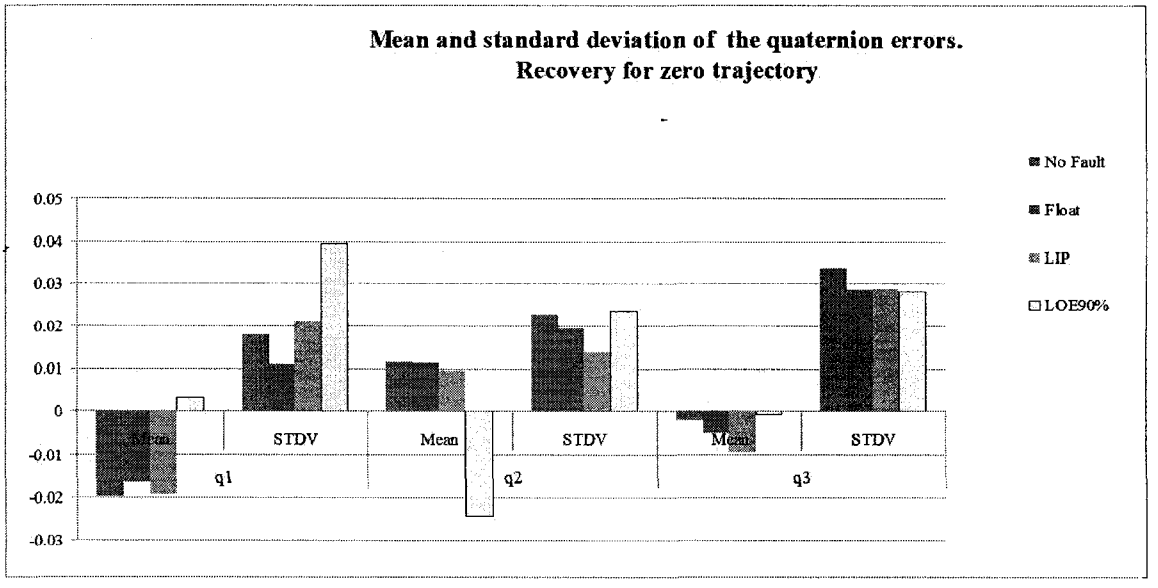

Figure 4.44: Mean and the standard deviation of the quaternion errors according to Table 4.7. Satellite is recovered from faults while following a zero reference trajectory.

Mean and standard deviation (Stdv) of the quaternion errors						
	q_1 Mean	q_1 Stdv	q_2 Mean	q_2 Stdv	q_3 Mean	q_3 Stdv
No Fault	-0.0198	0.0181	0.0115	0.0226	-0.0021	0.0336
Float	-0.0163	0.0109	0.0112	0.0194	-0.0048	0.0286
LIP	-0.0193	0.0209	0.0095	0.0140	-0.0095	0.0288
LOE 90%	0.0032	0.0394	-0.0241	0.0234	-0.0005	0.0281

Table 4.7: Mean and standard deviation of the quaternion errors in steady state. Satellite is recovered from faults while following a zero reference trajectory.

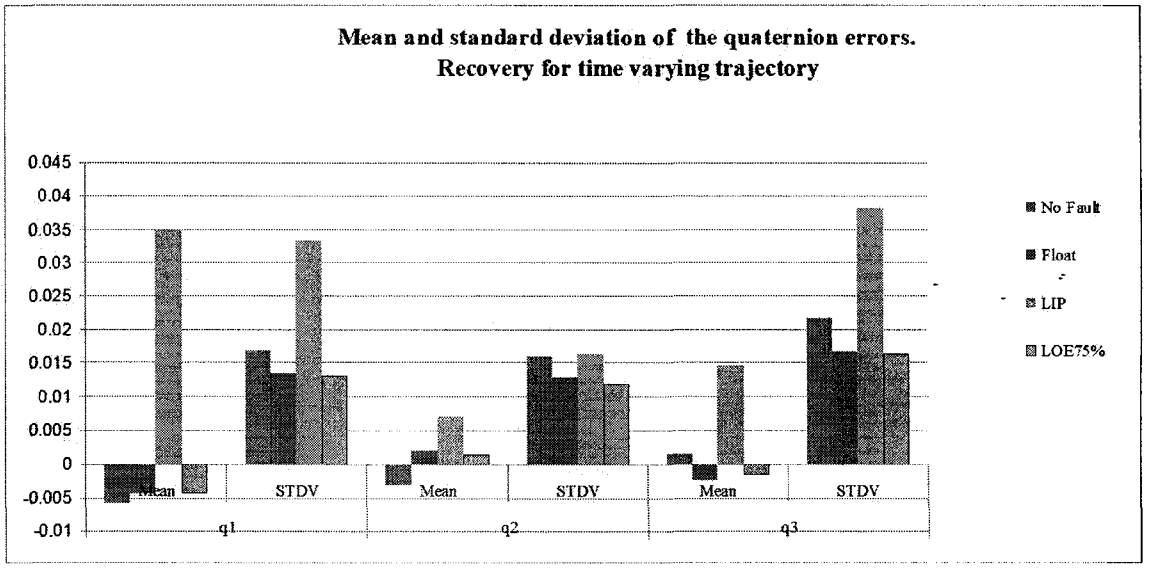

Figure 4.45: Mean and the standard deviation of quaternion errors according to Table 4.8. Satellite is recovered from faults while following a time varying trajectory.

Mean and standard deviation (Stdv) of the quaternion errors						
	q_1 **Mean**	q_1 **Stdv**	q_2 **Mean**	q_2 **Stdv**	q_3 **Mean**	q_3 **Stdv**
No Fault	-0.0058	0.0168	-0.0031	0.0159	0.0015	0.0217
Float	-0.0044	0.0134	0.0020	0.0127	-0.0024	0.0168
LIP	0.0032	0.0394	-0.0241	0.0234	-0.0005	0.0281
LOE 75%	-0.0043	0.0130	0.0014	0.0119	-0.0016	0.0163

Table 4.8: Mean and the standard deviation of quaternion errors in steady state. Satellite is recovered from faults while following a time varying trajectory.

4.4.2 Recovery From HO Fault

The HO fault can not be recovered by means of the recovery method that we have proposed since there is no solution to the constrained control reallocation for this particular case. In other words, the control effort required to overcome the forced saturation of an actuator surpasses the limited capabilities of the healthy magnetic torquers. It is suggested that since the system under float fault can be recovered, the HO failing actuator could be powered off and be considered as a float fault. Once an HO fault is detected, the action to follow will be to shut down the failing actuator and to report a float fault to the recovery system.

4.5 Effects of Delay of Fault Diagnosis in the Recovery System

The problem of delayed fault diagnosis is not addressed analytically in this thesis. However, simulations including delays in the response of the recovery are conducted in order to evaluate the response of the proposed recovery method. We have found that regardless of the applied delays of up to $5000s$ the simulated system did not become unstable under the effects of faults for the cases studied.

Simulation results show that fault detection delays in the order of up to one orbit have the consequence of larger overshoots during the transient phase of the recovery. By comparing the response of the system recovered from float at the time of the fault in Figure 4.32 and the faulty system recovered after $2,000s$ and $5,000s$ in Figures 4.46 and 4.48, respectively, it can be noticed that also the applied magnetic torques reach higher values when the fault is recovered late. A similar conclusion can be drawn for the case of an LIP fault that is recovered after $5,000s$, as shown in Figure 4.50.

In the special case of an HO fault, the response of the late-recovered system depends on the rate at which the actuator reaches saturation. The rate of change to the saturation of an HO fault was set to $0.001Am^2/s$ and to $0.005Am^2/s$ to show that the recovery was successful when invoked before and after the actuator had reached its saturation in Figures 4.52 and 4.54, respectively.

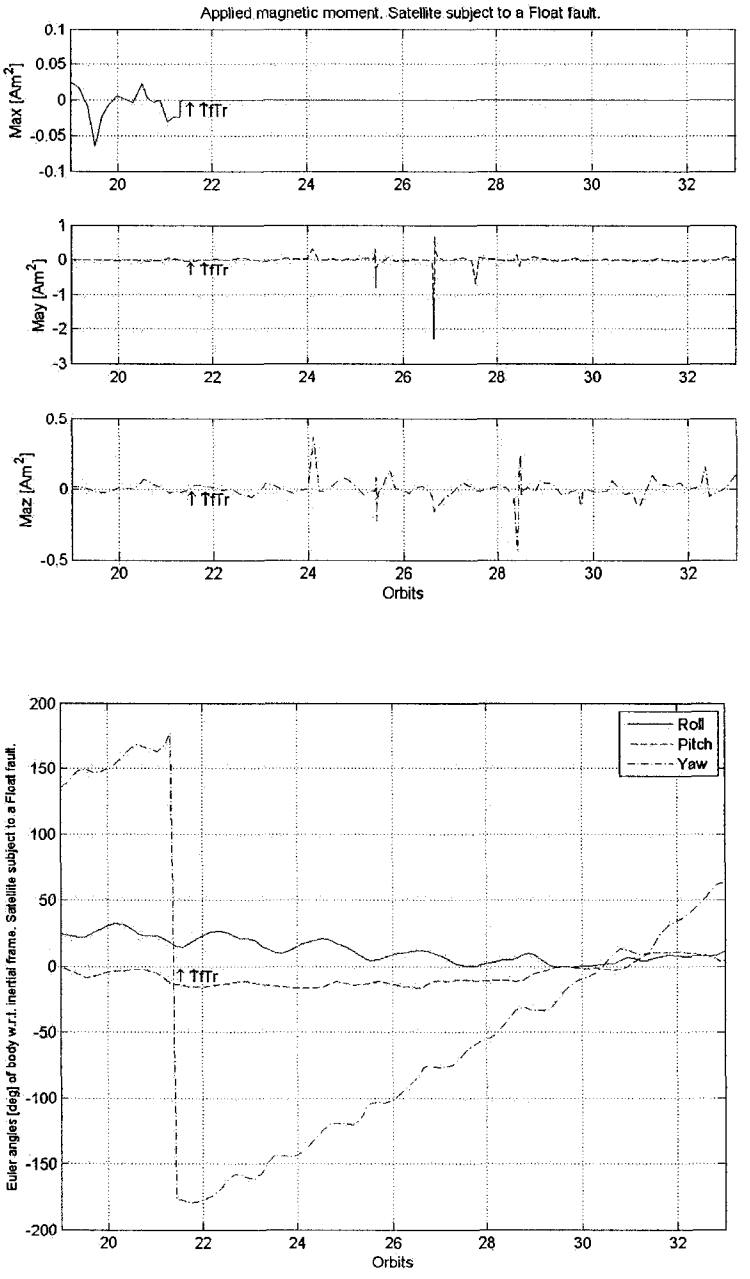

Figure 4.46: Response of the satellite that is recovered from a float fault after a 2000s delay (T_r) from the time $T_f = 21$ orbits when the fault is applied. Satellite is following the time varying reference of Figure 4.4.

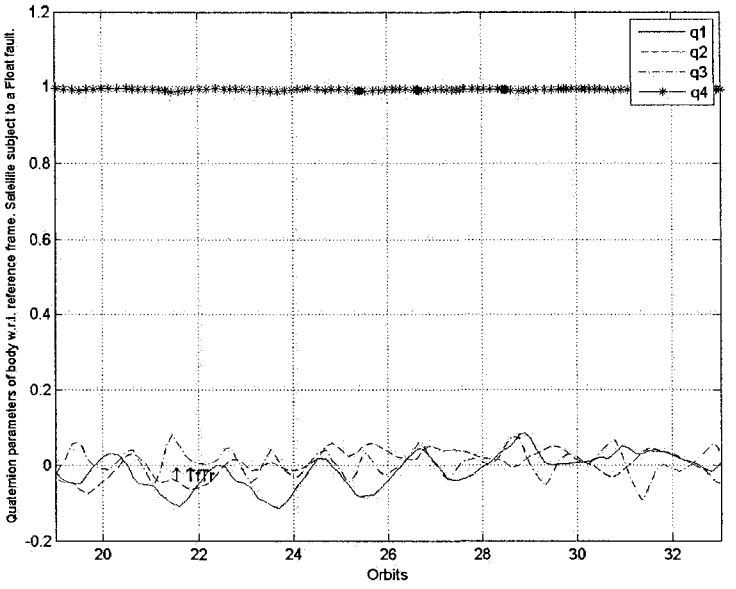

Figure 4.47: Quaternion errors. Response of the satellite that is recovered from a float fault after a 2000s (T_r) delay from the time $T_f = 21$ orbits when the fault is applied. Satellite is following the time varying reference of Figure 4.4.

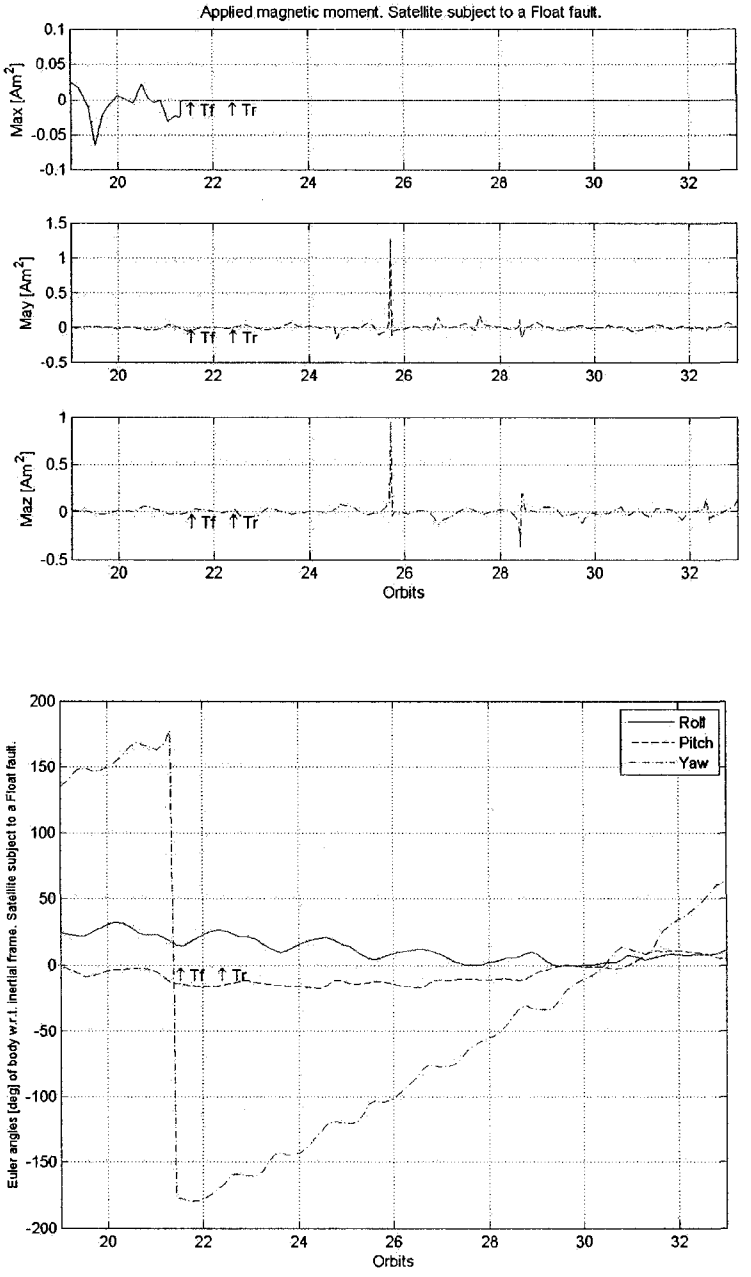

Figure 4.48: Response of the satellite that is recovered from a float fault after a 5000s delay (T_r) from the time T_f when the fault is applied. System is following the time varying trajectory of Figure 4.4.

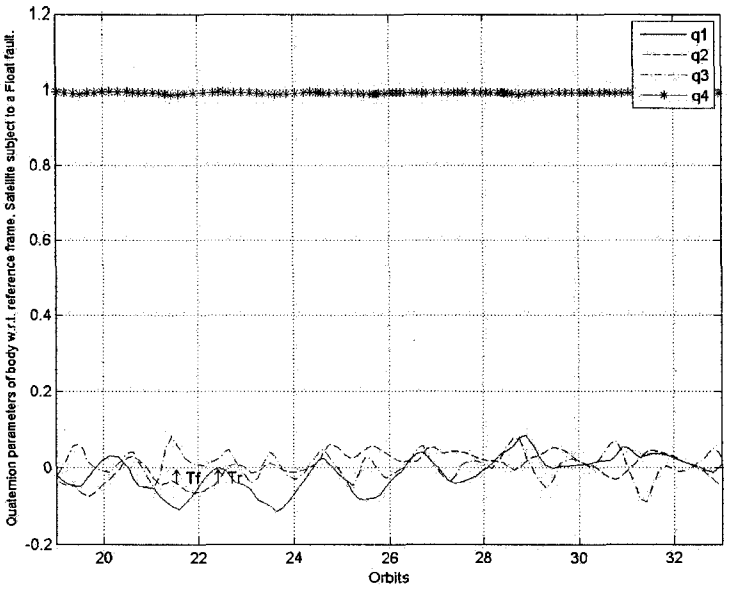

Figure 4.49: Quaternion errors. Response of the satellite that is recovered from a float fault after a 5000s delay (T_r) from the time $T_f = 21$ orbits when the fault is applied. Satellite is following the time varying reference of Figure 4.4.

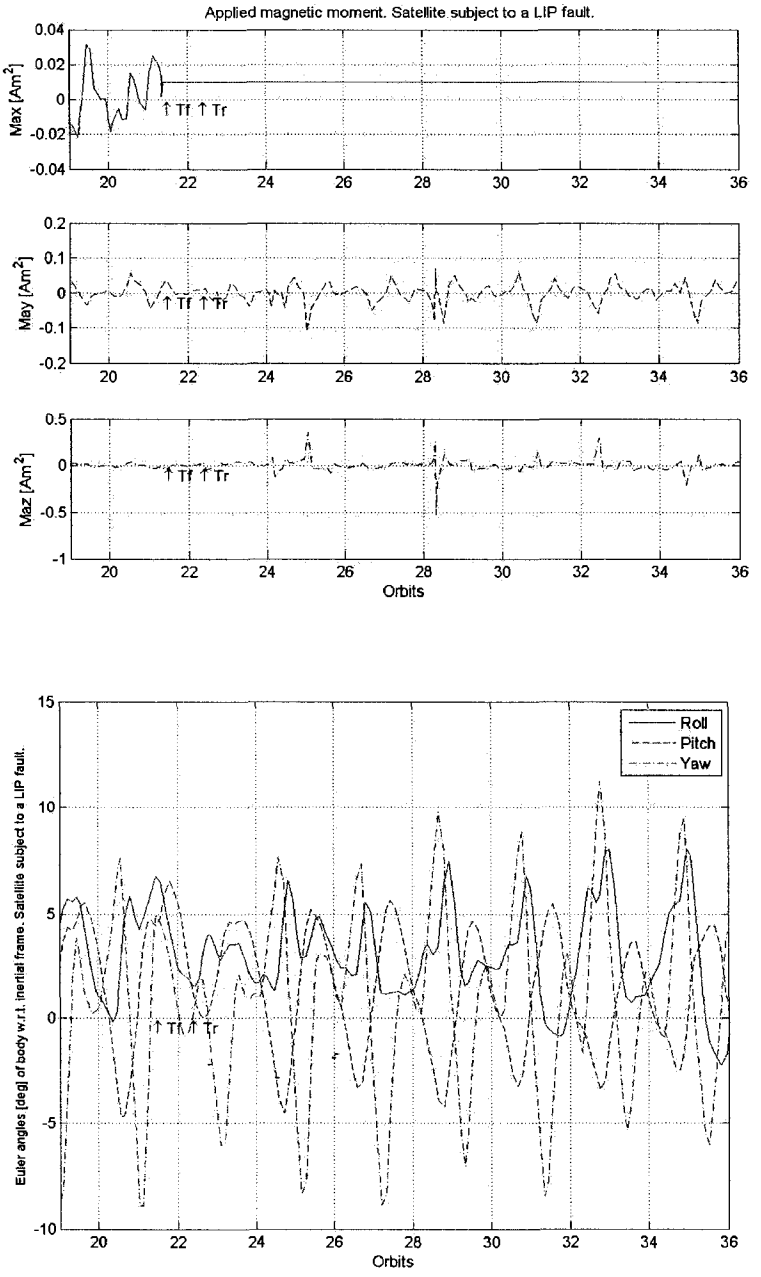

Figure 4.50: Response of the satellite that is recovered from an LIP fault after a 5000s delay (T_r) from the time $T_f = 21$ orbits when the fault is applied. Satellite is following a zero reference.

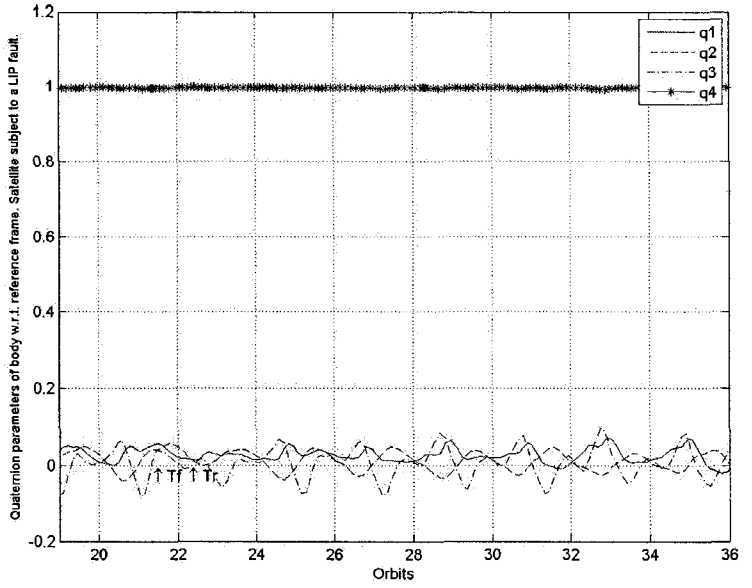

Figure 4.51: Quaternion errors. Response of the satellite that is recovered from an LIP fault after a 5000s delay (T_r) from the time $T_f = 21$ orbits when the fault is applied. Satellite is following a zero reference.

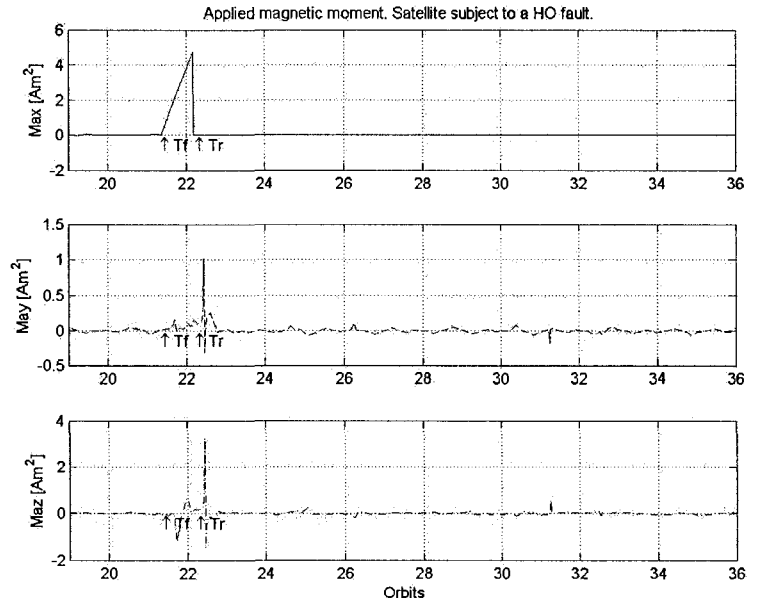

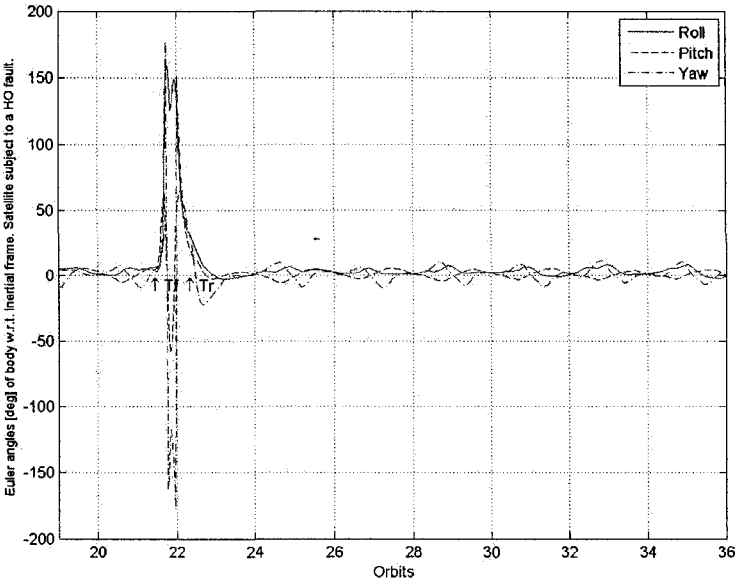

Figure 4.52: Response of the satellite that is recovered from an HO fault (with a $0.001 Am^2/s$ rate of change) after a 5000s delay (T_r) from the time $T_f = 21$ orbits when the fault is applied. Satellite is following a zero reference.

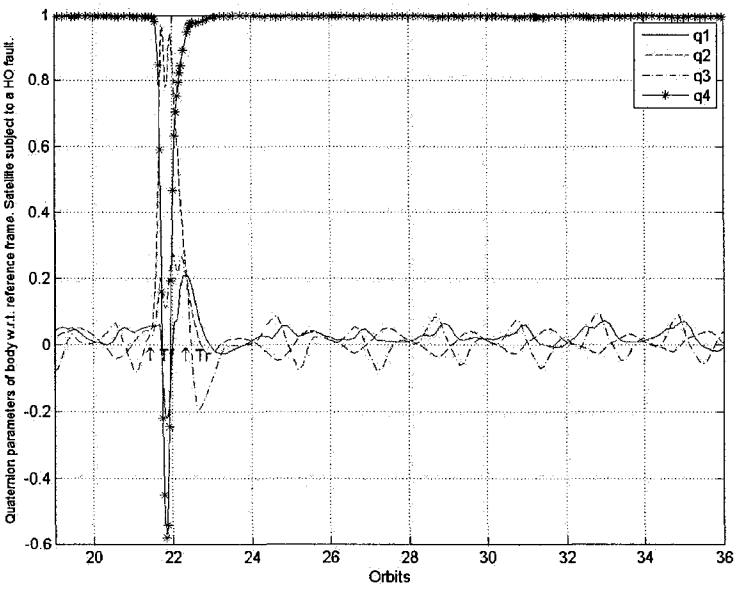

Figure 4.53: Quaternion errors. Response of the satellite that is recovered from an HO fault (with a $0.001 Am^2/s$ rate of change) after a 5000s delay (T_r) from the time $T_f = 21$ orbits when the fault is applied. Satellite is following a zero reference.

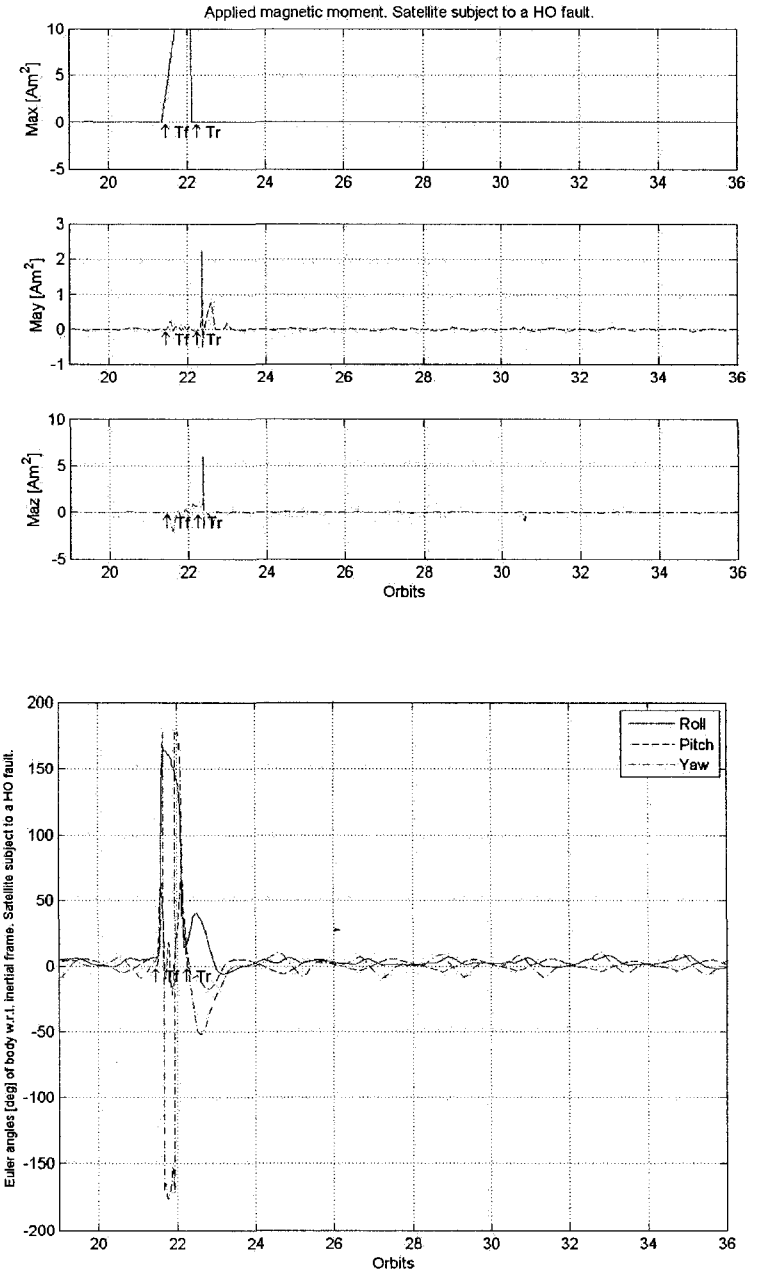

Figure 4.54: Response of the satellite that is recovered from an HO fault (with a $0.005 Am^2/s$ rate of change) after a 4500s (T_r) delay from the time $T_f = 21$ orbits when the fault is applied. Satellite is following a zero reference.

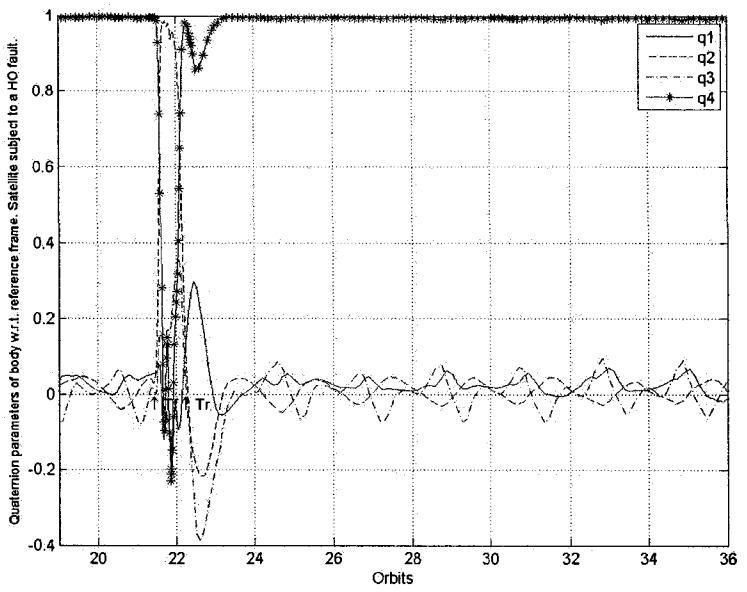

Figure 4.55: Quaternion errors. Response of the satellite that is recovered from an HO fault (with a $0.005 Am^2/s$ rate of change) after a 4500s (T_r) delay from the time $T_f = 21$ orbits when the fault is applied. Satellite is following a zero reference.

4.6 Recovery of the System that is Subject to Faults and Measurement Noise

The question of the effect of measurement noise arises due to the high importance of the value of the magnetic field for the calculation of the control action. The analytical discussion of this particular issue is beyond the scope of this thesis but for the sake of completeness the typical noise characteristics of the measurement signal from the magnetometer used in the sample satellite were investigated. Furthermore, simulations corresponding to the response of the system following a zero trajectory under normal conditions was carried out and compared to the response of the system recovered from a float fault, including the effect of noise in the magnetic field signal.

The authors in [60] state that the Ørsted satellite is equiped with two types of high precision magnetometers: a fluxgate magnetormer in charge of measuring the three vector components of the magnetic field and one overhauser magnetometer, which measures the absolute magnetic field strength and was intended mainly for intercalibration purposes. Considering then, that the fluxgate magnetometer would feed the attitude control system with the magnetic field data, the simulations below include the noise characteristics of this type of sensor according to [61].

By comparing the results of the performance of the system under normal conditions with and without presence of measurement noise, it can be seen that the steady state errors of the system that is subject to noise in the measurement of the magnetic field are larger.

The figure Figure 4.56 shows the proportion of the errors of the system with respect to those of the system that is subject to measurement noise.

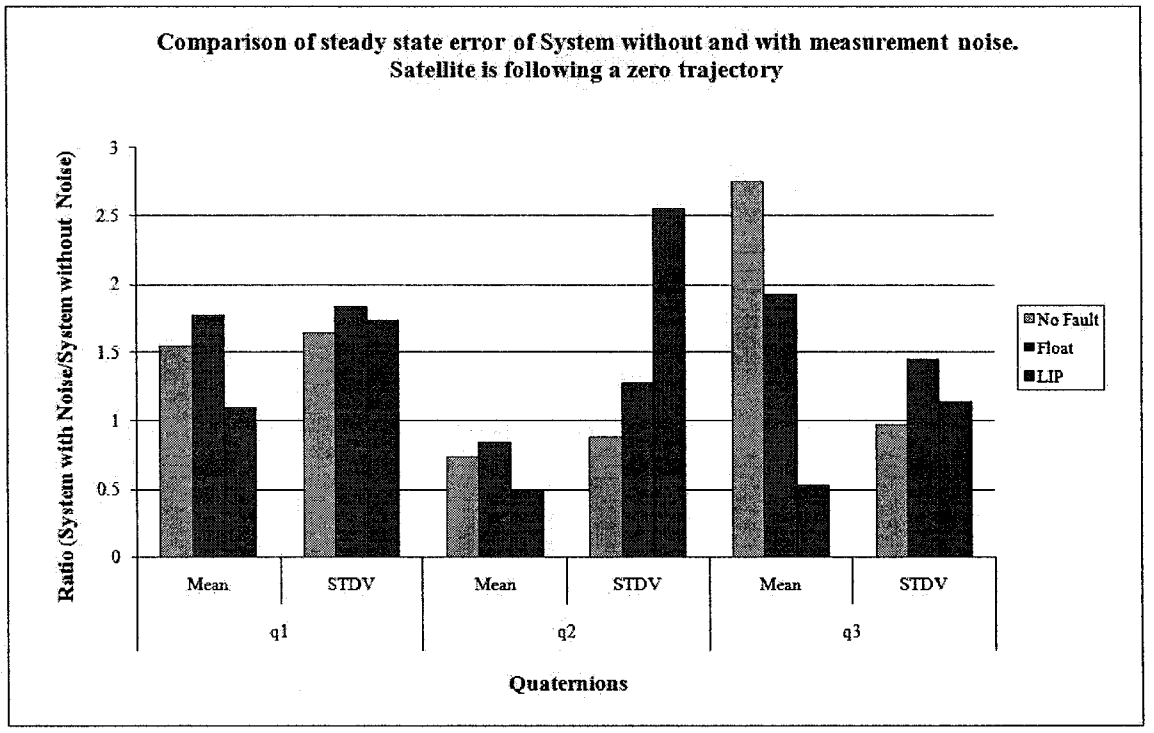

Figure 4.56: Comparison of steady state errors of system without and with measurement noise. System is following a zero trajectory.

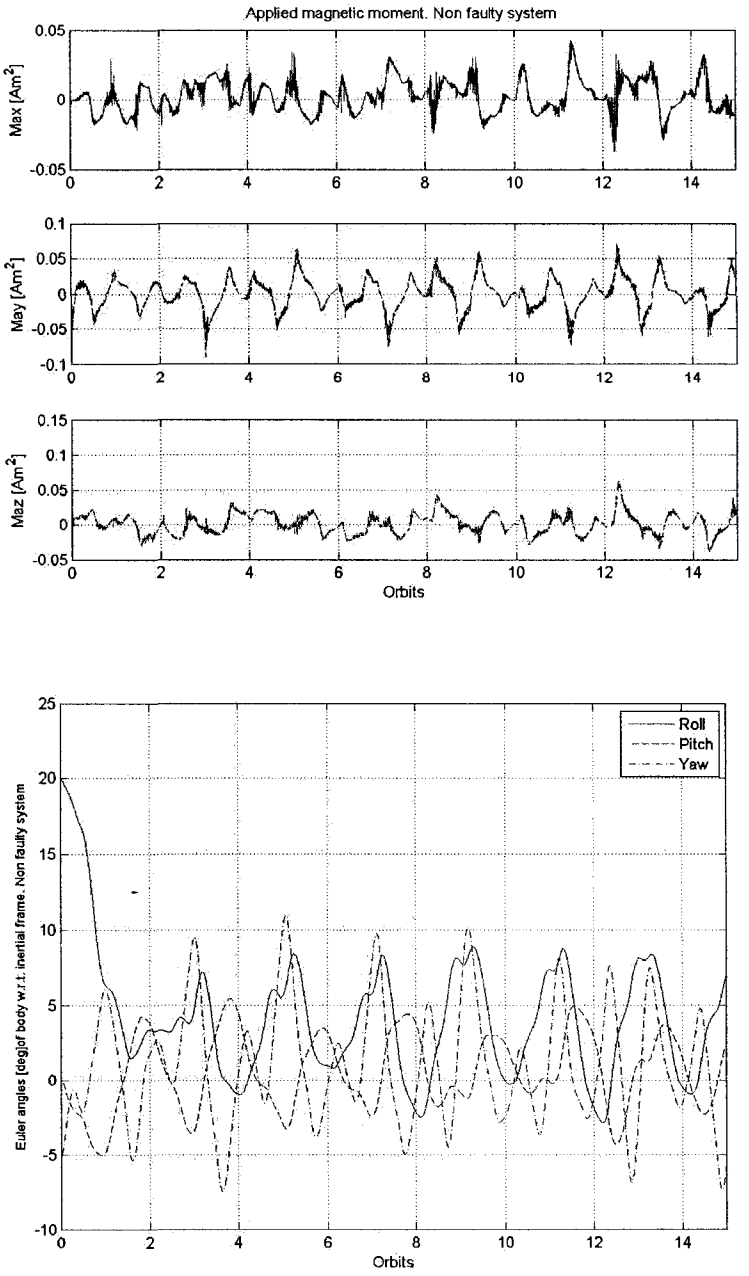

Figure 4.57: Response of the satellite under normal conditions that is subject to measurement noise from the magnetometers. Satellite is following a zero reference.

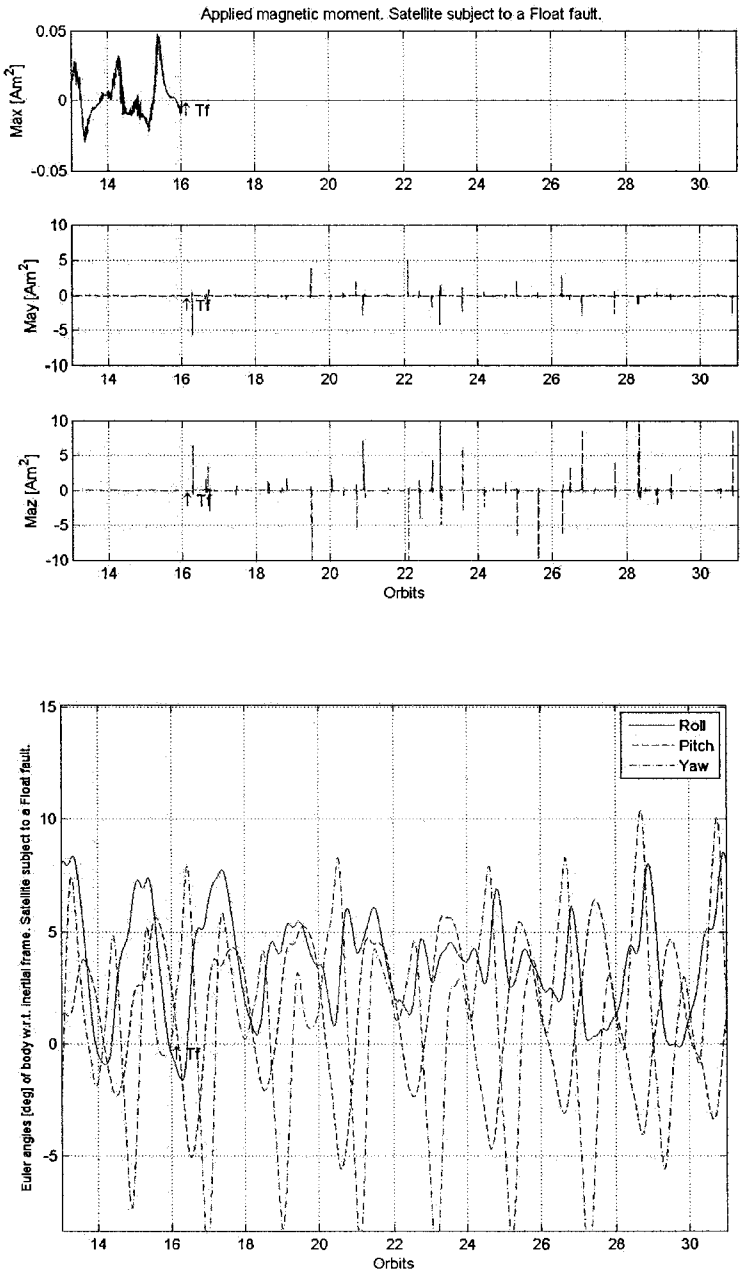

Figure 4.58: Response of the satellite under normal conditions that is subject to measurement noise from the magnetometers. Satellite is following a zero reference.

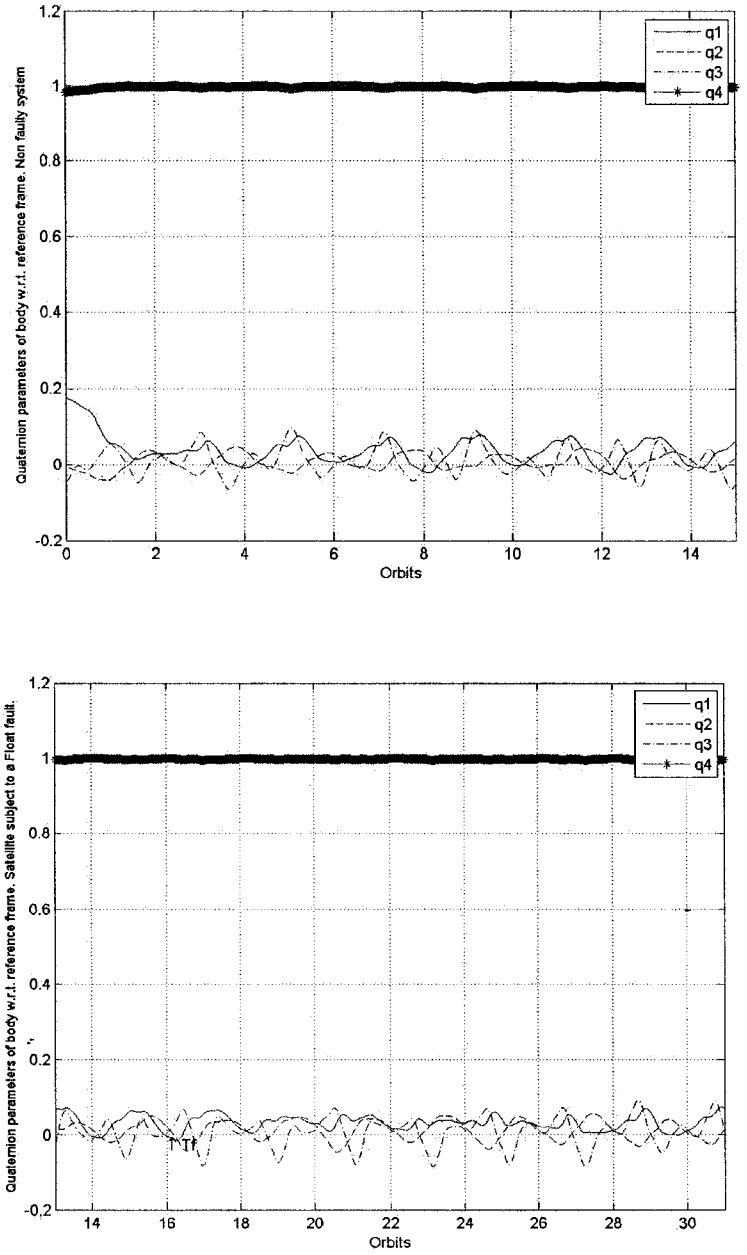

Figure 4.59: Quaternion errors. Response of the satellite under normal conditions and satellite that is recovered from a float fault that is applied at time T_f = orbits. Satellite is following a zero reference.

4.7 Recovery From Concurrent Faults

It is not possible to reallocate the control effort under all types of fault when a second fault appears. Due to the saturation moment restriction of the actuators, and the limited capability of the faulty magnetic torquers, a recovery without hardware redundancy may not be applicable. Nevertheless, the effects of the second fault in the system and the application of our proposed solution is evaluated in this section and simulation results are included.

Concurrent faults refer to non-simultaneous occurring faults. With this in mind, during the presence of one fault if a second fault occurs the recovery mechanism should reallocate the control effort within the capable actuators. For this purpose, an algorithm is implemented which applies the same optimization technique to reallocate the magnetic moment in order to have the resulting torque approximate the required control torque.

When a float, LIP or HO fault occurs, the magnetic moment from the actuator becomes fixed. In the case of an HO fault, the only choice that is available is to interrupt the circulation of the current in the coils of the saturated torquer. Nevertheless, under an LOE fault, it is possible to obtain a magnetic moment that is proportional (the multiplying factor is the loss of effectiveness gain) to the control input yielding a degree of freedom that is available for control regardless of the fault. Assuming that only two of the three actuators are subject to faults and that one of these faults is an LOE fault, the control effort can still be reallocated using the procedure that was developed in the previous chapter.

The Figures 4.60 and 4.61 show the case of 90% LOE faults ocurring at times $T_{f1} = 21$ orbits and at $T_{f2} = 43$ orbits in the actuators aligned to the X and Y axes, respectively. Figures 4.62 and 4.63 show the response of the system recovered from the avobe mentioned faults.

The second scenario that is presented in Figures 4.64 and 4.65 is the occurrence of a 75% LOE fault at $T_{f1} = 21$ orbits, followed by a LIP fault at time $T_{f2} = 43$ orbits. The corresponding response of the recovered system is shown in Figures 4.66 and 4.67.

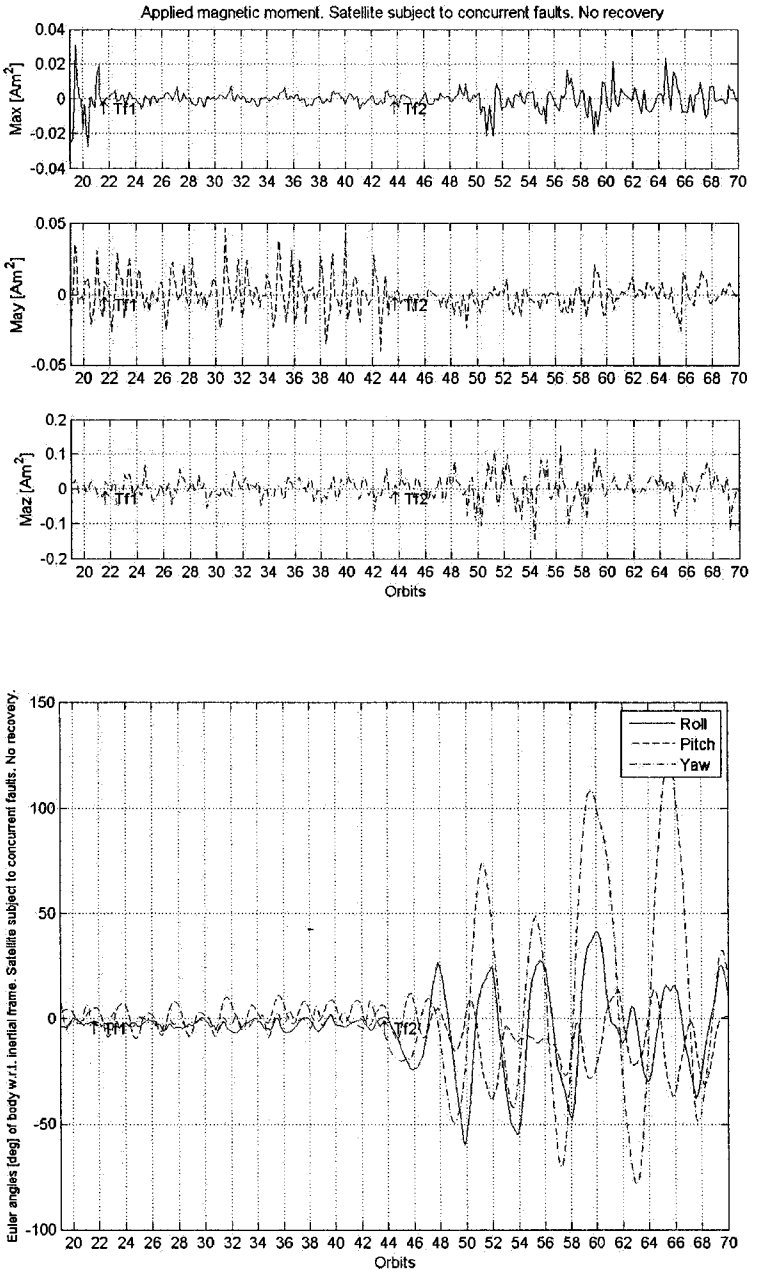

Figure 4.60: Response of the satellite that is subject to 90% LOE faults that are applied at times $T_{f1} = 21$ orbits and $T_{f2} = 43$ orbits in the torquers alligned to the X and Y axis, respectively. Satellite is following a zero reference.

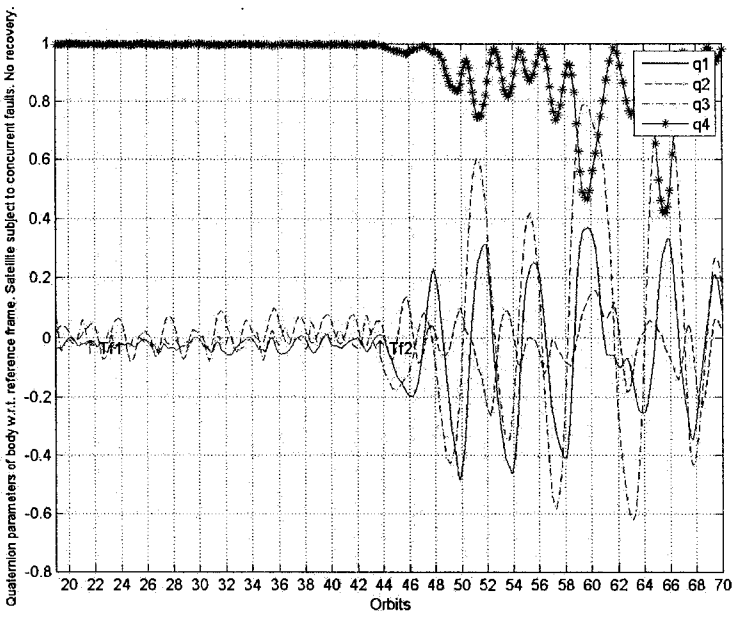

Figure 4.61: Quaternion errors. Response of the satellite that is subject to 90% LOE faults that are applied at times $T_{f1} = 21$ orbits and $T_{f2} = 43$ orbits in the torquers alligned to the X and Y axis, respectively. Satellite is following a zero reference.

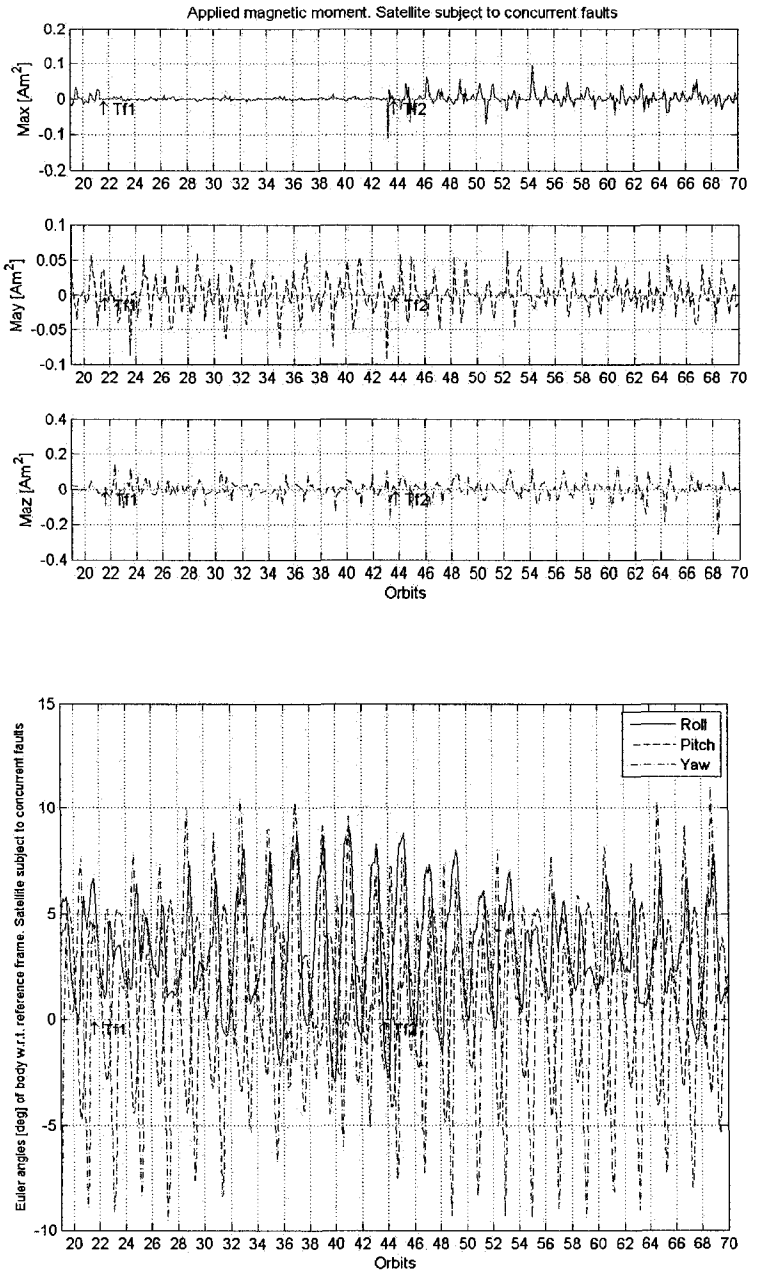

Figure 4.62: Response of the satellite that is recovered from 90% LOE faults that are applied at times $T_{f1} = 21$ orbits and $T_{f2} = 43$ orbits in the torquers alligned to the X and Y axis, respectively. Satellite is following a zero reference.

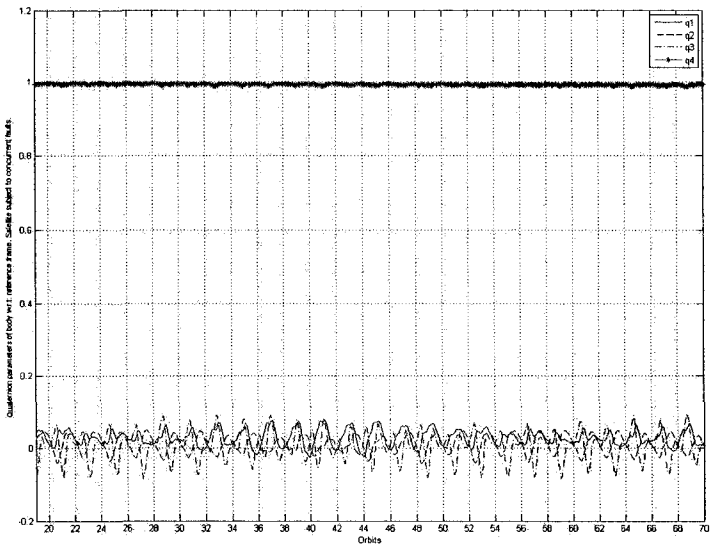

Figure 4.63: Quaternion errors. Response of the satellite that is recovered from a 90% LOE fault at time $T_{f1} = 21$ orbits and a second LOE of 90% at time $T_{f2} = 43$ orbits in the torquers alligned to the X and Y axis, respectively. Satellite is following a zero reference.

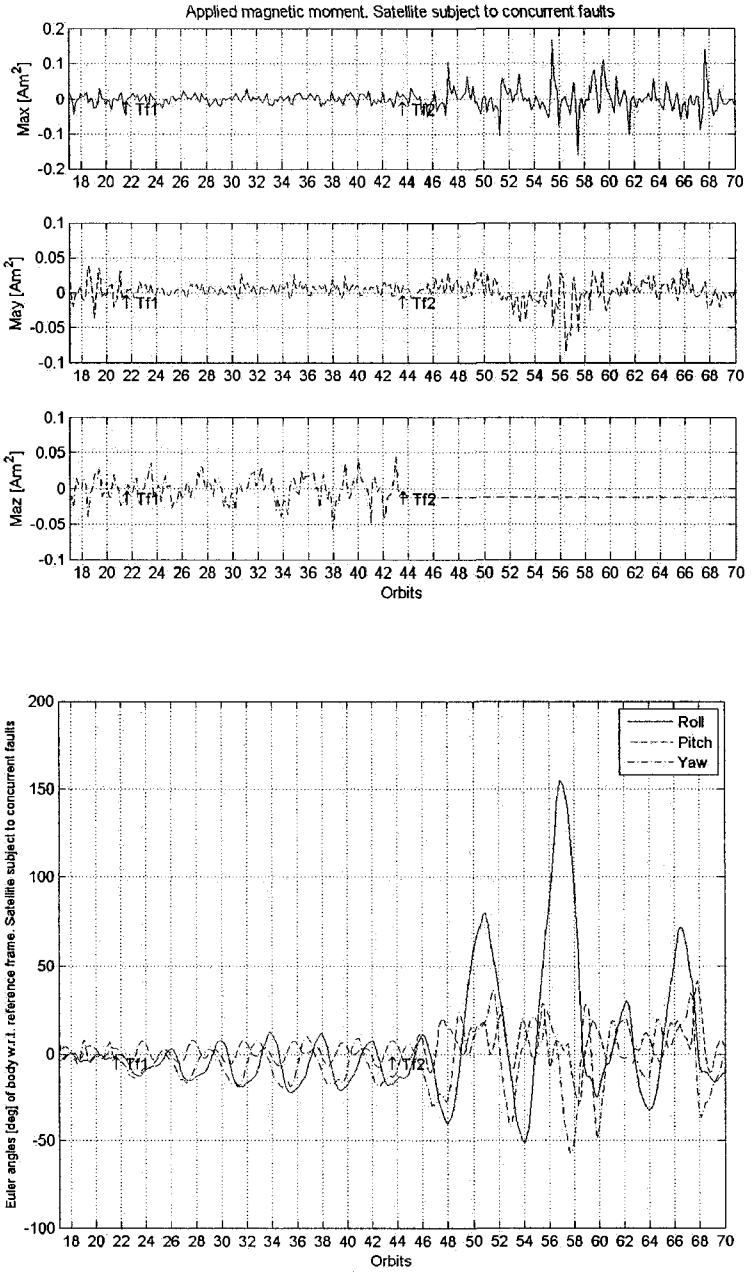

Figure 4.64: Response of the satellite that is subject to 75% LOE and LIP faults that are applied at times $T_{f1} = 21$ orbits and $T_{f2} = 43$ orbits in the torquers alligned to the Y and Z axis, respectively. Satellite is following a zero reference.

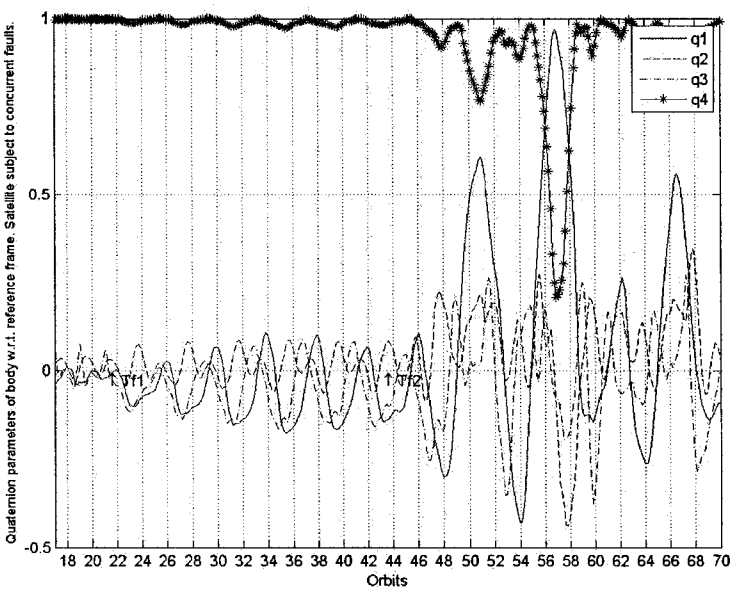

Figure 4.65: Quaternion errors. Response of the satellite that is subject to 75% LOE and LIP faults that are applied at times $T_{f1} = 21$ orbits and $T_{f2} = 43$ orbits in the torquers alligned to the Y and Z axis, respectively. Satellite is following a zero reference.

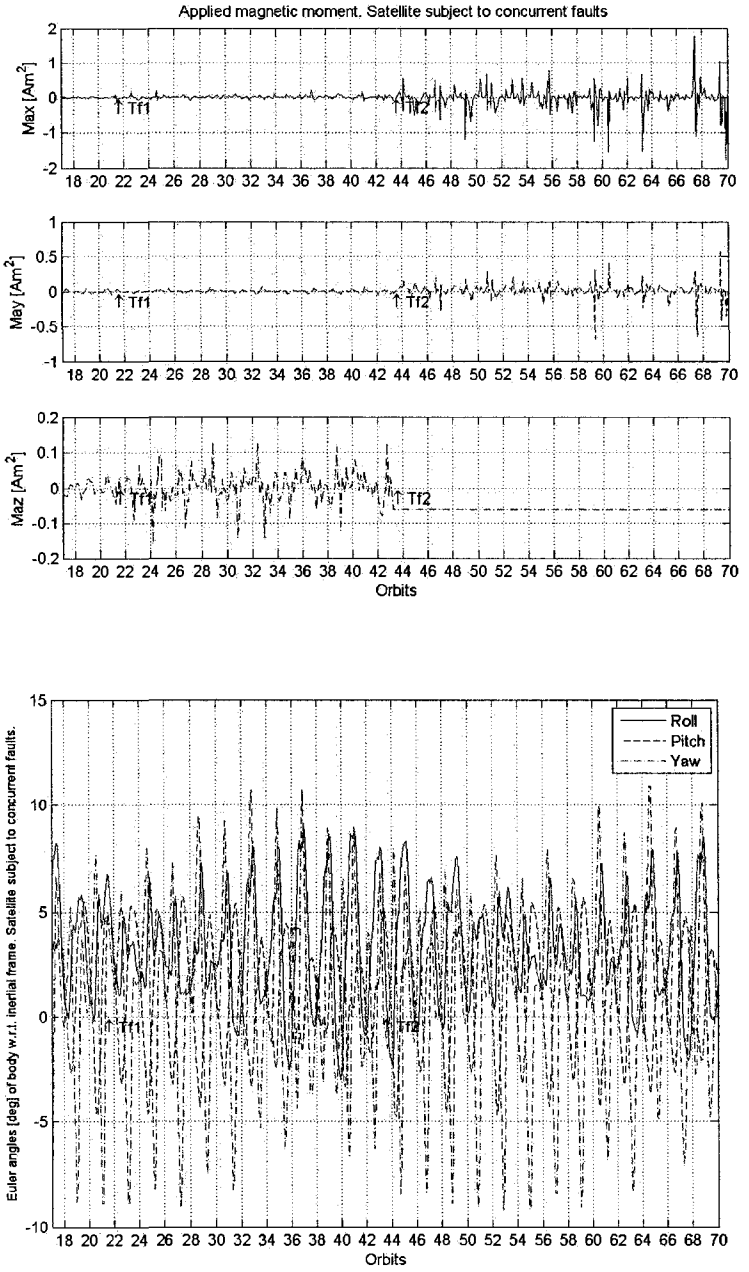

Figure 4.66: Response of the satellite that is recovered from 75% LOE and LIP faults that are applied at times $T_{f1} = 21$ orbits and $T_{f2} = 43$ orbits in the torquers alligned to the Y and Z, respectively. Satellite is following a zero reference.

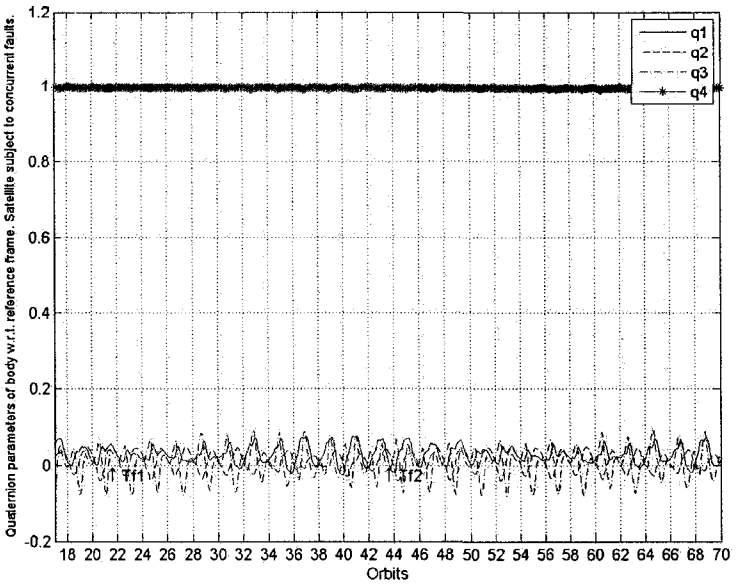

Figure 4.67: Quaternion errors. Response of the satellite that is recovered from a 75% LOE and LIP faults that are applied at times $T_{f1} = 21$ orbits and $T_{f2} = 43$ orbits in the torquers alligned to the Y and Z axis, respectively. Satellite is following a zero reference.

4.8 Chapter Summary

This chapter has presented the characteristics of the model that is implemented for simulating the attitude control system of a satellite using magnetic torquers. The parameters of the system, as well as the calculated environmental disturbances for sizing the actuators were also formulated.

In addition, the simulation results for each of the fault cases and the corresponding recovered systems as well as the effects of the delay in the fault detection and magnetic field measurement noise have been provided. A discussion about the response of the control

reallocation mechanism when the system is subject to concurrent faults is also included. Three scenarios were considered for the simulation of the system that is subject to faults and recovered from faults, namely, the command reference set to zero and two time varying references having different frequencies.

The next chapter will present the conclusions of this thesis and future work to be conducted on fault recovery of magnetic actuators in the attitude control subsystem of a satellite.

Chapter 5

Conclusions and Future Work

5.1 Conclusions

The dynamics and kinematics equations of motion for a LEO satellite are implemented in the Matlab's Simulink. The model includes the following features:

- Major environmental disturbances such as gravity gradient torque, magnetic disturbance and aerodynamic drag,
- Model of the orbital trajectory of the satellite,
- Model of the geomagnetic field at satellite's position in a given orbit,
- Model of a set of three orthogonal magnetic torques, including the fault modes (LIP, HO, LOE and Float),
- Nonlinear attitude controller for trajectory tracking, and
- Fault recovery system.

A comprehensive analysis of the environmental disturbances on the satellite simulated indicate that the most significant environmental disturbances correspond to the gravity gradient torque and the disturbance due to the residual magnetic moment on the satellite. Based on these results, the actuators are sized to be able to compensate for the environmental disturbances and maneuvering efforts.

In order to verify the satellite operation for calculating the desired magnetic moment from the torquers, a geometrical analysis of the torque and the magnetic moment as well as the magnetic field interaction was conducted. It was shown that the torque produced by the cross multiplying twice the desired torque (calculated using a nonlinear control law) with the magnetic field vector corresponds to the component of the desired torque in the plane that is perpendicular to the magnetic field. The resulting vector was shown to be the control moment that generates the closest torque to T_c (the desired control torque).

The stability analysis of the closed-loop system that is actuated by the magnetic torquers was presented. It was indicated that further work is required in the formal evaluation of the boundedness and the stability of closed-loop system when $T_{eq} \neq 0$ for the specific control law that was employed by assuming a normal operation of the actuators.

Different types of faults namely LIP, LOE, HO and Float in the actuators are utilized for the magnetic torquers. A complete analysis of the effects of each fault on the satellite attitude was also made. The solution proposed for the recovery from faults in the magnetic actuators was shown to be indeed effective for the recovery from Float, LOE and LIP faults.

The recovery of the system under HO fault by simply shutting down the actuator under the fault was considered. Results are shown to be satisfactory when after shutting down the faulty actuator, the fault was recovered as a float fault.

Unconstrained and constrained optimization recovery strategies are developed and implemented numerically in simulations for the faulty magnetic torquers. The closed-loop stability of the system that is recovered from a fault was shown analytically for the solution to the unconstrained optimization problem. Moreover, the simulation results are shown for different faults scenarios and reference trajectories.

The effects of the time delay on the response of the recovery system to active faults (due to the delay in the detection of a fault and subsequent late recovery reaction) were evaluated through simulations. It was observed that the delay has indeed an effect on the performance of the recovered system. However, for the duration of the delays that were considered, the recovery mechanism was still able to stabilize the system despite the presence of a fault. The effects of the presence of noise in the measurement of the magnetic field were also applied and through numerical simulations it could be seen that the steady state error of the sytem under this condition is larger.

The recovery algorithm was also evaluated for operation under concurrent faults in some applicable cases, such as those involving the LIP, HO and LOE faults along with the occurrence of a second LOE fault. Due to the capability of each magnetic torquer to have

an effect on two control axes the results obtained showed that our proposed recovery solution is also effective under these scenarios. Two examples of recovery from concurrent faults were also presented in simulations to verify our claims.

A quantitative evaluation of the results was also made in order to compare the performance of the satellite under faults with and without our proposed recovery strategy. The mean and the standard deviations of the angular positions are used for this analysis. The results demonstrate that the performance of the system under recovery is considerably better than the system under fault with no recovery solution.

5.2 Future Work

The control reallocation problem for the application considered in this thesis can be extended with a more complicated cost function that may involve parameters of the controller to be adjusted as well as the power consumption efficiency and fairness among the actuators. Other control laws may also be used as baseline controller with which the reallocation approach introduced in this dissertation could be evaluated.

In the particular case of magnetic torquers, the effort from each actuator had an effect on two of the control axes. Therefore, it is considered that this approach could be adapted for the application to other types of actuators, under similar conditions with hardware redundancy.

The present work has assumed that the magnetic torquers are capable of producing a moment that is equal to the control input. However, it is clear that the physical properties of the coil materials, as well as the circuitry to drive the control current (or voltage) increase the complexity of the operation and therefore the dynamics of the actuator may deviate from an ideal performance. Further work could be done by incorporating the dynamics of the magnetic torquers and its integration with the fault recovery system.

Finally, it is our opinion that the analysis of the system should incorporate the effects of delayed detection and inaccuracies in the magnetometer measurements. This would make it possible to determine formally the maximum allowable delays in the fault recovery (or fault detection) system to guarantee the stability of the closed-loop satellite as well as the required performance requirements and specifications under realistic situations.

Bibliography

[1] K. L. MAKOVEC, A Nonlinear Magnetic Controller for Three-Axis Stability of Nanosatellites, Master's thesis, Virginia Polytechnic Institute and State University, 2001. xi, 17

[2] S. MCLEAN, S. MACMILLAN, S. MAUS, V. LESUR, A. THOMSON, and D. DATER, The US/UK World Magnetic Model for 2005-2010. NOAA Technical Report NESDIS/NGDC-1, Technical report, NOAA National Geophysical Data Center (USA) and British Geological Survey - Geomagnetism Group (UK), 2004. xi, 21, 22, 23

[3] B. WIE, *Space Vehicle Dynamics and Control*, American Institute of Aeronautics and Astronautics, Inc., 1998. xi, 18, 19, 23, 24, 26, 41, 42

[4] J. WERTZ, H. APGAR, D. BEARDEN, R. BELL, J. BLAKE, and D. BODEN, *Space Mission Analysis and Design*, Microcosm Press and Kluwer Academic Publishers, 1999. xix, 27, 28, 29, 32, 89, 91

[5] R. WISNIEWSKI, *Satellite Attitude Control Using Only Electromagnetic Actuation*, PhD thesis, Department of Control Engineering, Aalborg University, Denmark, 1996.

xix, 4, 11, 34, 40, 41, 44, 86, 92, 94

[6] B.-S. LEE and J.-S. LEE, Sun interference Predictions for the KOMPSAT TT&C Station, in *J. Astron. Space Sci. 14(1)*, 1997. xix, 87

[7] H. PAIK, KOMPSAT-I Payloads, Technical report, Satellite Application Dept., Korea Research Institute, 1998, http://sol.oc.ntu.edu.tw/omisar/wksp.mtg/ocare98/Kompsat/KOMPSAT1.htm. xix, 87

[8] M. LOVERA, E. DE MARCHI, and S. BITTANI, Periodic Attitude Control Techniques for Small Satellites With Magnetic Actuators, in *IEEE Transactions on Control Systems Technology*, volume 10, number 1, pp. 90–95, 2002. 3

[9] M. LOVERA and A. ASTOLFI, Global Magnetic Attitude Control of Spacecraft, in *43rd IEEE Conference on Decision and Control. Atlantis, Paradise Island, Bahamas*, 2004. 3

[10] E. SILANI and M. LOVERA, Magnetic Spacecraft Attitude Control: A Survey and Some New Results, in *Control Engineering Practice*, volume 13, number 3, pp. 357–371, 2005. 3, 30, 39

[11] M. LOVERA and A. ASTOLFI, Global Magnetic Attitude Control of Spacecraft in the Presence of Gravity Gradient, in *Proceedings of the 42nd IEEE Conference on Decision and Control. Maui,HA*, volume 42, pp. 796–805, 2006. 3, 30

[12] M. GUELMAN, R. WALLER, A. SHIRYAEV, and M. PSIAKI, Design and Testing of Magnetic Controllers for Satellite Stabilization, in *Acta Astronautica.*, volume 56, number 1-2, pp. 231–239, 2005. 3

[13] P. WANG and Y. B. SHTESSEL, Satellite Attitude Control Using only Magnetorquers, in *Proceedings of the American Control Conference. Morgantown, WV*, pp. 500–504, 1998. 3

[14] T. R. KROGSTAD, J. T. GRAVDAHL, and P. TONDEL, Explicit Model Predictive Control of a Satellite with Magnetic Torquers, in *Proceedings of the 13th Mediterranean Conference on Control and Automation. Limassol, Cyprus*, pp. 491–496, 2005. 3

[15] N. SIVAPRAKASH and J. SHANMUGAM, Neural network based three axis satellite attitude control using only magnetic torquers, in *24th Digital Avionics Systems Conference. Washington, DC*, volume 2, p. 6, 2005. 3

[16] M. POLITES, C. QUARIES, and D. KADERBEK, Pulse Width Modulating Low Power Magnetic Torquers for Precise Spacecraft Attitude Stabilization, in *Proceedings of the I MECH E Part G Journal of Aerospace Engineering*, volume 219, pp. 471–482, 2005. 3, 30

[17] F. SHABANINIA and R. KHORSHIDI, A Control System for a single-spin LEO Satellite employing supervisory control with fuzzy logic and adaptive control under uncertainty, in *Journal of Intelligent and Fuzzy Systems*, volume 17, number 5, pp. 533–540, 2006. 3

[18] M. WOOD and W.-H. C., Regulation of Magnetically Actuated Satellites using Model Predictive Control with Disturbance Modelling, in *IEEE International Conference in Networking, Sensing and Control (ICNSC)*, pp. 692–697, 2008. 4

[19] R. WISNIEWSKI and M. BLANKE, Attitude Control for Magnetic Actuated Satellite, in *Control of Nonlinear Systems: Proceedings of Theory and Applications, EURACO Workshop. Algarve, Portugal*, 1996. 4, 11, 34, 40, 41

[20] R. WISNIEWSKI and M. BLANKE, Fully Magnetic Attitude Control for Spacecraft Subject to Gravity Gradient, in *Automatica*, volume 35, number 7, pp. 1201–1214, 1999. 4, 11, 34, 40, 41

[21] R. WISNIEWSKI and L. MARKLEY, Optimal Magnetic Attitude Control, in *IFAC World Congress, Beijing, China*, 1999. 4

[22] R. WISNIEWSKI, Linear Time Varying Aproach to Satellite Attitude Control Using Only Electromagnetic Actuation, in *AIAA Guidance, Navigation, and Control Conference. New Orleans, LA*, pp. 11–13, 1997. 4

[23] V. VENKATASUBRAMANIAN, R. RENGASWAMY, K. YIN, and S. N. KAVURI, A Review of Process Fault Detection and Diagnosis. Part I: Quantitative Model-based Methods, in *Computers and Chemical Engineering*, volume 27, number 3, pp. 293–311, 2003. 5, 6

[24] B. THUMMALA, Spacecraft Autonomy, Master's thesis, School of Engineering. Granfield University, UK, 2003. 5

[25] R. PATTON, C. LOPEZ-TORIBIO, and F. UPPAL, Artificial Intelligence Approaches to Fault Diagnosis, in *Condition Monitoring: Machinery, External Structures and Health*, volume 34, number 5, pp. 1–518, 1999. 5, 7

[26] R. MEHRA, C. RAGO, and S. SEEREERAM, Autonomous Failure Detection, Identification and Fault-tolerant Estimation with Aerospace Applications, in *Proceedings of the 37th IEEE Conference on Decision and Control. Tampa, Florida*, 1998. 6, 49

[27] J. D. BOSKOVIC, S.-M. LI, and R. K. MEHRA, Reconfigurable Flight Control Design Using Multiple Switching Controllers and On-line Estimation of Damage-Related Parameters, in *Proceedings of the 2000 IEEEInternational Conference on Control Applications. Anchorage, Alaska*, pp. 479–484, 2000. 6, 8

[28] Y. ZHAN and J. JIANG, An Interacting Multiple-model Based Fault Detection, Diagnosis and Fault-tolerant Control Approach, in *Proceedings of the 38th IEEE Conference on Decision and Control. Phoenix, Arizona*, volume 4, pp. 3593–3598 vol.4, 1999. 6, 9

[29] V. VENKATASUBRAMANIAN, R. RENGASWAMY, and S. N. KAVURI, A Review of Process Fault Detection and Diagnosis. Part II: Qualitative Models and Search Strategies, in *Computers and Chemical Engineering*, volume 27, number 3, pp. 313–326, 2003. 6

[30] V. VENKATASUBRAMANIAN, R. RENGASWAMY, K. YIN, and S. N. KAVURI, A Review of Process Fault Detection and Diagnosis. Part III: Process History Based

Methods., in *Computers and Chemical Engineering*, volume 27, number 3, pp. 327–346, 2003. 6, 7

[31] D. MYLARASWAMY and V. VENKATASUBRAMANIAN, A Hybrid Framework for Large scale Process Fault Diagnosis, in *Computers and Chemical Engineering*, volume 21, pp. S935–S940, 1997. 6, 7

[32] S. LAPP and G. POWERS, Computer-aided Synthesis of Fault-trees, in *IEEE Transactions on Reliability*, volume R-36, pp. 2–13, 1977. 7

[33] V. VENKATASUBRAMANIAN and S. H. RICH, An object-oriented two-tier architecture for integrating compiled and deep-level knowledge for process diagnosis., in *Computers and Chemical Engineering*, volume 12, number 9-10, pp. 903–921, 1988. 7

[34] W. TRUSZKOWSKI and H. HALLOCK, Agent Technology from a NASA Perspective, in *Lecture Notes in Computer Science. Cooperative Information Agents III*, volume 1652, pp. 1–33, Springer, 1999. 8

[35] M. N. SEETING, Y. HASHIDA, N. BEAN, M. S. HODGART, and H. STEYN, CERISE microsatellite recovery from first detected collision in low Earth orbit, in *Acta Astronautica 55*, pp. 139–147, 2004. 8, 9

[36] H. RAUCH, Intelligent Fault Diagnosis and Control Reconfiguration, in *IEEE Control Systems Magazine*, volume 14, number 3, pp. 6–12, 1994. 8

[37] H. RAUCH, Autonomous Control Reconfiguration, in *IEEE Control Systems Magazine*, volume 15, number 6, pp. 37–48, 1995. 8

[38] H. TALEBI and R. PATEL, An Intelligent Fault Detection and Recovery Scheme for Reaction Wheel Actuator of Satellite Attitude Control Systems, in *Proceedings of the 2006 IEEE International Conference on Control Applications. Munich, Germany*, pp. 3282–3287, 2006. 8, 9

[39] J. D. BOSKOVIC and R. K. MEHRA, Stable Adaptive Multiple Model-based Control Design for Accommodation of Sensor Failures, in *Proceedings of the American Control Conference. Anchorage,AK*, pp. 2046–2051, 2002. 8

[40] Y. ZHANG and J. JIANG, Bibliographical Review on Reconfigurable Fault-Tolerant Control Systems, in *Proceedings of the 5th IFAC Symposium on Fault Detection, Supervision and Safety for Technical Processes. Washington, DC*, 2003. 8

[41] F. BACCONI, D. ANGELI, and E. MOSCA, Attitude Control of Asymmetric Spacecrafts Subject to Actuator Failures, in *Proceedings of 2003 IEEE Conference on Control Applications. Istanbul,Turkey*,.volume 1, pp. 474–479, 2003. 9

[42] J. D. BOSKOVIC and R. K. MEHRA, Multiple Model Based Adaptive Reconfigurable Formation Flight Control Design, in *Proceedings of the 41st IEEE Conference on Decision and Control. Las Vegas, NV*, volume 2, pp. 1263– 1268, 2002. 9

[43] J. D. BOSKOVIC and R. K. MEHRA, Fault Accommodation Using Model Predictive Methods, in *Proceedings of the American Control Conference. Anchorage, AK*, volume 6, pp. 5104–5109, 2002. 9

[44] K. M. A. and F. SASSANI, Spacecraft Momentum Dumping Using Less Than Three External Control Torques, in *International Conference on Systems, Man and Cybernetics (ISIC)*, pp. 4031–4039, 2007. 9

[45] M. W. OPPENHEIMER and D. B. DOMAN, Control Allocation for Overactuated Systems (preprint), Technical report, Air Foce Research Laboratory, Control Theory and Optimization Branch, 2006, http://stinet.dtic.mil/cgi-bin/GetTRDoc?AD=ADA461485&Location=U2&doc=GetTRDoc.pdf. 10

[46] J. D. BOSKOVIC and R. K. MEHRA, An Adaptive Scheme for Compensation of Loss of Effectiveness of Flight Control Effectors, in *Proceedings of he 40th IEEE Conference on Decision and Control. Orlando, FL*, IEEE, 2001. 10

[47] J. BOSKOVIC and R. MEHRA, Control Allocation in Overactuated Aircraft Under Position and Rate Limiting, in *Proceedings of the 2002 American Control Conference. Anchorage, AK*, volume 1, pp. 791–796, 2002. 10

[48] O. HARKEGARD and S. T. GLAD, Resolving Actuator Redundancy - Optimal Control vs. Control Allocation, in *Automatica*, volume 41, number 1, pp. 137–144, 2004. 10

[49] N. G. D. CENTER, IGRF - International Geomagnetic Reference Field, Technical report, NOAA Satellite and Information Center, 2004, http://www.ngdc.noaa.gov/IAGA/vmod/igrf.html. 21

[50] S. S. and M. HARRIS, Spacecraft Magnetic Torques - NASA SP-8018, Technical report, National Aeornautics and Space Administration (NASA), 1969, http://trs.nis.nasa.gov/archive/00000014/01/sp8018.pdf. 29

[51] M. L. PSIAKI, Magnetic Torquer Attitude Control Via Asymptotic Periodic Linear Quadratic Regulation, in *Journal of Guidance, Control, and Dynamics*, volume 24, number 2, pp. 386–394, 2001. 30

[52] A. SI MOHAMMED, Modeling and Simulation of Magnetic Control and its Application on Alsat-1 First Algerian Microsatellite, in *Proceedings 18th European Simulation Multiconference. Magdeburg, Germany*, pp. 296–300, 2004. 30

[53] S. P. BHAT and A. S. DHAM, Controllability of Spacecraft Attitude Under Magnetic Actuation, in *Proceedings of 42nd IEEE Conference on Decision and Control*, 2003. 30, 40, 43

[54] R. WISNIEWSKI, Sliding Mode Attitude Control for Magnetic Actuated Satellite, in *Proceedings of 14th IFAC Symposium on Automatic Control in Aerospace. Seoul, Korea*, 1998. 34

[55] G. WILLIAMS, *Linear Algebra with Applications*, Stetson University, 1984. 35, 36

[56] H. K. KHALIL, *Nonlinear Systems*, Prentice Hall, 2002. 45

[57] E. K. P. CHONG and S. H. ZAK, *Introduction to Optimization, Second Edition*, John Wiley & Sons, Inc, 2001. 57, 60, 64, 66

[58] S. DONG, Methods for Constrained Optimization, in *Internal Project Publication*, Massachussets Institute of Technology, 2006, http://web.mit.edu/dongs/www/publications/projects/2006-05-23_18.086_ConstrainedOptimization.pdf. 77

[59] DANMARKS-METEOROLOGISKE-INSTITUT, The Ørsted Satellite, Danmark Meteorological Instutute, http://web.dmi.dk/projects/oersted/. 94

[60] DANMARKS-METEOROLOGISKE-INSTITUT, The Ørsted Satellite, Danmark Meteorological Instutute, http://www.dmi.dk/eng/index/research_and_development/solar-terrestrial_physics_division/the_oersted-satellite.htm. 151

[61] O. V. NIELSEN, J. R. PETERSEN, F. PRIMDAHL, P. BRAUER, B. HERNANDO, A. FERNANDEZ, J. M. G. MERAYO, and P. RIPKA, *Measurement Science and Technology* **6, issue 8**, 1099 (1995). 151